DEPARTMENT OF TRANSPORTATION

# Deck Reinforcement Detailing and Concrete Mix Additives to Reduce Bridge Deck Cracking

**Brock Hedegaard, Principal Investigator**
Department of Civil Engineering
University of Minnesota Duluth

**July 2025**

Research Project
Final Report 2025-38

To get this document in an alternative format or language, please call 651-366-4720 (711 or 1-800-627-3529 for MN Relay). You can also email your request to ADArequest.dot@state.mn.us. Please make your request at least two weeks before you need the document.

## Technical Report Documentation Page

| 1. Report No. | 2. | 3. Recipients Accession No. | |
|---|---|---|---|
| MN 2025-38 | | | |
| 4. Title and Subtitle<br>Deck Reinforcement Detailing and Concrete Mix Additives to Reduce Bridge Deck Cracking | | 5. Report Date<br>July 2025<br>6. | |
| 7. Author(s)<br>Brock Hedegaard, Eric Gibson, Lauren Linderman | | 8. Performing Organization Report No. | |
| 9. Performing Organization Name and Address<br>Department of Civil Engineering<br>University of Minnesota Duluth<br>1405 University Drive, Duluth, MN, 55812 | | 10. Project/Task/Work Unit No.<br>11. Contract (C) or Grant (G) No.<br>1036342 WO#86 | |
| 12. Sponsoring Organization Name and Address<br>Minnesota Department of Transportation<br>Office of Research & Innovation<br>395 John Ireland Boulevard, MS 330<br>St. Paul, Minnesota 55155-1899 | | 13. Type of Report and Period Covered<br>Final report<br>14. Sponsoring Agency Code | |
| 15. Supplementary Notes<br>http://mdl.mndot.gov/ | | | |


16. Abstract (Limit: 250 words)

Despite recent changes to MnDOT mix designs, transverse cracking has still been observed shortly after the bridge deck is poured. The goal of this research was to determine the causes of this cracking and to propose deck reinforcement or mix design practices that efficiently mitigate the problem. Initial investigations focused on synthesizing existing research relating to crack mitigation in concrete bridge decks, and how these practices aligned with current Minnesota Department of Transportation (MnDOT) design and construction practices. This was followed by laboratory testing of high-performance bridge deck mixes to test alterations to the accepted mix specifications, and computational modeling to determine the most critical bridge deck demands and effects of altered deck reinforcement. Computational results indicated that minimizing shrinkage and the temperature difference between the placed deck concrete on the girders are the most effective means to reduce tensile demands on the bridge deck. Introducing shrinkage reducing admixtures into the mix effectively reduced strain due to unrestrained shrinkage by approximately 25% and forces due to restrained shrinkage by approximately 50%. Changing deck reinforcement has no effect on crack initiation but may control crack width once it forms. Thus, recommendations include a combination of reduced shrinkage and increased top longitudinal reinforcement in the bridge deck.


| 17. Document Analysis/Descriptors | 18. Availability Statement | | |
|---|---|---|---|
| Bridge decks, concrete shrinkage, cracking, deck reinforcement | No restrictions. Document available from: National Technical Information Services, Alexandria, Virginia 22312 | | |
| 19. Security Class (this report)<br>Unclassified | 20. Security Class (this page)<br>Unclassified | 21. No. of Pages<br>86 | 22. Price |

# Deck Reinforcement Detailing and Concrete Mix Additives to Reduce Bridge Deck Cracking

# Final Report

*Prepared by:*

Dr. Brock Hedegaard
Department of Civil Engineering
University of Minnesota Duluth

Eric Gibson
Department of Civil Engineering
University of Minnesota Duluth

Dr. Lauren Linderman
Department of Civil, Environmental, and Geo- Engineering
University of Minnesota

# July 2025

*Published by:*

Minnesota Department of Transportation
Office of Research & Innovation
395 John Ireland Boulevard, MS 330
St. Paul, Minnesota 55155-1899

# Table of Contents

# List of Figures

# List of Tables

# Executive Summary

Early-age cracking in reinforced concrete bridge decks leads to costly maintenance activities and/or rapid deterioration of reinforcing steel, decreasing the lifespan of a bridge deck. Despite alterations to MnDOT mix designs, transverse cracking is still observed shortly after casting. Reducing early-age cracking will reduce the amount of rehabilitation needed and increase the service life of a bridge, significantly improving life cycle costs.

The primary demands on bridge decks post-curing include thermal demands and shrinkage. Thermal demands involve differences in temperature between the deck and girders. For example, if casting warmer deck concrete onto cooler girders, the deck concrete tries to contract as it hardens and cools but is restrained by the girders. This restraint induces tensile stress into the deck. Thermal gradients, where the top surface of the deck is either heated by solar radiation or cooled with wind and rain, also result in deck stresses. Finally, deck shrinkage can result in further tensile stresses as the deck tries to contract but the girders restrain this deformation. To mitigate early-age cracking, either these tensile stresses must be reduced, or the tensile strength of the bridge deck must be increased. Therefore, the goals of this research are to investigate the causes of bridge deck cracking and to propose practices that reduce or control these demands.

Initial investigations focused on synthesizing existing research relating to crack mitigation in concrete bridge decks, and how these practices aligned with current Minnesota Department of Transportation (MnDOT) design and construction practices. Promising alternatives found throughout the literature included introducing shrinkage reducing admixtures (SRA) to concrete mixes, adjusting the fiber content of currently used concrete mixes, investigating deck curing and placement practices, and adjusting steel reinforcement ratios. The following research plan was divided into two phases: laboratory tests of high-performance concrete (HPC) mixes, and finite element modeling of bridge decks subjected to thermal and shrinkage demands.

Laboratory testing was conducted to test the effects of introducing SRAs, adjusting fiber content, and adjusting curing periods in the currently accepted HPC mix design used by MnDOT. Twelve total mixes were performed, including six to investigate the standard control HPC mix provided by MnDOT, four to investigate the introduction of SRAs into the HPC mix, and two to investigate the effects of adjusting fiber content in the HPC mix. Fresh and hardened concrete properties were tested to ensure that all the mixes provided acceptable concrete characteristics aligning with MnDOT HPC mix requirements. Results of interest included slump, air content, compressive strength, flexural strength, strain due to unrestrained shrinkage, and force due to restrained shrinkage.

Computational modeling using finite element analysis (FEA) was also conducted to investigate the effects of concrete creep and shrinkage, thermal variations, and different reinforcement layouts on tensile stress demands in the bridge deck. A model bridge deck was created in ANSYS based on a typical MnDOT bridge. The bridge model included six prestressed concrete girders and a 9-inch-thick bridge deck that had a width of 43 feet with a 100-foot span length. Models were created to test the current standard bridge deck with top longitudinal reinforcement spaced at 18 inches and compare this to decks

with 12-inch spacing, 6-inch spacing, flipped reinforcement layering, and bridges with multiple spans. Loading scenarios included the investigation of positive thermal gradients (deck warmer than girders), negative thermal gradients (deck cooler than girders), temperature differentials during deck concrete placement, creep and shrinkage, and the interactions among these. Model results focused on computing the top surface tensile stresses which indicate the initiation of cracking, and stresses through the depth of the deck which indicate the progression of cracking through the depth of the deck.

Based on laboratory results from each mix, introducing SRAs into the HPC mix effectively reduced strain due to unrestrained shrinkage by approximately 25% and forces due to restrained shrinkage by approximately 50%. The introduction of SRA did negatively affect the workability of the concrete, but otherwise the fresh and hardened properties were acceptable and met HPC requirements. Results from the mixes with adjusted fiber contents indicated little to no benefit in reducing unrestrained shrinkage strain or force due to restrained shrinkage.

Computational modeling indicated that creep and shrinkage induced the largest tensile stresses, exceeding 500 psi in the bridge deck, which alone may be sufficient to initiate cracking. Creep and shrinkage may also act in conjunction with a negative thermal gradient, leading to potential tensile stresses exceeding 650 psi in the deck, which would certainly lead to crack initiation. While it is not possible to eliminate naturally occurring thermal gradients, these results indicate that minimizing shrinkage and the temperature difference between the placed deck concrete on the girders are the most effective means to reduce tensile demands on the bridge deck. The models also indicated that changing the reinforcement layout or reducing spacing between temperature and shrinkage steel have no effect on reducing tensile stresses in the deck. Thus, additional deck reinforcement is unlikely to reduce the initiation of cracks. However, previous studies indicate that, once cracking has occurred, additional reinforcement may help control crack widths in the bridge deck.

Based on the findings from this study, the following recommendations were made:

- Introduce shrinkage reducing admixtures (SRA) to the HPC mix design to reduce early-age deck stresses and thus limit crack formation.
- Create specification language for controlling the difference between placed deck concrete and the girders.
- Reduce spacing between reinforcing bars in the top mat of longitudinal reinforcement to control crack widths.

# Chapter 1: Introduction

## 1.1 Background

A bridge deck is the structural surface of a bridge used for vehicles to drive on, commonly made of concrete, steel, or wood. Concrete bridge decks can be either precast, where the slab is cast and cured in a manufacturing facility and moved to the desired location, or cast-in-place, where the slab is cast and cured in its final desired position. Bridge decks can be a major load-carrying element if composite with the girders or a simple structural slab that spans between girders. At times, they may be covered with a non-structural concrete or asphalt pavement wearing surface for additional protection against the influences of everyday use.

As concrete members cure, they experience shrinkage, which can lead to cracking of the concrete. Shrinkage is the volumetric reduction of a concrete member not subjected to an external force. Shrinkage can be caused by the loss of moisture from concrete, referred to as drying shrinkage, or by the chemical reaction during cement hydration, referred to as autogenous shrinkage. Because moisture loss and cement hydration occur as concrete hardens, shrinkage begins shortly after casting the concrete. Shrinkage can be limited by controlling the amount of water that is added to a mix. If a lower water to cement ratio can be maintained, the hardened concrete will experience less drying shrinkage due to the lower water content, but the mix may experience more autogenous shrinkage.

Thermal effects may also lead to concrete cracking. A recently cast concrete bridge deck may have a higher temperature than the previously cast girders. As the temperature and volume of the deck decrease, the girders may provide restraint and induce tensile forces which cause cracking. Negative thermal gradients, where the top surface of the bridge has a lower temperature than the rest of the bridge, also induce tensile forces through the bridge deck.

## 1.2 Motivation

Early-age cracking in reinforced concrete bridge decks poses costly maintenance activities or leads to rapid deterioration of reinforcing steel, decreasing the lifespan of a bridge deck. Despite alterations to MnDOT mix designs, transverse cracking is still observed shortly after casting. To mitigate cracking, either induced tensile stresses must be reduced or tensile strength of the bridge deck must be increased to combat them. Reducing early age cracking will reduce the amount of rehabilitation needed and increase the service life of a bridge, significantly improving life cycle costs.

## 1.3 Objectives

The goal of this research is to investigate the causes of early-age bridge deck cracking and propose methods to mitigate cracking. Concrete mix design, steel reinforcement ratio, thermal effects, and curing practices will be investigated to determine which factors most effectively reduce tensile stresses

in the bridge deck. Recommendations will be provided relating to which methods best reduce tensile stresses, control cracking, and can be implemented on a large scale in future bridge deck design.

This investigation will assume a cast-in-place concrete bridge deck with a rectangular cross section and no wearing course. This type of bridge deck will be supported by prestressed concrete girders and will have two layers of reinforcement in the longitudinal and transverse directions. To construct a cast-in-place bridge deck, formwork must first be built, and steel reinforcement must be put in place. After the formwork and reinforcement are installed, the concrete can be poured. The concrete must then be cured for a minimum seven-day period, at which time the formwork and curing material may be removed (MnDOT *Standard Specifications for Construction: 2020 Edition*). These practices represent the control scenario to gather baseline data relating to bridge deck cracking.

Research tasks included a literature review, laboratory testing, and computational modeling using finite element analysis. Chapter 2 contains the literature review, which presents a synthesis of research and a summary of existing MnDOT design and construction practices. This provided insight into potential solutions that may be implemented in current practices. Chapter 3 contains details of laboratory and computational modeling methodologies, summarizing standard procedures for concrete mixing and testing and computational modeling and testing. Chapter 4 provides results from all laboratory testing. We discuss each concrete mix and the associated results, providing comparisons between concrete characteristics. Chapter 5 provides results from all computational testing, including both initial and parametric model testing. Initial modeling focused primarily on developing a representative model that can accurately produce values for deck stresses caused by different loading scenarios. Once we developed an accurate model, parametric modeling focused on making changes to the original model to test different reinforcement layouts and loading conditions. Chapter 6 provides a summary of performed tests, a discussion of results, and recommendations based on the discussion.

# Chapter 2: Literature Review

Early-age cracking in reinforced concrete bridge decks results in costly maintenance activities and may significantly reduce the lifespan of a bridge deck. In this review, we will discuss existing research relating to early age cracking in concrete and early age cracking mitigation methods, and further examine current Minnesota Department of Transportation (MnDOT) design and construction practices. Finally, we will present ideas for testing to determine possible solutions that can be implemented by MnDOT.

## 2.1 Existing Research

Existing research points to multiple possible solutions that have the potential to decrease early-age cracking in concrete bridge decks. Common solutions include using shrinkage reducing admixtures (SRA), expansive agents (EA), internally cured concrete (ICC), fiber reinforcement, textured epoxy reinforcement, and other methods.

### 2.1.1 Shrinkage Reducing Admixtures

Shrinkage reducing admixtures (SRA) combat drying shrinkage by decreasing surface tension of concrete pores, which reduces capillary stresses. Multiple studies have demonstrated that SRAs effectively decrease shrinkage strains along with providing slower shrinkage rates.

Rahman et al. (2020) tested a scale bridge deck containing SRA compared to a control mixture (Portland cement with a 0.44 w/c ratio) and determined that shrinkage strain in the SRA mixture was 73% less than shrinkage in the control mixture. The SRA mixture also demonstrated a significantly slower shrinkage rate compared to the control mixture, 0.3 microstrain per day compared to 1.0 microstrain per day after 28 days.

Simonton et al. (2021) compared the effects of SRA mixtures and SRA with ICC mixtures to a control mix over a 28-day period. The SRA mix demonstrated a decrease in autogenous shrinkage of 47%, while the SRA with ICC mix resulted in a decrease in autogenous shrinkage of 84%. It was also found that drying shrinkage was reduced by 40% in both mixtures when using an SRA dosage of 3.0 gal/yd$^3$, which is double the maximum recommended dosage for products such as MasterLife SRA 035.

Ardeshirilajimi et al. (2016) fabricated and monitored scale bridge decks with SRA and ICC mixtures compared to a control mixture over a 182-day period and determined that drying shrinkage was considerably reduced in the SRA and ICC mixtures. They also found that the rate of shrinkage was significantly decreased, agreeing with conclusions by Rahman et al. (2020). The ICC mix that also included SRA produced the smallest overall strain change and tensile forces, creating the smallest cracking potential.

Ozyildirim et al. (2018) compared the effects of SRA in silica fume concrete (SFC) to a control SFC mix used on two bridges in Virginia. The SFC control mix had higher shrinkage values than recommended, but the SFC with SRA demonstrated lower shrinkage values with minimal cracking.

Lee et al. (2018) performed tests using SRA with latex modified concrete (LMC) to reduce plastic and drying shrinkage. It was found that the mixture containing 3% SRA by weight of binding material provided significant shrinkage reducing performance while maintaining other required concrete properties.

Tunstall et al. (2021) performed a review on air entraining admixtures (AEA) and explained the interaction between SRAs and AEAs. In some cases, the use of SRAs may affect the effectiveness of AEAs. It was found that strongly hydrophobic SRAs (that is, SRAs with a hydrophile-lipophile balance of less than seven) have especially adverse effects on AEAs.

California Department of Transportation (CDOT) (2022), Virginia Department of Transportation (VDOT) (2020), and Washington Department of Transportation (WSDOT), among others, all permit the use of SRAs in concrete bridge deck mixes. Typically, this is required to meet shrinkage limits of less than 0.04%. CDOT requires 0.75 gallons of SRA per cubic yard in all bridge deck mixes to achieve 0.032% shrinkage or less. When using rapid set concrete (RSC) CDOT does not require the incorporation of SRAs in mixes if shrinkage test results are 0.024% or less. VDOT states that SRAs may be used in mixes to achieve 0.035% shrinkage or less. WSDOT allows SRAs to be used to achieve 0.032% shrinkage or less.

### 2.1.2 Expansive Agents

Early age expansion of concrete induces compression into the system which counteracts tensile stresses caused by restrained shrinkage. Type-K cement can be used as a partial replacement to Portland cement to achieve expansive properties to counteract shrinkage.

Rahman et al. (2020) tested a Type-K cement mixture and a control Portland cement mixture to compare expansion and shrinkage data over a 182-day period. After seven days, expansion of the Type-K cement mix was 109% larger than that of the control mix, and after the full 182-day period the Type-K cement mix demonstrated a 15% shrinkage reduction compared to the control mix. However, the Type-K cement mix also demonstrated the highest shrinkage rate after 28 days at 1.1 microstrain per day compared to the control mix at 1.0 microstrain per day.

Ardeshirilajimi et al. (2016) tested Type-K cement with ICC mixtures compared to a control mixture over a 182-day period and found contradicting results. It was found that the total shrinkage of the Type-K cement mixture was comparable to the control mix, providing essentially no benefits to counteract shrinkage.

Khayat et al. (2019) tested a Type-G expansive agent for effects during field implementation. An initial expansion of 125 microstrain after three days was measured, along with a limiting shrinkage of 320 microstrain.

### 2.1.3 Internally Cured Concrete

Internally cured concrete utilizes pre-soaked aggregate to release water internally after concrete placement. The pre-soaked aggregate slows internal moisture loss of the concrete with the goal of decreasing shrinkage.

Ardeshirilajimi et al. (2016) studied the effects of ICC on drying and autogenous shrinkage and determined that it has a significant effect on autogenous shrinkage (that is, shrinkage caused by self-desiccation of the concrete induced by hydration), but little to no effect on drying shrinkage. An inverse relationship between autogenous shrinkage and the amount of water used for internal curing was also determined.

Rahman et al. (2020) tested the effects of ICC compared to a control mixture containing Portland cement with a 0.44 w/c ratio. After a drying period of 182 days, it was measured that the ICC mixture experienced a peak strain of 175 microstrain while the control mixture experienced a peak strain of 195 microstrain. Therefore, the ICC concrete mixture experienced 10% less shrinkage than the control mixture over the 6-month period.

Abdigaliyev et al. (2020) also found results determining that ICC successfully controls autogenous shrinkage and delays restrained shrinkage cracking. Hamid et al. (2022) studied ICC and conventional concrete to compare the time to shrinkage initiation. It was found that shrinkage initiated five hours after casting in both mixes, but autogenous shrinkage was eliminated in the ICC mix. Pacheco et al. (2021) determined that ICC resulted in a substantial increase in cracking resistance for restrained concrete but had little to no effect on concrete in non-restrained conditions.

### 2.1.4 Fiber Reinforcement

Early age cracking in concrete can be mitigated with the addition of fiber reinforcement to combat tensile stresses. Fiber reinforcement can significantly improve the tensile behavior of the concrete. Depending on fiber type and dosage, this may result in an increase in tensile capacity or improved post-peak (i.e., post cracking) behavior. Shafei et al. (2021) tested the effects of fiber reinforcement in concrete bridge decks by adding different dosages of microfibers and macrofibres to concrete mixes. It was determined that shrinkage cracking was significantly reduced by introducing polypropylene microfibers in a dosage as low as 0.25% by volume. However, due to the increased water content required with the introduction of microfibers, it is recommended to use a maximum 0.125% microfiber content. It was also found that alkali-resistant glass macrofibres produced the best post-peak strength compared to polypropylene and polyvinyl alcohol macrofibres when the mix contained both microfibers and macrofibres. Therefore, it was determined that the optimal mix should contain 0.125% polypropylene microfiber content and 0.25% alkali-resistant glass macrofibre content to best combat early age cracking in concrete bridge decks.

Patnaik (2017) studied the effects of adding fiber reinforcement to concrete bridge decks without changing steel reinforcement details. The addition of polypropylene fibers reduced plastic shrinkage by a factor of 8 and reduced the overall severity of cracking by a factor of 3 to 4. Saje et al. (2011) tested

the shrinkage of polypropylene fiber reinforced high performance concrete. It was observed that the total shrinkage of the fiber reinforced concrete was between 20% to 39% less than the total shrinkage of the control mix over the first 77 days. It was also found that moistening the fibers prior to mixing also assists in reducing drying and total shrinkage.

Different states may allow or even mandate the inclusion of fibers into bridge deck mixes. For example, the California Department of Transportation and Virginia Department of Transportation allow the usage of fiber reinforcement in concrete bridge deck mixes. CDOT requires bridge decks to contain at least 1 pound per cubic yard of polymer microfibers and at least 3 pounds per cubic yard of polymer macrofibres. When using rapid set concrete CDOT does not require the incorporation of fibers if shrinkage test results are 0.024% or less. VDOT states that fiber reinforcement may be used in deck slabs to combat shrinkage cracking but does not state quantities.

### 2.1.5 Textured Epoxy Coated Rebar

Epoxy coated rebar provides corrosion resistance for steel reinforcement. However, bond strength between the reinforcement and concrete decreases, leading to reduced cracking resistance. A proposed solution for this is textured epoxy coated (TEC) rebar, which is created by spraying a textured powder onto freshly coated conventional epoxy rebar. Kim et al. (2018) performed tests comparing TEC rebar to standard epoxy coated rebar and uncoated rebar. After performing direct pullout and flexure tests, it was found that the TEC bars provided comparable initial slip resistance to the uncoated bars, but degraded rapidly after the bond strength was surpassed. It was also found that, while the standard epoxy coated bars provided essentially no slip resistance under flexure, TEC bars and uncoated bars showed significantly better resistance with TEC bars exhibiting preferable crack widening resistance.

Andrawes et al. (2022) expanded on the prior research performed by Kim et al. (2018). During this study it was found that TEC bars provided higher initial slip resistance than uncoated and epoxy coated rebar, supporting the previous study. Finer cracks were also observed in the TEC rebar reinforced concrete than in the standard epoxy coated rebar reinforced concrete, also supporting the previous study. Ross et al. (2021) tested uncoated, conventional epoxy coated, TEC, hot-dipped galvanized, and continuously galvanized rebar to compare crack resistance for different coatings. It was determined that TEC bars performed 15% better than average in load crack control and 15% better than average in shrinkage crack control.

### 2.1.6 Reinforcement Spacing

Longitudinal steel in bridge decks is primarily used for shrinkage and temperature reinforcement, and thus may designed according the AASHTO LRFD (2020) section 5.10.6:

$$A_s \geq \frac{1.30(bh)}{2(b+h)(f_y)} \tag{2-1}$$

where $A_s$ is area of reinforcement in square inches per foot on each face in each direction and $0.11\ \text{in}^2/\text{ft} \leq A_s \leq 0.60\ \text{in}^2/\text{ft}$, *b* is least width of component section in inches, *h* is least thickness of component section in inches, and $f_y$ is the specific yield strength of reinforcing bars in ksi. For bridge decks that are 9-inches thick, this requires approximately 0.1 in$^2$/ft, and thus is less than the lower bound of 0.11 in$^2$/ft. This amount of steel can be provided using #4 bars at 18-inches on center, the largest allowable rebar spacing, matching current MnDOT practices as discussed below.

NCHRP Synthesis Report 500, *Control of Concrete Cracking in Bridges* (2017), summarizes bridge component cracking practices and research in different states, providing summaries of deck reinforcement practices. As part of research performed for the Indiana DOT, Frosch et al. (2002) presented an equation to determine the recommended area of reinforcing steel to control crack widths:

$$A_s \geq 6\frac{\sqrt{f_c'}}{f_y}A_g \tag{2-2}$$

where $f_c'$ is the design 28-day concrete strength in psi, $f_y$ is the steel yield stress in psi, and $A_g$ is the gross area of the deck. This equation represents the total amount of steel in each direction. The goal of this equation is to provide enough reinforcement such that no yielding occurs in the steel as it crosses the crack, theoretically controlling crack spacing. However, the equation does not directly address the steel-concrete bond. For a 9-inch-thick deck, this equation requires 0.68 in$^2$/ft split into two layers, which may be satisfied with two layers of #4 bars at 7-inches on center, though Frosch et al. further recommended a maximum 6-inch rebar spacing.

Observations by Texas DOT were also discussed in NCHRP Synthesis 500. Based on field observations, Texas DOT determined that the optimal top mat longitudinal reinforcement layout includes #4 bars spaced at 9-inches on center, meeting a reinforcement ratio of 0.27 $\text{in}^2/\text{ft}$ for the top mat. Utah Department of Transportation (UDOT) (2022) places additional emphasis on minimum rebar spacing to combat shrinkage cracking, requiring #4 bars spaced at 12 inches in slabs less than 18 inches thick.

Ge et al. (2021) monitored a reinforced concrete deck on a steel girder bridge for early age cracking. Decreasing bar spacing and increasing reinforcement ratio to achieve an area of longitudinal deck reinforcement that is approximately one percent of the concrete deck area effectively limited crack widths to 0.012 inches. However, it was also noted that more extensive cracks, covering 2.2% of the concrete deck area, occurred in the tested specimens that used a higher reinforcement ratio and larger bar sizes.

### 2.1.7 Shrinkage Testing Methods

Methods to note relating to shrinkage testing of concrete can be found in Simonton et al. (2021), Lee et al. (2018), and Shafei et al. (2021). Simonton et al. (2021) measured unrestrained deformation of specimens using procedures from ASTM C157. Specimen dimensions were 3-in. by 3-in. by 11.25-in. prisms which were measured using a H-3250D 10-in. effective length digital length comparator after 24

hours of curing and 28 days of curing. After the 28-day curing period, additional measurements were taken at 4, 7, 14, 28, and 56 days. A ring test was also performed following ASTM C1581 to determine the time to cracking due to restrained shrinkage.

Lee et al. (2018) performed a length change test using a 100-mm by 100-mm by 400-mm prismatic specimen and a both-end flange type gauge, taking measurements until 28 days of curing. A ring test was also performed following AASHTO PP 34 99 and was visually observed for 56 days.

Shafei et al. (2021) followed general procedures specified in ASTM C1579-13, Standard Test Method for Evaluating Plastic Shrinkage Cracking of Restrained Fiber Reinforced Concrete, with some changes to adapt to the specific research goals. A rectangular plywood mold was used to create slabs with dimensions 22 inches long by 15 inches wide by 4 inches tall. An internal restraint was used, and specimens were placed in an environmental chamber during curing. A handheld microscopic camera and scale bar were used to measure crack widths.

### 2.1.8 Miscellaneous Methods for Crack Control

Other methods for controlling early age cracking in bridge decks may include maintaining proper water to cement (w/c) ratio and using proper curing methods. Rettner et al. (2014) analyzed 20 concrete bridges in Minnesota for cracking mechanisms. It was found that an optimized w/c ratio of 0.38-0.42 should be utilized, as lower w/c ratios experience higher autogenous shrinkage and higher w/c ratios experience higher drying shrinkage.

California Department of Transportation (CDOT) (2022) and Virginia Department of Transportation (VDOT) (2020) place emphasis on curing practices to reduce shrinkage cracking. CDOT requires the curing compound to be applied immediately after finishing, before the moisture sheen dissipates. VDOT also requires the curing compound to be applied immediately after finishing, but states to wait until the moisture sheen dissipates before applying the compound. In a previous study performed by MnDOT, French et al (1999) investigated transverse cracking in bridge decks around Minneapolis. The study included field investigations of 72 bridges along with a laboratory shrinkage study and parametric study. Recommendations from the study include reducing shrinkage by limiting cement contents to 650 lb/yd$^3$ to 660 lb/yd$^3$, using a minimum air content of 5.5% to 6.0%, and maximizing fine and coarse aggregate contents. It was also recommended to use a minimum air temperature of 40°F and maximum air temperature of 90°F during casting, avoid casting when a temperature range of 50°F or more is expected, and reduce longitudinal restraint of the deck. French et al (1999) also recommended limiting transverse reinforcement sizing and maximizing spacing by using either #5 bars spaced at 5.5 inches or #6 bars at 6.5 to 7 inches, while avoiding thin decks (6.25-inch decks exhibited the most cracking). They did not recommend any provisions for longitudinal reinforcement, however.

## 2.2 Current MnDOT Practices

Current MnDOT practices relating to reinforced concrete bridge deck construction can be found in volume two of the MnDOT *Standard Specifications for Construction: 2020 Edition*, section 2401:

Concrete Bridge Construction. Of specific relevance to the topic of early-age transverse cracking in bridge decks are subsections 2401.2K: High Performance Concrete Bridge Decks, 2401.2K.7: Concrete Mix Design, and 2401.3G: Curing Practices. Section 2472: Metal Reinforcement will also be referred to in relation to construction practices for steel reinforcement installation. Further information is documented in the *MnDOT Service Life Design Guide for Bridges* (2023) and the *MnDOT LRFD Bridge Design Manual* (2023).

Section 2401.2K contains specifications relating to high performance concrete (HPC) bridge deck materials. This section contains requirements for aggregates, cementitious materials, and other additional ingredients such as admixtures and fiber reinforcement. Aggregate requirements are largely concerned with controlling alkali-silica reactivity. Water reducing admixture, retarding admixture, accelerating admixture, water reducing and retarding admixture, high range water reducing admixture, and specific performance-based admixtures may be used in concrete mixtures. It also states that fiber reinforcement is acceptable in mixtures, and indeed all currently accepted HPC mixes incorporate fibers at a nominal dosage to control cracking due to plastic shrinkage.

Section 2401.2K.7 contains specifications relating to concrete mix design. Figure 2.2.1 displays the water to cement (W/C) ratio, air content, supplementary cementitious material (SCM), slump, minimum compressive strength, and coarse aggregate requirements for high performance concrete used for concrete bridge decks. These specifications do not contain strength requirements at times other than 28 days, nor do they specify an allowable maximum strength, though these may be controlled indirectly by the rather narrow allowable W/C ratio limits.

**High Performance Bridge Deck Concrete Mix Design Requirements**

| Concrete Grade | Mix Number* | Intended Use | W/C Ratio | Target Air Content | Maximum percent SCM (Fly Ash/Slag/ Silica Fume/ Ternary) ‖ | Slump Range†, inches | Minimum Compressive Strength, f'c (28 Calendar Day) | 3137, "Coarse Aggregate for Portland Cement Concrete" |
|---|---|---|---|---|---|---|---|---|
| HPC | 3YHPC-M | Bridge Deck – Monolithic | 0.42-0.45 | 6.5 percent | 30/35/5/40 | 2 - 5 | 4000 psi | 2.D.2 |
| | 3YHPC-S | Bridge – Structural Slab | | | | | | |

* Provide a Job Mix Formula in accordance with 2401.2K.8, "Job Mix Formula." Use any good standard practice to develop a job mix formula and gradation working range by using procedures such as but not limited to 8-18, 8-20 gradation control, Shilstone process, FHWA 0.45 power chart, or any other performance related gradation control to produce a workable and pumpable concrete mixture meeting all the requirements of the Contract.
‖ The individual limits of each SCM shall apply to ternary mixtures.
† Keep the consistency of the concrete uniform during entire placement.

**Figure 2.2.1. MnDOT high performance concrete mix design requirements (Table 2401.2-4)**

Figure 2.2.2 shows specifications for hardened high-performance concrete used in bridge decks. These specifications include 28-day compressive strength, rapid chloride permeability, freeze-thaw durability, shrinkage, and scaling requirements. Specifications related to early-age strength gain and shrinkage may be of particular importance for early-age cracking. Of note, the standard shrinkage test per ASTM C157 measures the relative shrinkage of concrete for 28 days after an initial 28-day water bath cure. This does not align with MnDOT field curing procedures, as discussed below; the curing procedure may have a significant impact on the amount of shrinkage and the ability of that concrete to resist shrinkage related stresses.

**Required Hardened Concrete Properties for Mixes 3YHPC-M and 3YHPC-S**

| Test | Requirement | Test Method |
|---|---|---|
| Required Strength (Average of 3 cylinders) | 4000 psi at 28 Calendar Days | *ASTM C31** |
| Rapid Chloride Permeability | ≤ 2500 coulombs at 28 Calendar Days (for Preliminary Approval)<br>≤ 1500 coulombs at 56 Calendar Days | *ASTM C1202‖* |
| Freeze-Thaw Durability | Greater than 90 percent at 300 cycles | *ASTM C666†*, Procedure A |
| Shrinkage | No greater than 0.040 percent at 28 Calendar Days | *ASTM C157‡* |
| Scaling | Visual rating not greater than 2 at 50 cycles | *ASTM C672#* |

** ASTM C31, Standard Practice for Making and Curing Concrete Test Specimens in the Field*
*‖ ASTM C1202, Standard Test Method for Electrical Indication of Concrete's Ability to Resist Chloride Ion Penetration*
*† ASTM C666, Standard Test Method for Resistance of Concrete to Rapid Freezing and Thawing*
*‡ ASTM C157, Standard Test Method for Length Change of Hardened Hydraulic-Cement Mortar and Concrete*
*# ASTM 672, Standard Test Method for Scaling Resistance of Concrete Surfaces Exposed to Deicing Chemicals*

**Figure 2.2.2. MnDOT properties for hardened concrete used in bridge decks (Table 2401.2-5)**

Section 2401.3G.6 contains specifications relating to allowable curing methods and protection for concrete bridge decks. Section G.6.a states that, three hours prior to concrete placement, the engineer and contractor must review the National Weather Service forecast to ensure that there is no precipitation predicted two hours prior to, during, and two hours after placement, there is less than a 30 percent chance of precipitation for the entire placement window, and the combined air temperature, relative humidity, concrete temperature, and wind velocity creates an evaporation rate of less than 0.2 pounds per square foot of surface area per hour. Rapid surface evaporation can accelerate drying

shrinkage, which may increase the risk of early-age cracking. Figure 2.2.3 provides a chart that may be used to estimate the rate of evaporation.

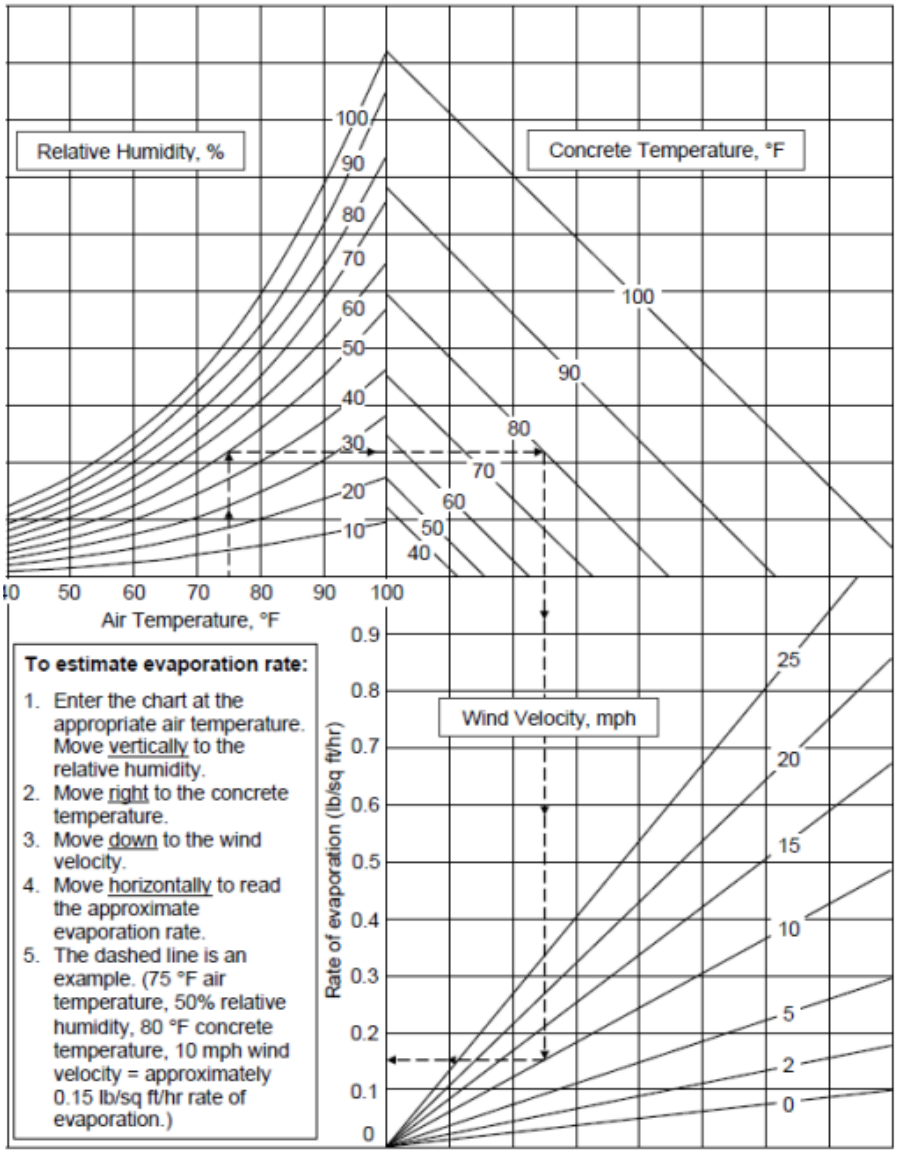


**Figure 2.2.3. Estimating rate of evaporation based on air temp, concrete temp, and wind velocity (2401.3-1)**

Section 2401.3G.6.b provides specifications for concrete bridge deck curing methods. Bridge slabs require a minimum 7-day curing period (Table 2401.3-2). Allowable curing methods for concrete bridge decks include conventional wet curing after carpet drag, conventional wet curing after tined texturing, Poly-Alpha Methyl Styrene (AMS) curing compound after wet cure, and conventional wet curing after applying transverse broom finish AMS curing compound after wet cure period. Figure 2.2.4 shows required curing methods for concrete bridge decks based on the deck type and surface type. When using wet curing, pre-wetted burlap must be applied to cover 100 percent of the deck area within 30

minutes of the final strike-off of the surface, and the slab surface must be kept continuously wet for at least seven calendar days.

**Required Curing Method Based on Final Bridge Deck Surface**

| Bridge Deck Type | Final Bridge Deck Surface | Required Curing Method ‖ |
|---|---|---|
| Bridge Structural Slab curing (3YHPC-S) (3YLCHPC-S) (3Y42-S) | Low Slump Wearing Course | Conventional wet curing after carpet drag |
| Bridge Deck Slab curing (3YHPC-M) (3YLCHPC-M) (3Y42-M) | Epoxy Chip Seal Wearing Course or Premixed Polymer Wearing Course | Conventional wet curing after carpet drag |
| | Bridge Deck Planing | Conventional wet curing after carpet drag |
| | Tined Texturing* | Conventional wet curing after tine texturing. AMS curing compound after wet cure period |
| | Finished Sidewalk or Trail Portion of Deck (without separate pour above)* | Conventional wet curing after applying transverse broom finish AMS curing compound after wet cure period |
| * Prevent marring of broomed finish or tined textured surface by careful placement of wet curing. ‖ Apply conventional wet curing to Bridge Slab following the concrete finishing. | | |

**Figure 2.2.4. Required methods for curing based on bridge deck surface (2401.3-4)**

Section 2401.3G.6.c(1) provides specifications for cold weather protection for concrete bridge slabs. If temperatures below 36°F are expected, concrete may only be poured within heated housing over the pour area while a pour temperature of at least 60°F is maintained. If a temperature of greater than 36°F is expected during placement but below 34°F during curing, concrete must be poured after all required insulation or housing and heating has been placed in order to protect concrete from freezing.

Section 2401.3G.6.d provides specifications for concrete bridge deck drying periods. It is mentioned that slabs cast after October 14 and are open to traffic before April 15 of the following year must have a drying period of 21 days after removing the curing material or until after April 15, whichever comes first. Heat and housing must be provided to maintain a concrete temperature of at least 40°F, and air circulation must be ensured to dry the concrete.

*MnDOT Service Life Design Guide for Bridges* section 3.3.2 states that most of the rebar used on MnDOT bridge projects is epoxy coated rebar. To reach enhanced or maximum service life, the guide recommends that decks should be reinforced with alternative rebar materials such as epoxy-coated 4% chromium, GFRP, or stainless-steel bars, and should have a 14-day wet cure duration rather than the standard specified 7-day cure.

The *MnDOT LRFD Bridge Design Manual* provides tables with epoxy coated reinforcement spacing requirements, shown in figures 2.2.5 and 2.2.6 for decks supported on prestressed concrete or steel girders, respectively. Spacing of transverse reinforcement (both top and bottom mat) and longitudinal

reinforcement (bottom mat only) varies depending on the bridge deck supports, beam spacing, and deck thickness. However, longitudinal top mat reinforcement is always specified as #4 bars at 18-in. spacing; these bars are the most likely to control transverse cracking due to early-age shrinkage or temperature effects. As noted above, these satisfy the AASHTO LRFD requirements for shrinkage and temperature reinforcement, but many state practices and other researchers recommend more tightly spaced top longitudinal reinforcement.

| Maximum Beam Spacing① | Transverse Reinforcement Size and Spacing | | | | Deck Thickness T② | Longitudinal Reinforcement Size and Spacing, Bottom Mat③ | Longitudinal Reinforcement Size and Spacing, Top Mat③ |
|---|---|---|---|---|---|---|---|
| | Bottom Mat | | Top Mat | | | | |
| | With Wearing Course | Without Wearing Course | Deck on I-Beam | Deck on Rectangular Beam | | | |
| 5'-0" | 4 @ 6.5" | 4 @ 9" | 4 @ 10" | 4 @ 9.5" | 9" | 4 @ 9" | 4 @ 1'-6" |
| 5'-6" | 4 @ 6.5" | 4 @ 8.5" | 4 @ 9" | 4 @ 8.5" | 9" | 4 @ 9" | 4 @ 1'-6" |
| 6'-0" | 4 @ 6.5" | 4 @ 8" | 4 @ 8.5" | 4 @ 8" | 9" | 4 @ 9" | 4 @ 1'-6" |
| 6'-6" | 4 @ 6" | 4 @ 8" | 4 @ 8" | 4 @ 7.5" | 9" | 4 @ 9" | 4 @ 1'-6" |
| 7'-0" | 4 @ 5.5" | 4 @ 7.5" | 4 @ 7.5" | 4 @ 7" | 9" | 4 @ 8" | 4 @ 1'-6" |
| 7'-6" | 4 @ 5.5" | 4 @ 7" | 4 @ 7" | 4 @ 6.5" | 9" | 4 @ 8" | 4 @ 1'-6" |
| 8'-0" | 4 @ 5" | 4 @ 6.5" | 4 @ 6.5" | 4 @ 6.5" | 9" | 4 @ 7" | 4 @ 1'-6" |
| 8'-6" | 5 @ 7.5" | 4 @ 6" | 4 @ 6.5" | 4 @ 6" | 9" | 4 @ 7" | 4 @ 1'-6" |
| 9'-0" | 5 @ 7" | 4 @ 6" | 4 @ 6" | 4 @ 6" | 9" | 5 @ 10" | 4 @ 1'-6" |
| 9'-6" | 5 @ 6.5" | 4 @ 5.5" | 4 @ 6" | 4 @ 5.5" | 9" | 5 @ 9" | 4 @ 1'-6" |
| 10'-0" | 5 @ 6" | 4 @ 5.5" | 4 @ 5.5" | 4 @ 5" | 9" | 5 @ 8" | 4 @ 1'-6" |
| 10'-6" | 5 @ 6" | 4 @ 5" | 4 @ 5" | 5 @ 6.5" | 9" | 5 @ 8" | 4 @ 1'-6" |
| 11'-0" | 5 @ 5.5" | 5 @ 7.5" | 5 @ 6" | 5 @ 6" | 9" | 5 @ 8" | 4 @ 1'-6" |
| 11'-6" | 5 @ 5.5" | 5 @ 7" | 5 @ 5.5" | 5 @ 5.5" | 9" | 5 @ 8" | 4 @ 1'-6" |
| 12'-0" | 5 @ 5" | 5 @ 6.5" | 5 @ 5.5" | 5 @ 5.5" | 9" | 5 @ 7" | 4 @ 1'-6" |
| 12'-6" | 6 @ 7" | 5 @ 6.5" | 5 @ 5" | 5 @ 5" | 9" | 5 @ 7" | 4 @ 1'-6" |
| 13'-0" | 6 @ 7" | 5 @ 6.5" | 5 @ 5" | 5 @ 5" | 9.5" | 5 @ 7" | 4 @ 1'-6" |
| 13'-6" | 6 @ 7.5" | 5 @ 6.5" | 5 @ 5" | 5 @ 5" | 9.75" | 5 @ 8" | 4 @ 1'-6" |
| 14'-0" | 6 @ 7" | 5 @ 6.5" | 5 @ 5" | 6 @ 6" | 10" | 5 @ 8" | 4 @ 1'-6" |
| 14'-6" | 6 @ 7.5" | 5 @ 6.5" | 5 @ 5" | 6 @ 6" | 10.25" | 5 @ 8" | 4 @ 1'-6" |
| 15'-0" | 6 @ 7.5" | 5 @ 6.5" | 5 @ 5" | 6 @ 6" | 10.5" | 5 @ 8" | 4 @ 1'-6" |

① For skews ≤ 20°, beam spacing is measured along the skew.
For skews > 20°, beam spacing is measured normal to roadway centerline.

② Deck thickness includes wearing course.

③ Reinforcement shown is for deck regions in non-pier areas only and is based on LRFD 5.10.6. Note that additional reinforcement is required for deck regions over/near piers. See Figure 9.2.1.8 for additional top longitudinal reinforcement required in deck regions over/near piers when only deck is continuous. For beams made continuous, design longitudinal reinforcement in deck regions over/near piers for factored negative moment.

**Figure 2.2.5. Rebar spacing for decks supported on pretensioned concrete beams (Table 9.2.1.1)**

| Maximum Beam Spacing① | Transverse Reinforcement Size and Spacing | | | Deck Thickness T ② | Longitudinal Reinforcement Size and Spacing, Bottom Mat ③ | Longitudinal Reinforcement Size and Spacing, Top Mat ③ |
|---|---|---|---|---|---|---|
| | Bottom Mat | | Top Mat | | | |
| | With Wearing Course | Without Wearing Course | | | | |
| 5'-0" | 4 @ 6.5" | 4 @ 9" | 4 @ 8" | 9" | 4 @ 9" | 4 @ 1'-6" |
| 5'-6" | 4 @ 6.5" | 4 @ 8.5" | 4 @ 7" | 9" | 4 @ 9" | 4 @ 1'-6" |
| 6'-0" | 4 @ 6.5" | 4 @ 8" | 4 @ 6.5" | 9" | 4 @ 9" | 4 @ 1'-6" |
| 6'-6" | 4 @ 6" | 4 @ 8" | 4 @ 6" | 9" | 4 @ 9" | 4 @ 1'-6" |
| 7'-0" | 4 @ 5.5" | 4 @ 7.5" | 4 @ 5.5" | 9" | 4 @ 8" | 4 @ 1'-6" |
| 7'-6" | 4 @ 5.5" | 4 @ 7" | 4 @ 5.5" | 9" | 4 @ 8" | 4 @ 1'-6" |
| 8'-0" | 4 @ 5" | 4 @ 6.5" | 4 @ 5" | 9" | 4 @ 7" | 4 @ 1'-6" |
| 8'-6" | 5 @ 7.5" | 4 @ 6" | 5 @ 6.5" | 9" | 4 @ 7" | 4 @ 1'-6" |
| 9'-0" | 5 @ 7" | 4 @ 6" | 5 @ 6.5" | 9" | 4 @ 6" | 4 @ 1'-6" |
| 9'-6" | 5 @ 6.5" | 4 @ 5.5" | 5 @ 6" | 9" | 4 @ 6" | 4 @ 1'-6" |
| 10'-0" | 5 @ 6" | 4 @ 5.5" | 5 @ 6" | 9" | 4 @ 5" | 4 @ 1'-6" |
| 10'-6" | 5 @ 6" | 4 @ 5" | 5 @ 5.5" | 9" | 4 @ 5" | 4 @ 1'-6" |
| 11'-0" | 5 @ 6" | 4 @ 5" | 5 @ 5.5" | 9.25" | 4 @ 5" | 4 @ 1'-6" |
| 11'-6" | 5 @ 6" | 4 @ 5" | 5 @ 5" | 9.5" | 4 @ 5" | 4 @ 1'-6" |
| 12'-0" | 5 @ 6" | 5 @ 7.5" | 5 @ 5" | 9.75" | 4 @ 6" | 4 @ 1'-6" |
| 12'-6" | 5 @ 6" | 5 @ 7.5" | 5 @ 5" | 10" | 4 @ 6" | 4 @ 1'-6" |
| 13'-0" | 5 @ 6" | 5 @ 7.5" | 6 @ 6.5" | 10.25" | 4 @ 6" | 4 @ 1'-6" |
| 13'-6" | 5 @ 6" | 5 @ 7" | 6 @ 6.5" | 10.5" | 4 @ 6" | 4 @ 1'-6" |
| 14'-0" | 5 @ 6" | 5 @ 7" | 6 @ 6.5" | 10.75" | 4 @ 6" | 4 @ 1'-6" |
| 14'-6" | 5 @ 5.5" | 5 @ 7" | 6 @ 6.5" | 11" | 4 @ 6" | 4 @ 1'-6" |
| 15'-0" | 5 @ 5.5" | 5 @ 7" | 6 @ 6.5" | 11.25" | 4 @ 6" | 4 @ 1'-6" |

① For skews ≤ 20°, beam spacing is measured along the skew.
For skews > 20°, beam spacing is measured normal to roadway centerline.

② Deck thickness includes wearing course.

③ Reinforcement shown is for positive moment region only and is based on LRFD 5.10.6. Where deck and steel beams are continuous, design longitudinal reinforcement in negative moment regions for the factored negative moment and meet requirements of LRFD Article 6.10.1.7. See Figure 9.2.1.9 for longitudinal reinforcing requirements in negative moment regions.

**Figure 2.2.6. Rebar spacing for decks supported on steel beams (Table 9.2.1.2)**

## 2.3 Ideas for Testing

In consideration of the presented literature and in consultation with the TAP, the research team investigated multiple strategies to mitigate early-age transverse cracking. These strategies included introducing SRAs to the currently accepted HPC mix design, adjusting fiber content in the currently accepted HPC mix design, investigating curing and placement practices, and adjusting reinforcement ratios of the top longitudinal deck reinforcement.

The research plan is founded upon the following hypotheses. Due to concrete shrinkage being a potential factor leading to early age cracking, the use of SRAs may reduce shrinkage enough to effectively reduce or eliminate early age cracking. Similarly, increasing the fiber content in the concrete mix may also effectively reduce or eliminate early age cracking due to the added benefits in controlling plastic shrinkage. Increasing curing duration may both increase the strength of concrete and reduce the shrinkage strain, thus reducing cracking potential. Limiting temperature differences between the placed deck concrete and the supporting girders may minimize the amount of restraint stresses developed as the deck concrete hardens. As previously discussed, MnDOT specified spacing requirements for top longitudinal deck reinforcement are significantly larger than many other state DOT requirements. Reducing the spacing of the top longitudinal reinforcement may reduce crack widths but may also increase the restraint on the deck and thus increase tensile stresses; the balance between these two competing factors may determine the efficacy of increasing the amount of steel in the deck.

# Chapter 3: Methods

## 3.1 Scope and Goals of Testing

This research investigated the effectiveness of different techniques that can be implemented to combat early-age cracking in concrete bridge decks. The research was split into two main phases: material testing and computational modeling. Material testing involved measurement of fresh and hardened properties of control high-performance concrete (HPC) mixes, HPC mixes with added SRA, and HPC mixes with adjusted fiber content. A total of four mixes were performed using shrinkage reducing admixtures provided by Master Builders. The first three mixes were performed using MasterLife SRA (Shrinkage Reducing Admixture) 035 admixture, with the fourth mix being performed using MasterLife CRA (Crack Reducing Admixture) 007 admixture. Two mixes were performed following the MnDOT HPC mix design described in Tables 3.2.1 and 3.2.2, but with adjusted fiber contents. The first mix was performed using a lower fiber content of 2 pounds per cubic yard, as opposed to a fiber content of 4 pounds per cubic yard used in the control mixes, while the second mix was performed using a higher fiber content of 6 pounds per cubic yard. When adding SRA or adjusting fiber content, four main properties were tested for the hardened concrete: compressive strength, modulus of rupture, unrestrained shrinkage strain, and force developed under restrained shrinkage. To test the effects of different curing times, multiple compression test cylinders and unrestrained shrinkage prisms were cast and cured for different lengths of time. Computational modeling using ANSYS, a finite element analysis software, was also performed to investigate different reinforcement ratios and replicate different thermal changes that a bridge deck may experience.

## 3.2 Laboratory Testing

### 3.2.1 Mix Criteria and Quantities

High-performance concrete (HPC) mix designs must meet certain design criteria to be approved for use by MnDOT. Criteria followed for this investigation include a water to cement ratio (w/c) of 0.42-0.45, fly ash (SCM) of 25%, and an aggregate content of 45% fine aggregate and 55% coarse aggregate with gradations as shown in Table 3.2.1. Mixes must also meet certain fresh and hardened concrete properties including a slump of two to five inches, air content of 6.5% plus or minus 0.5%, and a 28-day compressive strength of 4000 pounds per square inch. Currently approved MnDOT bridge deck mix materials of interest include type 1L cement, fly ash, coarse aggregate, fine aggregate, synthetic fibers, air entrainment admixture, and superplasticizer. Material quantities were determined using the job mix formula provided by MnDOT as shown in Table 3.2.2.

Laboratory testing involved a total of 12 batches of concrete, including six control mixes that followed the provided job mix formula, four mixes incorporating a shrinkage reducing admixture or crack reducing admixture (CRA), and two mixes with an adjusted fiber content. The specific quantities for each mix are provided in Chapter 4.

**Table 3.2.1. Aggregate gradation provided in MnDOT job mix formula**

| Sieve Size | Fine Aggregate (% Passing) | Coarse Aggregate (% Passing) | Total % Passing | Working Range Limits |
|---|---|---|---|---|
| **2”** | 100.0 | 100.0 | 100 | ±5 |
| **1 ½”** | 100.0 | 100.0 | 100 | ±5 |
| **1”** | 100.0 | 100.0 | 100 | ±5 |
| **¾”** | 100.0 | 100.0 | 100 | ±5 |
| **½”** | 100.0 | 65.0 | 81 | ±5 |
| **3/8”** | 100.0 | 31.0 | 62 | ±5 |
| **#4** | 100.0 | 4.0 | 47 | ±5 |
| **#8** | 91.0 | 0.0 | 41 | ±4 |
| **#16** | 72.0 | 0.0 | 32 | ±4 |
| **#30** | 47.0 | 0.0 | 21 | ±4 |
| **#50** | 17.0 | 0.0 | 8 | ±3 |
| **#100** | 1.0 | 0.0 | 0 | ±2 |
| **#200** | 0.2 | 0.0 | 0 | ≤1.6 |

**Table 3.2.2. Mix designs used for determining material quantities from MnDOT job mix formula**

| Material | Quantity (lb/yd$^3$) | Source |
|---|---|---|
| **Type-1L Cement** | 446 | Holcim, Alpena, MI |
| **Class-F Fly Ash** | 149 | Coal Creek |
| **Fine Aggregate** | 1338 | Unspecified |
| **#67 Coarse Aggregate** | 1678 | Martin Marietta Quarry, St. Cloud, MN |
| **FORTA-FERRO Synthetic Fibers** | 4.0 | Forta Corporation |
| **Water** | 250 | -- |

## 3.2.2 Mix Procedure

Unless otherwise noted, all concrete mixes were performed following the same procedure to maintain consistent control variables. To begin, coarse and fine aggregates were laid out to air dry for a minimum of 3 days. After the coarse aggregate dried, it was sieved and separated into 1/4-inch, 3/8-inch, and 1/4-inch piles in accordance with ASTM C192. On the day of each mix, moisture content was determined for coarse and fine aggregate in accordance with ASTM D2216. Next, all materials were weighed according to the batch size. A 1.0 cubic foot butter batch, scaled according to each given mix, was then mixed to coat the inside of the drum. After the butter batch was completed, the full-scale test batch was then mixed in accordance with ASTM C192. After the concrete had been thoroughly mixed, fresh concrete tests were performed. Slump was checked first in accordance with ASTM C143, and then air content was

determined in accordance with ASTM C231. After the fresh concrete tests satisfied the necessary criteria, unrestrained shrinkage prism molds, restrained shrinkage prism molds, cylinder molds, and a modulus of rupture mold were filled using the remaining concrete. Prior to casting the full test batches, several initial trial mixes were conducted to practice the mixing and testing protocols, helping ensure the full tested batches were consistent. The results of these trial batches are not presented herein.

### 3.2.3 Fresh Concrete Tests

Fresh concrete tests were performed to determine slump and air content of each mix. Per the job mix formula provided by MnDOT, the acceptable slump range was 2.0 to 5.0 inches, and the acceptable air content range is 6% to 7%. If the slump was below the two-inch minimum, more superplasticizer was added to increase workability until the slump was adequate. In all tested batches, the measured slump was never greater than the five-inch maximum. After the slump was within the required range, air content was tested using a Type-B meter to determine if it was within the acceptable range. If air content was too low, more air entrainment admixture (AEA) was added. Due to the inability to reduce air content in the wet concrete, in cases where the air content was too high, the resulting air content was simply noted and then specimens were cast. Otherwise, if the air content was in the target range, the resulting concrete was cast into molds for hardened concrete testing. When adding additional AEA or superplasticizer, the admixture was mixed with 5 milliliters of water and dispersed directly onto the wet concrete in the mixer. The concrete was then mixed again for 3 minutes, followed by a 3-minute rest, and ending with an additional 2-minute mix. Cylinder molds were capped with plastic caps, while the remaining molds were covered with wet burlap for the remainder of their curing durations.

### 3.2.4 Hardened Concrete Tests

Material properties of interest include compressive strength, unrestrained shrinkage strain, restrained shrinkage forces, and modulus of rupture. Unrestrained shrinkage prisms, restrained shrinkage prisms, and modulus of rupture beams were all cured in their forms for 24 hours, with wet burlap covering the exposed face of the specimens. Empty forms for each test are shown in Figure 3.2.1.

Compression tests were performed in accordance with ASTM C39. During each mix, twelve 4-in. x 8-in. cylinders were cast in order to observe compressive strength. Cylinders were tested at 3, 7, 14, and 28 days with three cylinders being tested at each interval. Cylinders were sealed and cured in their molds for the entirety of the curing period, being removed from the mold immediately before testing.


**Figure 3.2.1. Empty forms for each hardened concrete test to be performed**

Unrestrained shrinkage was tested in accordance with ASTM C157. Eleven 3-in. x 3-in. x 11.25-in. prisms were cast during each mix to observe unrestrained shrinkage. These prisms were cured under wet burlap for 24 hours after being cast, and then taken out of the forms, weighed, and measured using a length comparator. Three of the prisms were then left out as the 24-hour cure specimens, while the remaining prisms were placed in a saturated lime water bath for the remainder of their cure periods. Two prisms were removed each at 7, 14, 21, and 28 days after casting. After being taken out of the bath, the prisms were dried with a rag and then were immediately measured for length and weight. Prisms remained exposed in the laboratory environment after that, being placed on metal grates to ensure air exposure on all sides. Prisms were weighed and measured every one to four days for the first 28 days after being taken out of the bath, and every seven to ten days thereafter. Testing of unrestrained shrinkage prisms concluded 90 days after the casting date.

Three 3-in. x 3-in. x 15.75-in. restrained shrinkage prisms were also cast for each mix and placed in three different restrained shrinkage testing apparatuses. Each restrained shrinkage apparatus was made up of 3.0-inch wide by 0.75-inch-thick steel plates connected using 0.25-inch diameter shoulder bolts. Each apparatus also has a threaded rod through the top plate and bottom plate. The threaded rod on the bottom is cast into the concrete with a nut placed with two inches of clear space between its inside face and the bottom of the prism. Another nut is then placed on the bottom of the threaded rod on the

exterior face of the apparatus, restraining the bottom end of the prism, as shown in Figure 3.2.2. The threaded rod on the top end is also cast into the concrete with a nut placed with two inches of clear space between its inside face and the top of the prism. This threaded rod passes through a load cell on top of the apparatus, where another nut is placed on top of the load cell. As the specimen shrinks the load is transferred to the load cell which reads the force, in pounds, caused by the shrinkage. One-inch, 0.75-inch, and 0.5-inch diameter threaded rods were used to test different levels of restraint, with larger rods providing more restraint and therefore expected to develop more tensile stress in the concrete. Figure 3.2.3 shows all three restrained shrinkage tests being performed.

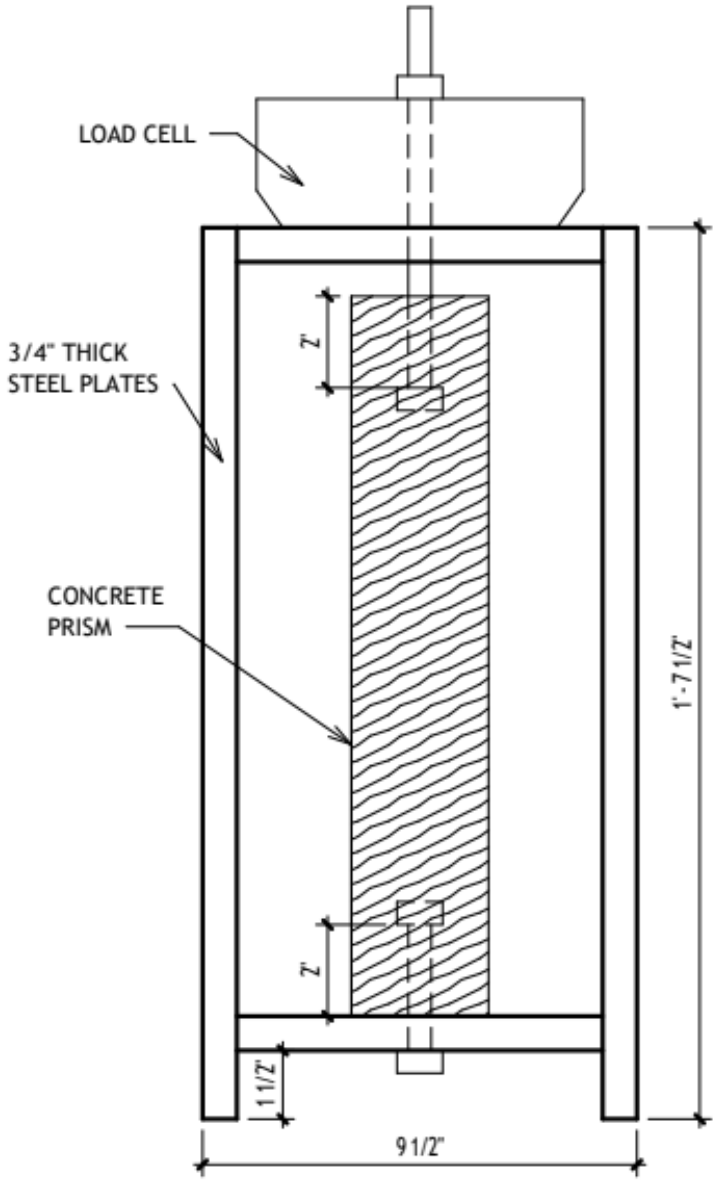


**Figure 3.2.2. Restrained shrinkage test setup**

**Figure 3.2.3. Restrained shrinkage tests in operation**

Flexure tests were performed in accordance with ASTM C78. Except for one of the control mixes, one 6-in. x 6-in. x 21-in. modulus of rupture beam was cast during each mix. The beam was demolded after 24 hours of curing in the form and placed in a cure chamber for the remainder of its curing period of 28 days. The cure chamber was maintained at a temperature of 23°C (73.4°F) and 95% relative humidity. Six modulus of rupture beams were cast for one control mix with variable curing durations. The procedure was identical to that described above, but two beams were cured for 7 days, two for 14 days, and the remaining two for 28 days. All modulus of rupture tests were performed at 28 days or later.

## 3.3 Finite Element Analysis

Finite element modeling was performed to determine stress distribution due to thermal variations, shrinkage, and creep in a model representative of a typical bridge section. Modeling was completed in two phases: initial modeling and parametric modeling. Initial modeling consisted of basic geometric

modeling along with general shrinkage loading and thermal loading scenarios. Results from the initial modeling informed the scope of parametric modeling. Parametric modeling included the addition of more structural detail, multiple scenarios for deck reinforcement placement, and more advanced loading scenarios in order to achieve a more accurate representation of field conditions.

### 3.3.1 Initial Computational Modeling

Geometric modeling was performed using SolidWorks and imported into Ansys Workbench for analysis. Bridge geometry consists of a 9.0-inch-thick bridge deck resting on six MN45 girders as shown in Figure 3.3.1 and Figure 3.3.2.

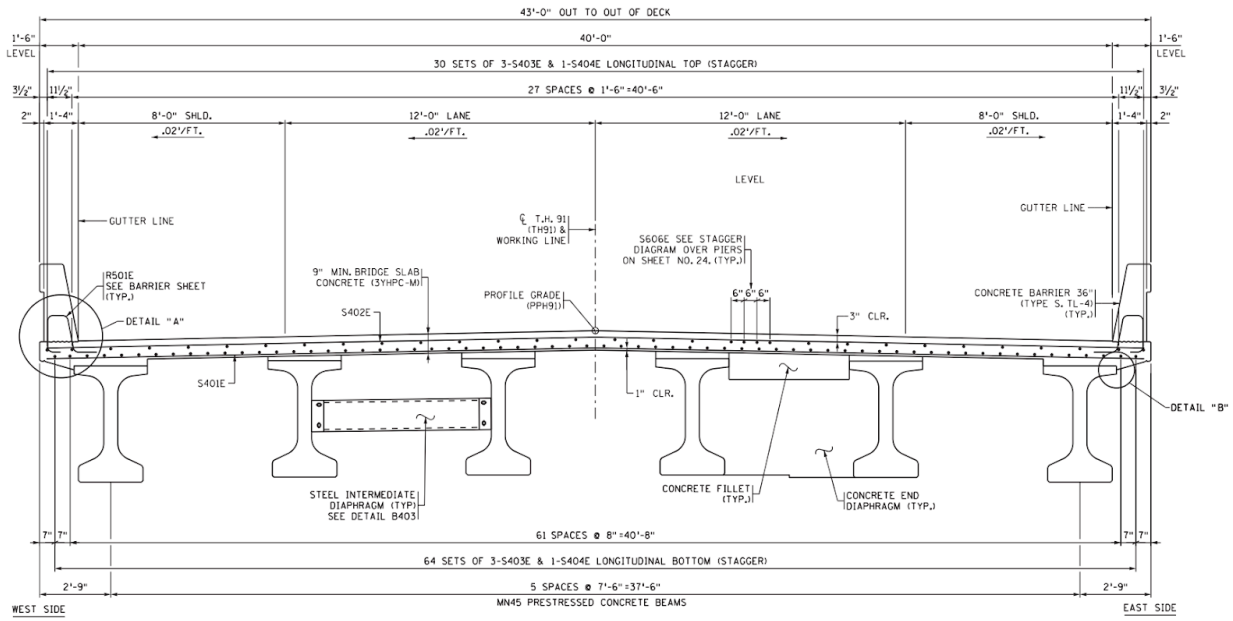


**Figure 3.3.1. Bridge section showing typical geometry and reinforcement details**

The modeled bridge was 43-feet wide with a span of 100 feet. The crown of the bridge deck was ignored in the model due to the added difficulty in geometric modeling but negligible effect it would have on the analysis. Four layers of reinforcement were placed in the deck, modeled using “truss” type elements that carry only axial force. All deck reinforcement consisted of #4 bars (0.5-in. diameter). Top transverse reinforcement was placed 3.25 inches below the top of the deck and spaced at 7 inches on center. Top longitudinal reinforcement was placed 3.75 inches from the top of the deck with the first bar placed 15 inches from the edge of the deck and remaining bars spanning throughout the deck spaced 18 inches on center. Bottom transverse reinforcement was placed 1.25 inches up from the bottom of the slab and spaced 7 inches on center. Bottom longitudinal reinforcement was placed 1.75 inches up from the bottom of the deck with the first bar placed 6 inches from the side of the deck and the remaining bars spanning throughout the deck spaced 8 inches on center. Initial modelling neglected mild steel reinforcement and prestressing in the MN45 girders, the barrier, and the steel intermediate and concrete end diaphragms.

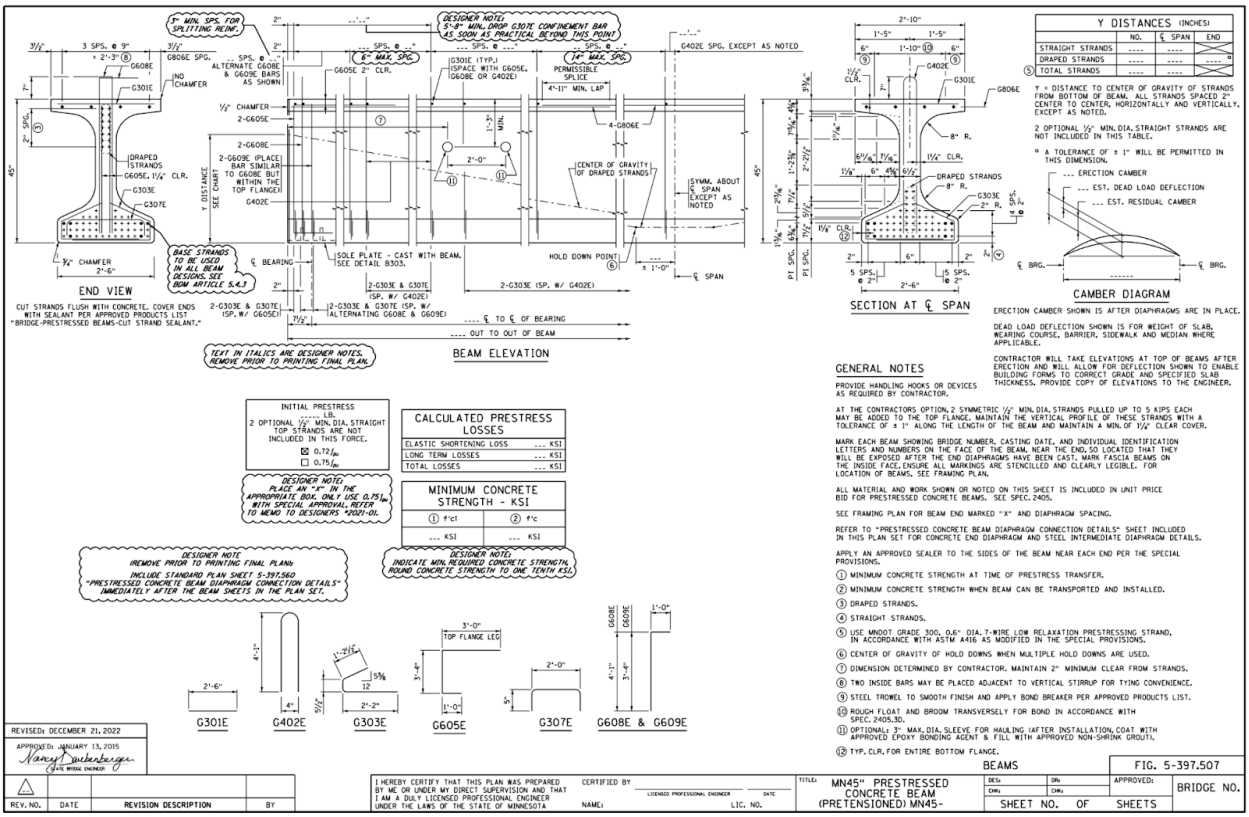


**Figure 3.3.2. MN45 girder details**

Meshing was applied to the concrete deck, steel reinforcement, and the girders. An 18-inch mesh was applied to the reinforcement, while the deck had an 18-inch mesh applied to the horizontal surface (X-Z plane) and a 1.5-inch mesh applied vertically (Y-direction). An 18-inch mesh was also applied to the girders. Boundary conditions included a pinned condition on one end and a roller condition on the other. The meshed model is shown in Figure 3.3.3.

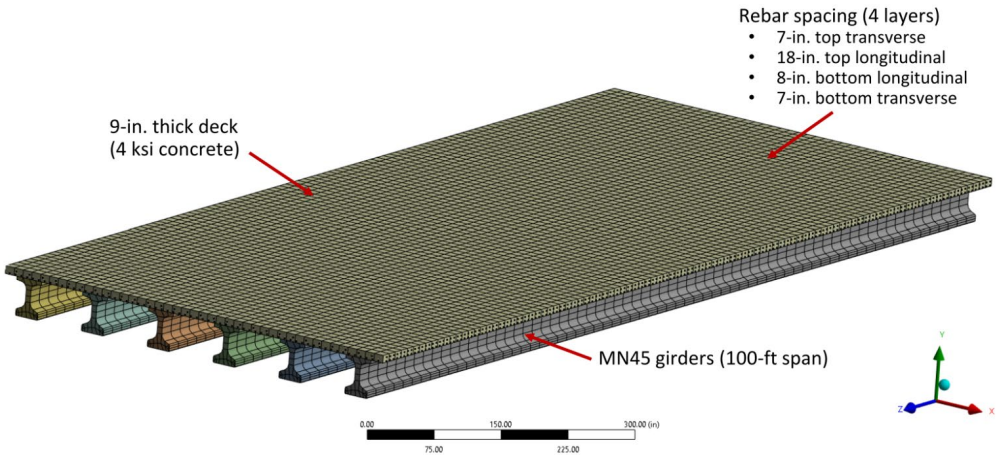


**Figure 3.3.3. Full model bridge deck and girders with meshing applied**

Material properties of interest for concrete and steel in the model include density, coefficient of thermal expansion, Young's modulus, and Poisson's ratio, as described in Table 3.3.1. Shrinkage was applied to this model by changing the concrete temperature by a specific value resulting in an equivalent shrinkage strain. The effects of creep were not examined. Later models will include the CPRH creep and shrinkage model (Hedegaard et al. 2023) to directly consider time-dependent strains.

**Table 3.3.1. Material properties used in ANSYS model**

| Property | Concrete | Steel (Rebar) |
|---|---|---|
| Density ($\mathrm{lb/ft^3}$) | 150 | 490 |
| Coefficient of Thermal Expansion (strain/°F) | $5.56 \times 10^{-6}$ | $6.67 \times 10^{-6}$ |
| Young's Modulus (ksi) | 4000 | 29000 |
| Poisson's Ratio | 0.2 | 0.3 |

The initial model was investigated under the following loading scenarios:

1. Uniform temperature changes
2. Positive thermal gradients
3. Negative thermal gradients
4. Uniform deck shrinkage of 400 microstrain (equal to 0.04% strain)
5. Deck-to-girder uniform temperature difference.

Uniform temperature changes refer to a thermal change applied to all components of the model. Because the bridge is simply supported, the only stresses that develop are due to the different coefficients of thermal expansion for the concrete and steel.

Thermal gradients refer to a temperature difference through the depth of the section. A positive thermal gradient occurs when the top surface is warmer than the rest of the structure, and a negative thermal gradient occurs when the top surface is cooler than the rest of the structure. Thermal gradients create nonuniform thermal strains and thus can induce stresses through the depth of the cross section due to strain compatibility. Positive thermal gradients put the deck into compression while negative thermal gradients put the deck into tension.

The AASHTO LRFD (2020) design positive thermal gradient is shown in Figure 3.3.4. The negative gradient is equivalent to the positive gradient but multiplied by a factor of –0.3 for plain concrete decks. This design gradient is contrasted with the Priestley (1978) fifth-order curve and linear gradients. Previous investigations of box girder bridges in Minnesota (Hedegaard et al. 2013) showed that the measured thermal gradients more closely match the Priestley gradient, and that this gradient furthermore causes greater stresses in bridges than the AASHTO LRFD design gradient. However, the magnitude of the AASHTO LRFD design thermal gradients, defined as the difference between the top surface temperature and the lower superstructure temperature, closely matches field observations in

Minnesota. Therefore, the applied thermal gradients in this study take the shape of the Priestley (1978) gradients but use AASHTO LRFD magnitudes of +46°F for the positive gradient and –14°F for the negative gradient.

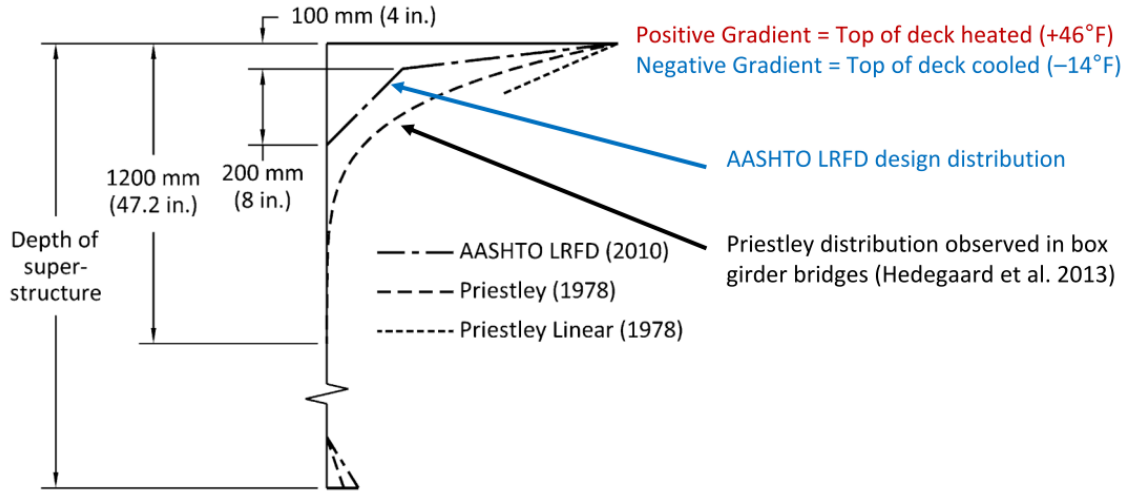


**Figure 3.3.4. Design thermal gradients applied to concrete bridges**

Shrinkage of the deck was applied by changing the temperature of the deck concrete (and only the concrete, as the reinforcing steel does not shrink). A temperature change of –72°F was applied, as this would result in a thermal contraction of 400 microstrain in the concrete if it were unrestrained, thus matching the MnDOT-specified shrinkage strain limit for HPC mixes described in Figure 2.2.2. When restrained by the reinforcement and the girders, this strain results in tensile stresses in the deck.

Deck-to-girder uniform temperature changes were applied to both the deck concrete and reinforcing steel, modeling a difference in temperature between the deck and the girders. This type of loading corresponds to a warm deck concrete poured onto a cooler girder; as the deck concrete cools to match the girder temperature, it contracts and places the deck into tension.

## 3.3.2 Parametric Computational Modeling

To further explore how deck reinforcing details may contribute to or control transverse deck cracking, more detailed computational models were developed. Refinements to the model included the addition of girder reinforcement and elastomeric bearing pads as shown in Figures 3.3.5 and 3.3.6, and explicitly modeling time-dependent aging, creep, and shrinkage in accordance with the CPRH model (Hedegaard et al. 2023). Otherwise, details for the geometry and mesh were similar to that for the initial model described above.

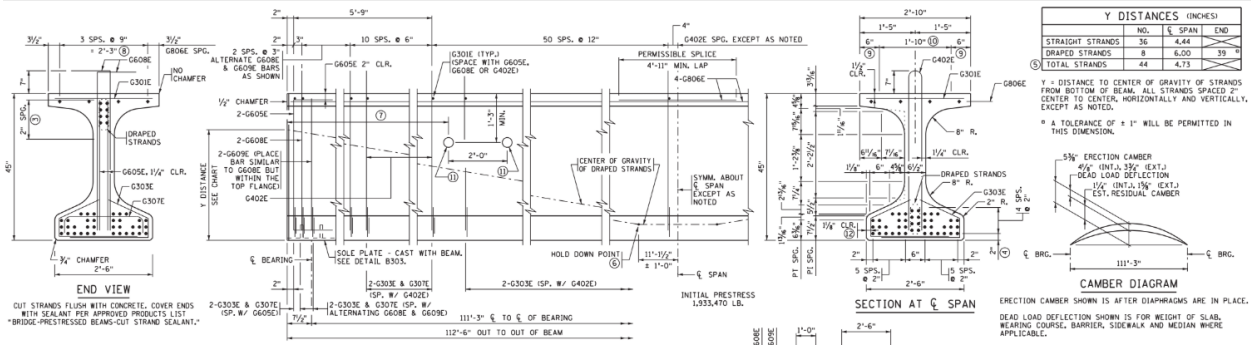


**Figure 3.3.5. MN45 girder reinforcement details**

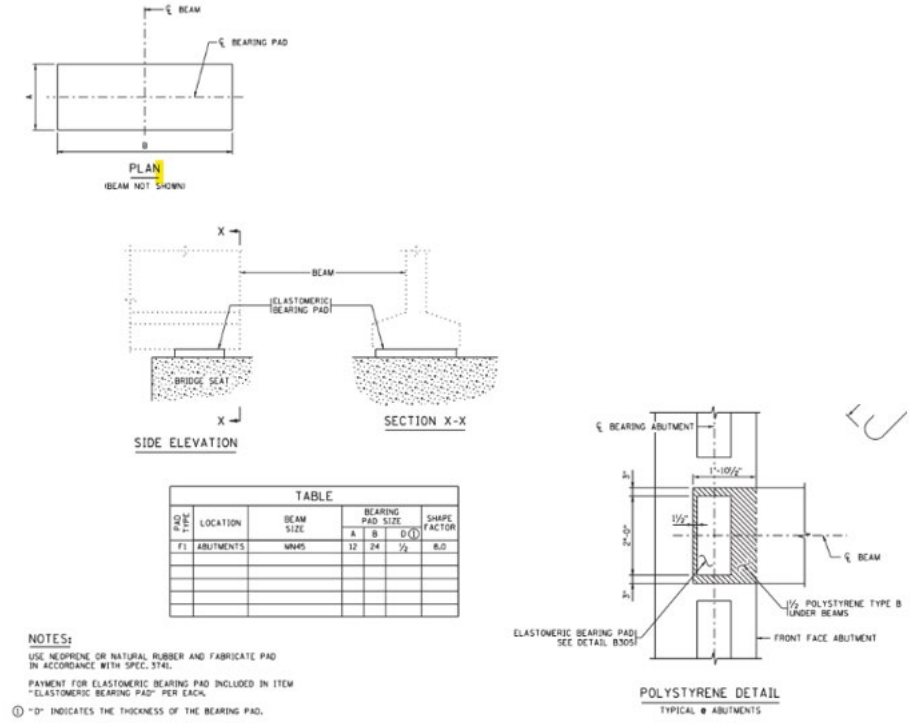


**Figure 3.3.6. Elastomeric bearing pad details**

Additional material properties were necessary to predict the shrinkage and creep behavior of the concrete, as shown in Table 3.3.2. Three different concrete materials were applied to the bridge deck to more accurately represent shrinkage throughout the deck. The exposed top surface of the deck is expected to shrink faster than the concrete below the surface, which can be controlled by the volume-to-surface ratio in the CPRH model. A 1.5-inch concrete mesh was applied through the depth of the deck to split it into six layers, with the top layer (Concrete Deck Top) having a volume to surface ratio of 1.5 inches, the second layer (Concrete Deck Middle) having a volume to surface ratio of 3 inches, and the bottom four layers (Concrete Deck Lower) having a volume to surface ratio of 4.5 inches. The CPRH model also includes aging of the elastic modulus of the concrete that depends on the cement type classification and the mean 28-day concrete strength (assumed to be approximately 1160 psi higher than the 28-day design strength). The curing duration changes the onset of drying in the model, material

properties remain consistent in all of the new models. The age at analysis start is used to capture the difference in concrete ages between the deck and the girders; the girders were assumed to be 93 days old (i.e., 3 months old) when the deck was poured.

**Table 3.3.2. Material properties for parametric modeling**

| Property | Concrete Deck Lower | Concrete Deck Middle | Concrete Deck Top | Concrete Girder | Steel (Rebar/ Strand) | Bearing Pad |
|---|---|---|---|---|---|---|
| Density (lb/ft$^3$) | 150 | 150 | 150 | 150 | 490 | 58 |
| Coefficient of Thermal Expansion (strain/°F) | $5.56x10^{-6}$ | $5.56x10^{-6}$ | $5.56x10^{-6}$ | $5.56x10^{-6}$ | $6.67x10^{-6}$ | $4.4x10^{-5}$ |
| Young's Modulus (ksi) | Per CPRH | Per CPRH | Per CPRH | Per CPRH | 29,000 | 1850 |
| Poisson's Ratio | 0.2 | 0.2 | 0.2 | 0.2 | 0.3 | 0.49 |
| Mean 28-Day Strength (psi) | 5160 | 5160 | 5160 | 8160 | N/A | N/A |
| Aggregate Volume Fraction | 0.666 | 0.666 | 0.666 | 0.666 | N/A | N/A |
| Volume-Surface Ratio (in.) | 4.5 | 3 | 1.5 | 3.74 | N/A | N/A |
| Cement Type | I | I | I | III | N/A | N/A |
| Curing Duration (days) | 7 | 7 | 7 | 1 | N/A | N/A |
| Age at Start of Analysis (days) | 7 | 7 | 7 | 100 | N/A | N/A |

The parametric model was used to investigate four different reinforcement configurations. The first of the four models (**18TLR**) was the typical model bridge used in the initial modeling with top longitudinal reinforcement spaced at 18 inches. This model was also investigated for a two-span continuous system (**2 span 18TLR**) by adding boundary conditions to the deck face on one side of the bridge so that it had no longitudinal displacement or rotation. Adding this condition causes the bridge to act as a multi-span bridge (i.e., a continuous deck cast over simply supported girders) due to the restraint in that direction.

The second model (**flipped 18TLR**) also included the typical model bridge with top longitudinal reinforcement spaced at 18 inches. However, the layering of the transverse and longitudinal reinforcement was as follows from top down: top transverse, top longitudinal, bottom longitudinal, bottom transverse. The reinforcement of the second "flipped" model is as follows: top longitudinal, top transverse, bottom transverse, bottom longitudinal.

The third and fourth models included a change in the spacing of the top longitudinal reinforcement. Rather than being spaced at 18 inches, the reinforcement was spaced at 12 inches (**12TLR**) or 6 inches (**6TLR**). All of the transverse and bottom longitudinal reinforcement remains unchanged.

All parametric models were investigated under the following loading scenarios:

1. Elastic behavior under positive thermal gradients
2. Elastic behavior under negative thermal gradients
3. Elastic behavior under deck-to-girder uniform temperature difference
4. 28-day creep and shrinkage analysis with constant temperature conditions
5. 28-day creep and shrinkage analysis with cycled thermal gradients

The three loading cases for elastic behavior were identical to those from the initial model, but with the model refinements as discussed above. Elastic modulus values for the deck and girder concrete corresponded to those at the age of analysis start, that is, 7 days and 100 days for the deck and girders, respectively. The elastic modulus for the concrete materials for these models followed the aging expression presented in the CPRH creep and shrinkage model (Hedegaard et al. 2023). Thus, the deck concrete, with an expected 28-day strength of 5160 psi, had a 7-day modulus of 3664 ksi, while the girder concrete, with an expected 28-day strength of 8160 psi, had a 100-day modulus of 5302 ksi. For the creep and shrinkage analyses, these represent the initial elastic moduli which then increased throughout the 28-day duration.

The two creep and shrinkage analyses were conducted using the Kelvin Chain rate type method described by Bazant and Xi (1995) and adapted to the CPRH model. Using this method, shrinkage and creep are computed over incremental time steps while considering the full time-history of stresses and strains. Both time-dependent analyses modeled a duration beginning at end of curing for the deck and concluding 28 days later with ambient relative humidity held constant at 70%. According to Figure 5.4.2.3.3-1 of AASHTO LRFD (2020), the average ambient relative humidity throughout the state of Minnesota varies between 70% and 75%. The CPRH model accounts for temperature effects in the rate of creep and shrinkage, such that these strains accelerate under high temperatures and decelerate for lower temperatures.

The creep and shrinkage analysis with constant temperature conditions held the temperature at 68°F throughout the entire analysis and throughout the entire model, as this temperature corresponds to the standard assumed ambient conditions of the CPRH model. Time steps for this analysis were 1 day each. The modeled constant-temperature shrinkage strains experienced by the four concrete materials defined in Table 3.3.2 are shown in Figure 3.3.7. As will be shown in Chapter 4, these strains were less than those measured in lab testing because of the increased volume-to-surface ratio and the increased ambient relative humidity considered in the model. Lab testing was conducted at 50% ambient relative humidity, and lower humidity results in more drying shrinkage. The lab prisms had a volume-to-surface (V/S) ratio of 0.75-in., and thus shrank faster than even the top modeled layer of the deck with V/S = 1.5-in. Because the duration of the shrinkage analysis was only 28 days, the reduced rate of shrinkage appeared similar to an overall reduction in shrinkage strain. Given enough time, concrete with larger V/S

will shrink for longer and thus begin to catch up with the lower V/S concrete which quickly completes shrinking. However, this process takes months or years, and therefore is not relevant for early-age cracking that occurs within the first month. As a final note, using the CPRH model to estimate the lab shrinkage results of the control mix for 28-days of shrinkage following a 28-day cure resulted in a predicted 532 microstrain. As presented in Chapter 4, this overpredicted the measured shrinkage of the control mixes by approximately 30%.

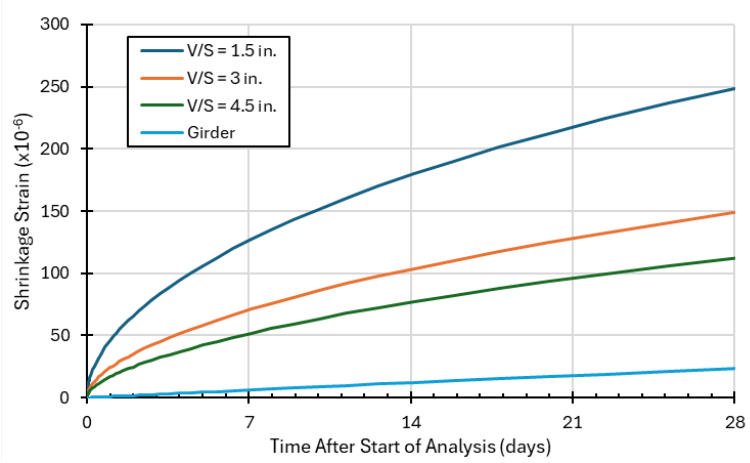


**Figure 3.3.7. Modeled shrinkage strains in parametric models**

For the creep and shrinkage analysis with cycled thermal gradients, thermal gradients were applied and removed during each analysis day. The analysis began at the end of deck curing with a uniform temperature of 68°F, but over the course of each day ramped up to a design positive thermal gradient (top deck temperature = 68°F + 46°F = 114°F), down to a design negative thermal gradient (top deck temperature = 68°F – 14°F = 54°F), and then back to the uniform temperature to begin the next day, all following a daily sinusoidal function. These cycled gradients were repeated for 28 days, using time steps of 0.1 days throughout the analysis. The application of cycled gradients induced a stress history into the deck, which altered the creep response. Furthermore, the top surface of the deck was on average warmer than the rest of the structure because the positive gradient was greater than the negative gradient; this accelerated both creep and shrinkage in the deck. Repeating the design gradients daily reflected an unrealistic weather pattern, as positive design gradients only occur during days of high solar radiation, while negative gradients tend to develop during evenings if rain or wind is present. However, the daily cycles used herein are believed to exacerbate the tension caused by deck shrinkage, so these may be considered as upper bound values of deck tensile stress under unfavorable thermal conditions.

# Chapter 4: Laboratory Testing Results

## 4.1 Laboratory Testing Summary

Laboratory testing involved a total of 12 batches of concrete, including six control mixes, four mixes incorporating a shrinkage reducing admixture or crack reducing admixture (CRA), and two mixes with an adjusted fiber content. Actual material quantities used in each mix are shown in Table 4.1.1. The effective water-to-binder (*w*/*b*) for each mix is tabulated in Table 4.1.2. This represents the weight of the total mix water divided by the combined weight of the cement and fly ash. For the SRA and CRA mixes, two *w*/*b* ratios are given: one using just the mix water for weight *w*, and the other using the weight of the water plus SRA or CRA for weight *w*. This distinction is made because, according to the supplier's data sheets, the SRA dosage is intended to offset an equal amount of mix water.

**Table 4.1.1. Actual material quantities used during laboratory testing**

| Mix | Volume ($ft^3$) | Cement (lb) | Fly Ash (lb) | Fine Agg. (lb) | Coarse Agg. (lb) | Fibers (lb) | Water (lb) | WR (oz.) | AEA (oz.) | SRA /CRA (oz.) |
|---|---|---|---|---|---|---|---|---|---|---|
| **Control Mix 1** | 3.0 | 49.6 | 16.56 | 148.6 | 186.4 | 0.44 | 27.78 | 1.34 | 0.85 | -- |
| **Control Mix 2** | 3.0 | 49.6 | 16.56 | 148.7 | 186.4 | 0.44 | 27.78 | 0.85 | 0.85 | -- |
| **Control Mix 3** | 3.0 | 49.6 | 16.56 | 148.7 | 186.4 | 0.44 | 27.78 | 0.85 | 0.34 | -- |
| **Control Mix 4** | 2.3 | 38.0 | 12.69 | 114.0 | 142.9 | 0.34 | 21.30 | 0.95 | 0.14 | -- |
| **Control Mix 5** | 3.25 | 53.7 | 17.94 | 161.1 | 202.0 | 0.48 | 30.09 | 1.34 | 0.10 | -- |
| **Control Mix 6** | 4.0 | 66.1 | 22.07 | 198.2 | 248.6 | 0.59 | 37.87 | 2.37 | 0.14 | -- |
| **SRA Mix 1** | 3.25 | 53.7 | 17.94 | 161.1 | 202.0 | 0.48 | 31.19 | 2.03 | 0.20 | 15.22 |
| **SRA Mix 2** | 3.25 | 53.7 | 17.94 | 161.1 | 202.0 | 0.48 | 29.10 | 2.20 | 0.17 | 15.22 |
| **SRA Mix 3** | 3.25 | 53.7 | 17.94 | 161.1 | 202.0 | 0.48 | 29.10 | 2.20 | 0.17 | 15.22 |
| **CRA Mix 1** | 3.25 | 53.7 | 17.94 | 161.1 | 202.0 | 0.48 | 28.44 | 1.34 | 0.17 | 23.67 |
| **Fiber Mix 1** | 3.25 | 53.7 | 17.94 | 161.1 | 202.0 | 0.72 | 33.99 | 2.87 | 0.17 | -- |
| **Fiber Mix 2** | 3.25 | 53.7 | 17.94 | 161.1 | 202.0 | 0.24 | 30.09 | 1.72 | 0.10 | -- |

**Table 4.1.2. Effective water-to-binder ratios for laboratory mixes**

| Mix | Mix Water (lb) | Total Binder (lb) | w/b ratio | Water + SRA (lb) | (w+SRA)/b ratio |
|---|---|---|---|---|---|
| **Control Mix 1** | 27.78 | 66.12 | 0.420 | 27.78 | 0.420 |
| **Control Mix 2** | 27.78 | 66.12 | 0.420 | 27.78 | 0.420 |
| **Control Mix 3** | 27.78 | 66.12 | 0.420 | 27.78 | 0.420 |
| **Control Mix 4** | 21.3 | 50.68 | 0.420 | 21.30 | 0.420 |
| **Control Mix 5** | 30.09 | 71.63 | 0.420 | 30.09 | 0.420 |
| **Control Mix 6** | 37.87 | 88.14 | 0.430 | 37.87 | 0.430 |
| **SRA Mix 1** | 31.19 | 71.63 | 0.435 | 32.17 | 0.449 |
| **SRA Mix 2** | 29.1 | 71.63 | 0.406 | 30.08 | 0.420 |
| **SRA Mix 3** | 29.1 | 71.63 | 0.406 | 30.08 | 0.420 |
| **CRA Mix 1** | 28.44 | 71.63 | 0.397 | 29.97 | 0.418 |
| **Fiber Mix 1** | 33.99 | 71.63 | 0.475 | 33.99 | 0.475 |
| **Fiber Mix 2** | 30.09 | 71.63 | 0.420 | 30.09 | 0.420 |

Control mixes 1,2,3, and 5 were performed to capture concrete strength and shrinkage. The first three batches were 3.0 cubic feet in volume with the intention of performing two slump tests and two air entrainment tests, along with filling twelve cylindrical molds for compression tests, eleven rectangular prism molds for unrestrained shrinkage tests, and one rectangular prism mold for a modulus of rupture test. Control Mix 5 was 3.25 cubic feet in volume with the intention of performing all the same tests as stated above with the addition of filling three molds for restrained shrinkage tests. The fourth control mix was performed to investigate 28-day compressive strength of cylinders cured for different periods of time. This batch was 2.3 cubic feet in volume with the intention of performing one slump test, one air entrainment test, and casting 21 cylinders for compressive tests. Control Mix 6 was performed to investigate the effects of different curing times on flexural strength of the control HPC mix. This mix was 4.0 cubic feet in volume with the intention of performing one slump test, one air entrainment test, casting 12 cylinders for compressive tests, and casting six rectangular prism molds for modulus of rupture tests. Due to a delay in load cell manufacturing, restrained shrinkage tests were only performed for Control Mix 5.

A total of four mixes were performed using shrinkage reducing admixtures provided by Master Builders. All of the mixes were 3.25 cubic feet in volume with the intention of performing two slump tests and two air entrainment tests, along with filling twelve cylindrical molds for compression tests, eleven rectangular prism molds for unrestrained shrinkage tests, three rectangular prism molds for restrained shrinkage tests, and one rectangular prism mold for a modulus of rupture test. As noted above, shrinkage reducing admixtures are intended as a substitute for water in the mix, so an equivalent amount of water was left out when the admixtures were added. Master Builders recommends using 0.5 to 1.5 gallons per cubic yard of type SRA admixture, so 15.22 fluid ounces (roughly 1 gallon per cubic yard) was used for these mixes. Master Builders recommends using 1 to 2 gallons per cubic yard of type CRA admixture, so 23.67 ounces (roughly 1.5 gallons per cubic yard) was used for this mix. It should be

noted that although SRA and CRA are a substitute for water, they appeared to have a negative impact on the workability of the concrete and SRA Mix 1 required additional water to reach the target slump.

Two mixes were performed following the MnDOT HPC mix design described in section 3.2.1 but with adjusted fiber contents. Both mixes were 3.25 cubic feet in volume with the intention of performing two slump tests and two air entrainment tests, along with filling twelve cylindrical molds for compression tests, eleven rectangular prism molds for unrestrained shrinkage tests, three rectangular prism molds for restrained shrinkage tests, and one rectangular prism mold for a modulus of rupture test.

Fresh and hardened concrete tests were performed with each batch. Test results for each mix are summarized in Table 4.1.3, excluding restrained shrinkage testing results. Note that values for shrinkage strain are given for the 28-day cure specimens after 28 days of drying shrinkage (i.e., 56 days after casting). Further details on these results are presented in the following sections.

**Table 4.1.3. Summary of fresh and hardened concrete test results**

| Mix | Slump | Air Content | Average 28-day Comp. Strength (psi) | Modulus of Rupture (psi) | Shrinkage Strain |
|---|---|---|---|---|---|
| **Control Mix 1** | 1.75” | 7.8% | 4230 | -- | 420 |
| **Control Mix 2** | 2.125” | 10.0% | 2945 | 613 | 422 |
| **Control Mix 3** | 3.25” | 15.3% | 3164 | 656 | 402 |
| **Control Mix 4** | 3.75” | 11.0% | -- | -- | -- |
| **Control Mix 5** | 3.5” | 8.0% | 5321 | 551 | 378 |
| **Control Mix 6** | 3.5” | 7.9% | 4699 | 411 | -- |
| **SRA Mix 1** | 2.5” | 10.0% | 4113 | -- | -- |
| **SRA Mix 2** | 2.0” | 5.2% | 6689 | 612 | 260 |
| **SRA Mix 3** | 5.0” | 7.4% | 6099 | 607 | 278 |
| **CRA Mix 1** | 2.5” | 6.4% | 6625 | 560 | 225 |
| **Fiber Mix 1** | 2.5” | 8.5% | 5017 | 589 | 375 |
| **Fiber Mix 2** | 2.25” | 6.0% | 5985 | 650 | 360 |

## 4.2 Mixing Log and Fresh Concrete Properties

Control Mix 1, conducted on April 10, 2024, presented an initial slump of 1.5 inches and air content of 7.8 percent. The maximum amount of superplasticizer recommended in the JMF, 1.34 oz total, was added to the mix to increase workability, but the slump only increased to 1.75 inches. It should be noted that a butter batch was not performed prior to this mix, which is likely the cause behind the low slump. Eleven unrestrained shrinkage specimens and ten compression test cylinders were formed. Due to the excess amount of slump tests performed, there was not enough concrete to create a prism for the modulus of rupture test.

Control Mix 2, conducted on April 22, 2024, provided a slump of 2.125 inches and an air content of 10.0 percent despite using less superplasticizer and the same amount of AEA. Eleven unrestrained shrinkage specimens, twelve compression test cylinders, and one modulus of rupture specimen were formed. Including the butter batch into the mixing procedure appeared to increase air content and workability; it is likely that the paste coating the mixer contained entrained air and superplasticizer which was then added into the main batch.

Control Mix 3, conducted on May 3, 2024, provided a slump of 3.25 inches and an air content of 15.3 percent. As with the second full mix, the air content was extremely high despite reducing the amount of AEA. Eleven unrestrained shrinkage specimens, twelve compression test cylinders, and one modulus of rupture specimen were formed.

Control Mix 4 was conducted on May 24, 2024, to investigate 28-day compressive strength of cylinders cured for different periods of time. This mix was 2.3 cubic feet in volume with the intention of performing one slump test and one air entrainment test, along with casting 21 cylinders for compressive tests. This mix provided a slump of 3.75 inches and an air content of 11%.

Control Mix 5 was conducted on November 5, 2024, and provided a slump of 3.5 inches and air content of 8.0 percent. Eleven unrestrained shrinkage specimens, three restrained shrinkage prisms, twelve compression test cylinders, and one modulus of rupture specimen were formed.

Control Mix 6 was conducted on May 5, 2025, and provided an initial slump of 1.5 inches with an initial superplasticizer dosage of 1.69 ounces. An additional 0.68 ounces of superplasticizer was added, but the slump remained unchanged. An additional 33.8 ounces of water was added to the mix, which then provided a slump of 3.5 inches and air content of 7.9 percent. Three compression test cylinders and six modulus of rupture specimens were formed.

SRA Mix 1, conducted on July 9, 2024, presented an initial slump of 1.0 inch. The initial dosage of superplasticizer was 0.67 ounces, and following the first slump test an additional 0.68 ounces of superplasticizer was added, but the slump remained the same. Two more slump tests were performed, adding 15.22 and 16.9 ounces of water, with no change to the slump. After the fourth slump test 0.68 more ounces of superplasticizer was added, for a total of 2.03 ounces of superplasticizer, which increased the slump to 2.5 inches. Air content was determined to be 10 percent, which may have been increased due to the additional superplasticizer. Due to the amount of concrete used on the additional slump tests, only three unrestrained shrinkage prisms and twelve compression test cylinders were able to be formed.

SRA Mix 2 was conducted on July 18, 2024, and provided a slump of two inches and air content of 5.3 percent. Eleven unrestrained shrinkage specimens, three restrained shrinkage prisms, 12 compression test cylinders, and one modulus of rupture specimen were formed.

SRA Mix 3, conducted on August 8, 2024, provided a slump of 5 inches and air content of 7.4 percent. It should be noted that some water, believed to be roughly 33.8 ounces, was spilled during the mix process, so an additional 33.8 ounces was then added to the mix. The larger slump may be in part due to

the exact amount of water spilled being unknown, so likely the mix was more “wet” than indicated by the w/b ratio in Table 4.1.2. Eleven unrestrained shrinkage specimens, three restrained shrinkage prisms, 12 compression test cylinders, and one modulus of rupture specimen were formed.

The CRA mix, conducted on September 3, 2024, provided a slump of 2.5 inches and air content of 6.4 percent. Eleven unrestrained shrinkage specimens, three restrained shrinkage prisms, 12 compression test cylinders, and one modulus of rupture specimen were formed.

Fiber Mix 1, conducted on September 20, 2024, initially would not have provided an acceptable slump, by inspection, when using 1.34 ounces of superplasticizer. An additional 0.85 ounces of superplasticizer was added to the mix, which was also visually determined to fail. An additional 0.68 ounces of superplasticizer was added to the mix which provided a slump of 1.0 inches. An additional 50.72 ounces of water was added to the mix. However, the mix was still visually determined not to be workable enough, so an additional 67.63 ounces of water was added to the mix. The mix then provided a slump of 2.75 inches and air content of 8.5 percent. Eleven unrestrained shrinkage specimens, three restrained shrinkage prisms, 12 compression test cylinders, and one modulus of rupture specimen were formed.

Fiber Mix 2, conducted on October 8, 2024, initially would not have provided an acceptable slump, by inspection, when using 0.51 ounces of superplasticizer. It was then noticed that the incorrect amount of water was initially used, so an additional 35.5 ounces of water was added to the mix. However, it was visually determined not to pass slump, so more superplasticizer was added. 0.34 ounces of superplasticizer was added, followed by an additional 0.34 ounces, and then 0.2 ounces. Each time, the mix was visually determined not to be within the desired range. A final 0.34 ounces of superplasticizer was added to the mix, which then provided a slump of 2.25 inches and air content of 6.0 percent. Eleven unrestrained shrinkage specimens, three restrained shrinkage prisms, 12 compression test cylinders, and one modulus of rupture specimen were formed.

## 4.3 Hardened Concrete Properties

Not all control mixes met the target 28-day strength target of 4000 psi. Control Mixes 2 and 3 both failed to reach 4000 psi, likely caused by their high entrained air content. Compression test results for these four control mixes are shown in Figure 4.3.1.

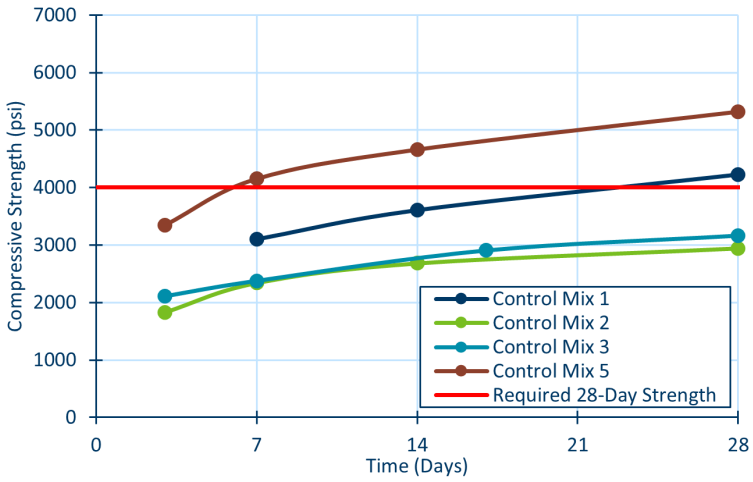


**Figure 4.3.1. Control Mix 1,2,3, and 5 compression test results**

Flexure tests were performed for Control Mixes 2, 3, and 5. Control Mix 2 had a modulus of rupture of 613 psi at 70 days, Control Mix 3 had a modulus of rupture of 656 psi at 59 days, and Control Mix 5 had a modulus of rupture of 551 psi at 28 days. Interestingly, these were not correlated with the 28-day compressive strengths, though likely because only one flexural sample was tested. The measured flexural strengths were all higher than would be expected for a typical modulus of rupture from Section 19.2.3.1 of ACI-318-19 or Section 5.4.2.6 of AASHTO LRFD (2020), which for 4000-psi concrete would be expected to be approximately equal to 480 psi. However, commentary C5.4.2.6 in AASHTO LRFD notes that this prediction is at the lower end of expected tensile strength, and that an upper value of 740 psi may be achievable, which places the measured results into the typical expected range. Lastly, curing duration may have an impact on the modulus of rupture, but that was not investigated herein. Carrasquillo et al. (1981) noted that the 28-day modulus of rupture may be reduced by 15 to 26% if the concrete is cured for 7 days and then left exposed for 21 days as compared to concrete that has been moist cured for 28 days. Therefore, the modulus of rupture for in-field cast-in-place HPC decks is likely similar to the AASHTO LRFD and ACI-318 predictions.

Control Mix 4 tested 21 cylinders cured for different cure periods. Compressive tests were all performed at 28-day strength, with three cylinders cured for one day, three cured for three days, three cured for ten days, three cured for fourteen days, three cured for 21 days, and three cured for 28 days. Cylinders were demolded at 24 hours and were all cured in a curing chamber at 95% relative humidity for the specified durations, except for the one-day cure specimens which were not placed in the curing chamber and were left out of the chamber immediately upon demolding. Once the designated curing durations were complete, the cylinders were removed from the chamber and left out in the lab until reaching an age of 28 days. An additional three cylinders were not placed in the curing chamber and were instead left in their cylindrical molds for 28 days. Results for 28-day compressive strengths are presented in Figure 4.3.2 below. It can be noted that the one-day curing period appeared to present a lower compressive strength by roughly 600 psi minimum, but the curing periods of three days or more appeared to have little to no effect on compressive strength.

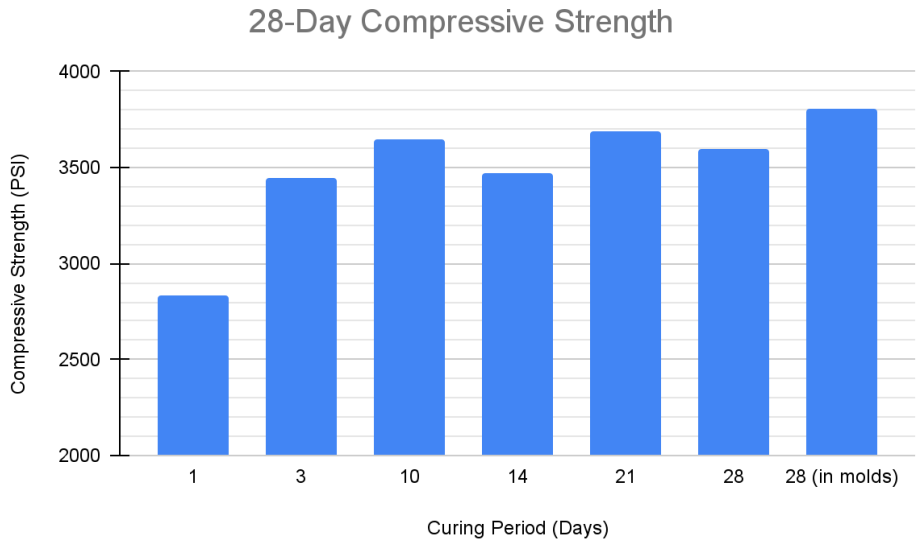


**Figure 4.3.2. 28-day compressive strength of cylinders cured for different lengths of time**

Control Mix 6 tested six modulus of rupture beams and three compression test cylinders at 28 days from casting. The cylinders were left to cure in their forms for the full 28-day period, and the average 28-day compressive strength was 4699 psi. Two of the modulus of rupture beams were cured for seven days, two were cured for 14 days, and two were cured for 28 days. Beams were cured in their forms covered by wet burlap for 24 hours and then taken out of the forms and placed in a curing chamber for the remainder of their cure periods. After being removed from the curing chamber, the 7-day and 14-day cure beams were left exposed in the lab until being tested at an age of 28 days. Flexural strength results are shown in Table 4.3.1. Despite the differences in curing durations, the 28-day modulus of rupture values were not significantly different.

**Table 4.3.1. Modulus of rupture values for different curing durations**

| Curing Duration (days) | Beam 1 Modulus of Rupture (psi) | Beam 2 Modulus of Rupture (psi) | Average |
|---|---|---|---|
| 7 | 391 | 410 | 401 |
| 14 | 406 | 351 | 379 |
| 28 | 439 | 383 | 411 |

All SRA mixes achieved the target 28-day compressive strength. Compression tests results for mixes containing SRAs are shown in Figure 4.3.3. These strengths were greater overall than those of the control mixes, though the most likely cause of this was the better accuracy in achieving the target air content with the SRA mixes.

Flexure tests were performed for SRA Mixes 2 and 3, and CRA Mix 1. SRA Mix 2 had a modulus of rupture of 612 psi at 71 days, SRA Mix 3 had a modulus of rupture of 607 at 50 days, and CRA Mix 1 had a modulus of rupture of 560 psi at 28 days. Again, these values were not correlated with the

compressive strength results and were comparable with the modulus of rupture measured with the control mix.

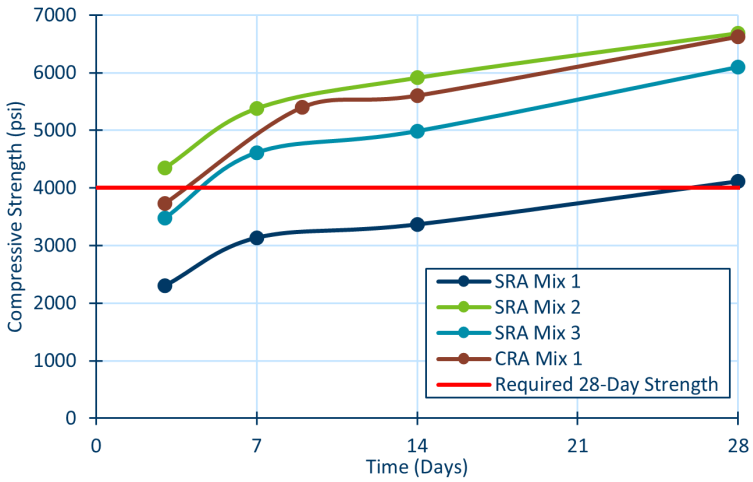


**Figure 4.3.3. Compressive strength results for SRA and CRA mixes**

Both Fiber Mix 1 and Fiber Mix 2 met the required 28-day compressive strength, reaching 5017 psi or 5985 psi, respectively. Compression test results for both fiber mixes are shown in Figure 4.3.4. Flexural tests were performed for both mixes at 28 days, achieving a modulus of rupture of 589 psi and 650 psi for Fiber Mix 1 and 2, respectively. These values for modulus of rupture did not strongly differ from those of either the control mixes or SRA mixes.

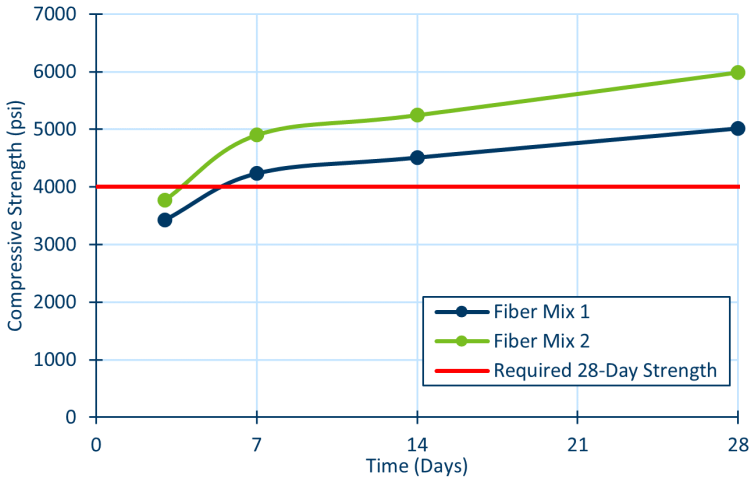


**Figure 4.3.4. Compressive strength results for Fiber Mix 1 and 2**

## 4.4 Shrinkage Testing

### 4.4.1 Unrestrained Shrinkage Results

Control Mix 1 provided ten unrestrained shrinkage specimens that were weighed and their length measured; one additional specimen was weighed but not measured due to one of the end pins falling out. Eight of the shrinkage specimens were placed in the lime-water bath for the remainder of their curing periods of 7 days, 14 days, 23 days, and 28 days (two samples for each curing duration), and two were left out of the bath to be tested as the 24-hour curing period specimens. Resulting strain due to unrestrained shrinkage is shown in Figure 4.4.1(a). The 28-day cure specimen exceeded the 400 microstrain limit, reaching 420 microstrain after 28 days of drying. The 1-day cure specimens experienced exceptionally high shrinkage, reaching over 700 microstrain. The cause of this is unknown, though it may have been caused by loose pins in those specimens.

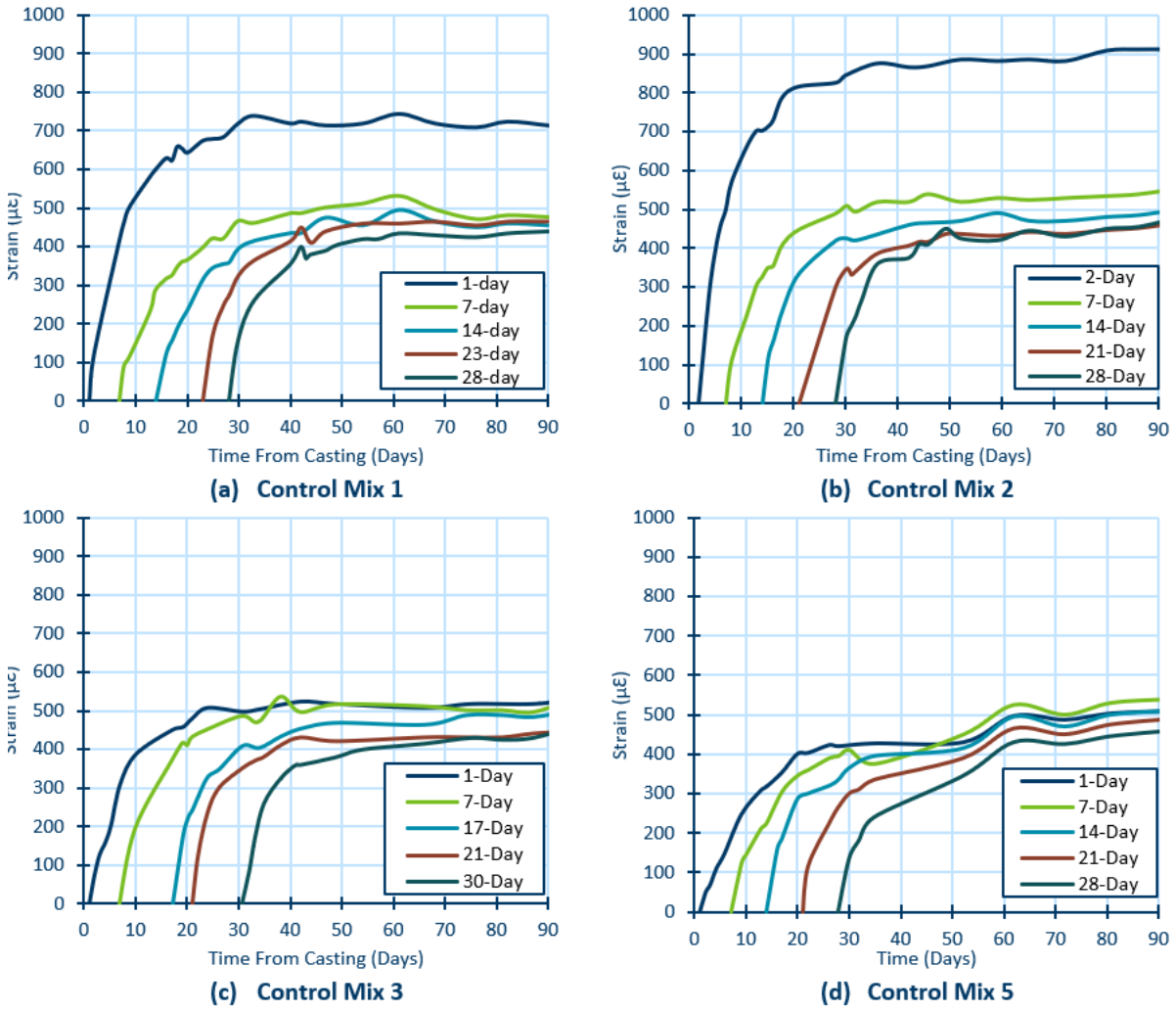


**Figure 4.4.1. Strain due to unrestrained shrinkage for Control Mixes**

Due to scheduling issues for Control Mix 2, all the unrestrained shrinkage specimens were demolded, weighed, and measured at 2-days age. Eight of these were placed in the lime-water bath for the remainder of their curing periods of 7 days, 14 days, 21 days, and 28 days (two samples for each curing duration), while three were left out to be tested immediately without a lime-water bath cure. Results for strain due to unrestrained shrinkage are shown in Figure 4.4.1(b). The 28-day cure specimen again exceeded the 400 microstrain limit reaching 422 microstrain after 28 days of drying, as with Control Mix 1. The 2-day cure specimens experienced exceptionally high shrinkage, reaching over 900 microstrain. This observation is consistent with Control Mix 1, indicating either a consistent mistake or consistent shrinkage behavior.

All the unrestrained shrinkage specimens in Control Mix 3 were demolded, weighed, and measured at 24 hours. Eight of these were placed in the lime-water bath for the remainder of their curing periods of 7 days, 17 days, 21 days, and 30 days (two samples for each curing duration), while three were left out to be tested immediately without a lime-water bath cure. Resulting strain due to unrestrained shrinkage is shown in Figure 4.4.1(c). The 30-day cure specimen slightly exceeded the 400 microstrain limit, reaching 402 microstrain after 28 days of drying. However, the 1-day cure specimens provided less shrinkage than in Control Mix 1 and 2, slightly exceeding 500 microstrain.

All the unrestrained shrinkage specimens for Control Mix 5 were demolded, weighed, and measured at 24 hours. Eight of these were placed in the lime-water bath for the remainder of their curing periods of 7 days, 14 days, 21 days, and 28 days (two samples for each curing duration), while three were left out to be tested immediately without a lime-water bath cure. Resulting strain due to unrestrained shrinkage is shown in Figure 4.4.1(d). The 28-day cure specimen did not exceed the 400 microstrain limit, reaching 378 microstrain at 28 days of drying. The 1-day cure specimens slightly exceeded 500 microstrain, remaining consistent with observations from Control Mix 3.

The three unrestrained shrinkage prisms in SRA Mix 1 were cured in their forms for 24 hours and then taken out, weighed, measured, and left to be tested without the lime-water bath cure. Results for strain due to unrestrained shrinkage are shown in Figure 4.4.2(a). Even the 1-day cure specimens only slightly exceeded the 400 microstrain limit at 90 days, indicating significant improvement compared to the control mixes.

All the unrestrained shrinkage specimens in SRA Mix 2 were demolded, weighed, and measured at 24 hours. Eight of these were placed in the lime-water bath for the remainder of their curing periods of 7 days, 14 days, 21 days, and 28 days (two samples for each curing duration), while three were left out to be tested immediately without a lime-water bath cure. The specimens intended to be taken out at 14 days were taken out and weighed at 14 days, but length was not measured until 18 days after casting. Results for strain due to unrestrained shrinkage are shown in Figure 4.4.2(b). None of the specimens exceeded the 400 microstrain limit within the 90-day observation time, with the 7-day cure specimens reaching a maximum 395 microstrain. The 28-day cure specimen reached 260 microstrain after 28 days of drying, which is well below the 400 microstrain limit.

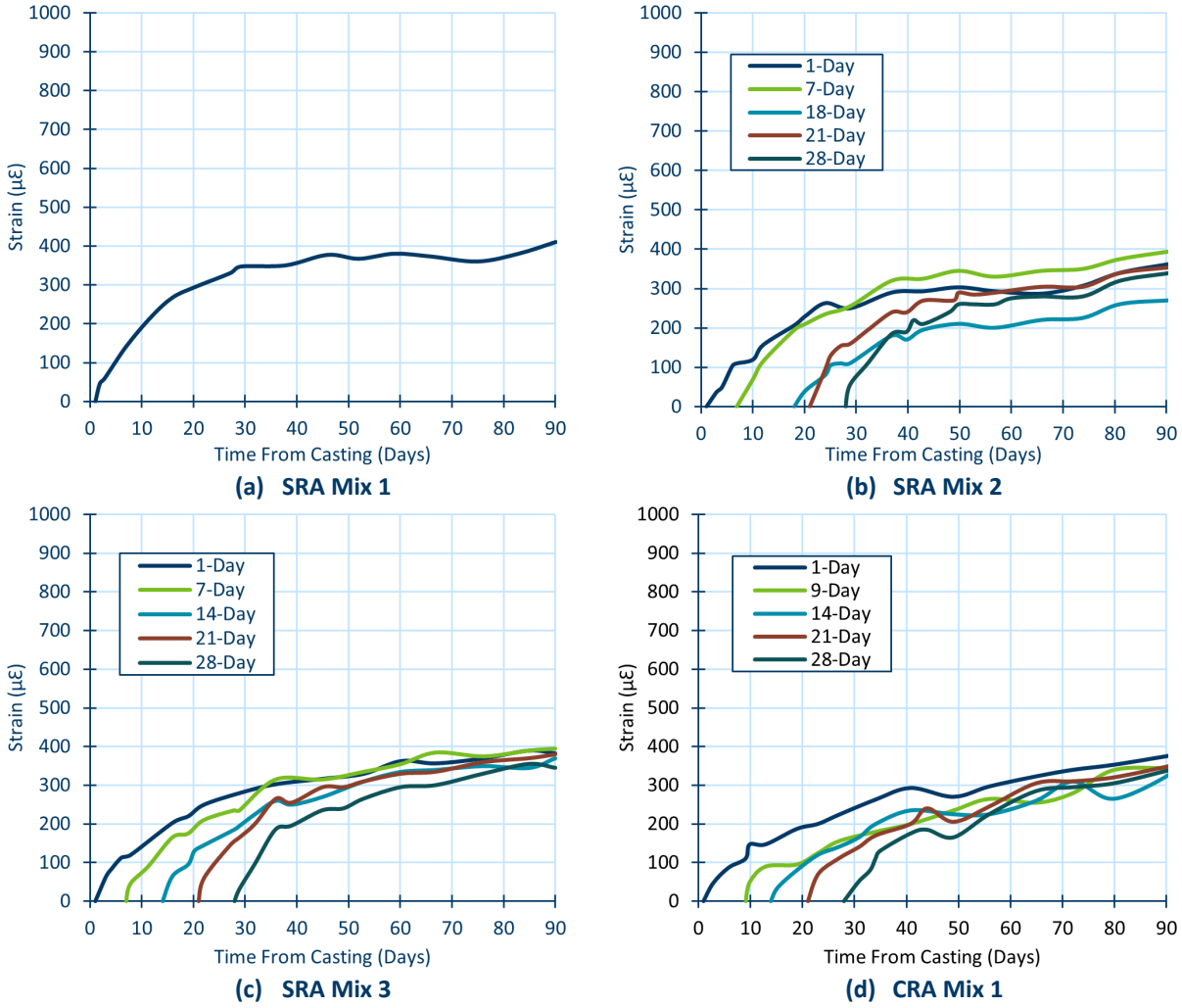


**Figure 4.4.2. Strain due to unrestrained shrinkage for SRA Mixes**

All the unrestrained shrinkage specimens in SRA Mix 3 were demolded, weighed, and measured at 24 hours. Eight of these were placed in the lime-water bath for the remainder of their curing periods of 7 days, 14 days, 21 days, and 28 days (two samples for each curing duration), while three were left out to be tested immediately without a lime-water bath cure. Resulting strain due to unrestrained shrinkage is shown in Figure 4.4.2(c). Again, none of the specimens exceeded the 400 microstrain limit, with the 7-day cure specimens reaching a maximum 395 microstrain. The 28-day cure specimen reached 278 microstrain after 28 days of drying, again, well below the 400 microstrain limit.

All the unrestrained shrinkage specimens in CRA Mix 1 were demolded, weighed, and measured at 24 hours. Eight of these were placed in the lime-water bath for the remainder of their curing periods of 9 days, 14 days, 21 days, and 28 days (two samples for each curing duration), while three were left out to be tested immediately without a lime-water bath cure. Results for strain due to unrestrained shrinkage are shown in Figure 4.4.2(d). None of the specimens exceeded the 400 microstrain limit, with the 1-day cure specimens reaching a maximum 377 microstrain. The 28-day cure specimen reached 225 microstrain after 28 days of drying, which is slightly above half of the 400 microstrain limit.

All the unrestrained shrinkage specimens in Fiber Mix 1 were demolded, weighed, and measured at 24 hours. Eight of these were placed in the lime-water bath for the remainder of their curing periods of 10 days, 14 days, 21 days, and 28 days (two samples for each curing duration), while three were left out to be tested immediately without a lime-water bath cure. Results for strain due to unrestrained shrinkage are shown in Figure 4.4.3(a). It can be observed that the 28-day cure specimen did not exceed the 400 microstrain limit, reaching 375 microstrain after 28 days of drying.

All the unrestrained shrinkage specimens in Fiber Mix 2 were demolded, weighed, and measured at 24 hours. Eight of these were placed in the lime-water bath for the remainder of their curing periods of 7 days, 14 days, 21 days, and 28 days (two samples for each curing duration), while three were left out to be tested immediately without a lime-water bath cure. Results for strain due to unrestrained shrinkage are shown in Figure 4.4.3(b). It can be observed that the 28-day cure specimen did not exceed the 400 microstrain limit, reaching 360 microstrain after 28 days of drying. It should be noted that the slight increase in shrinkage strain at the 90-day reading may have been caused by varying laboratory conditions leading to a slightly higher shrinkage reading, in which case the 28-day cure specimen may have experienced strain less than 400 microstrain.

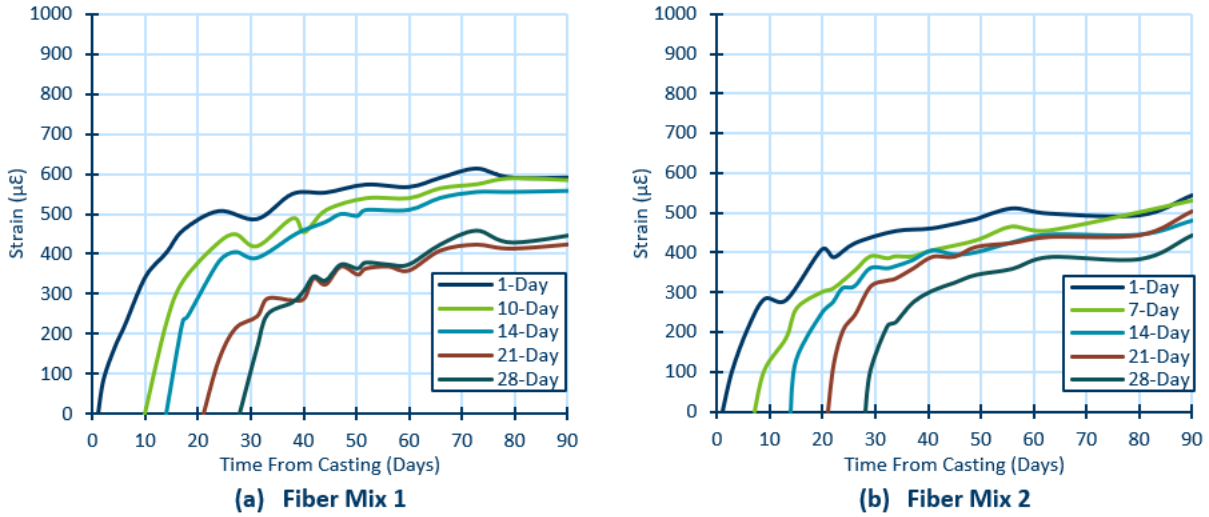


**Figure 4.4.3. Strain due to unrestrained shrinkage for Fiber Mixes**

## 4.4.2 Restrained Shrinkage Results

Restrained shrinkage prisms for Control Mix 5 were demolded after 24 hours and placed into the restrained shrinkage apparatuses, with data being recorded for 28 days. The resulting forces due to restrained shrinkage are shown in Figure 4.4.4. It can be observed that the maximum forces were 132, 101, and 55 pounds at 28 days for the 1-inch, 0.75-inch, and 0.5-inch bars, respectively.

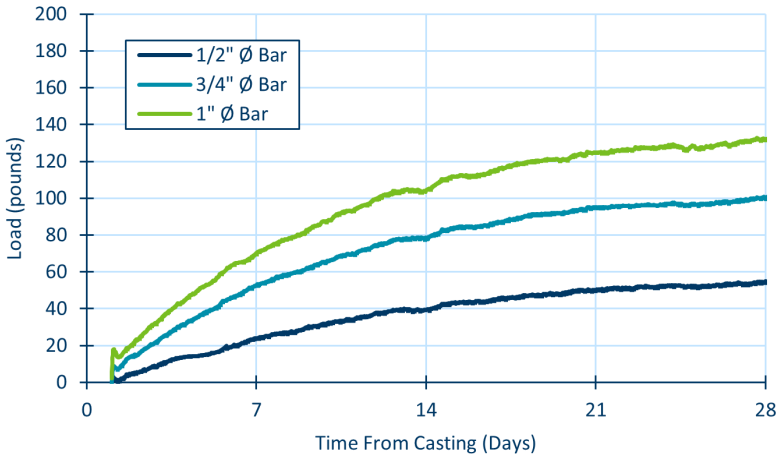


**Figure 4.4.4. Force due to restrained shrinkage for Control Mix 5**

Restrained shrinkage prisms for SRA Mix 2 were demolded after 24 hours and placed into the restrained shrinkage apparatuses, with data being recorded for 22 days. Results for strain due to restrained shrinkage are shown in Figure 4.4.5(a). The maximum forces were 61, 52, and 39 pounds for the 1-inch, 0.75-inch, and 0.5-inch bars, respectively.

Restrained shrinkage prisms for SRA Mix 3 were demolded after 24 hours and placed into the restrained shrinkage apparatuses, with data being recorded for 27 days. Results for strain due to restrained shrinkage are shown in Figure 4.4.5(b). It can be observed that the maximum forces were 64, 64, and 31 pounds for the 1-inch, 0.75-inch, and 0.5-inch bars, respectively.

Restrained shrinkage prisms for CRA Mix 1 were demolded after 24 hours and placed into the restrained shrinkage apparatuses, with data being recorded for 18 days. Results for strain due to restrained shrinkage are shown in Figure 4.4.5(c). It can be observed that the maximum forces were 54, 49, and 23 pounds for the 1-inch, 0.75-inch, and 0.5-inch bars, respectively.

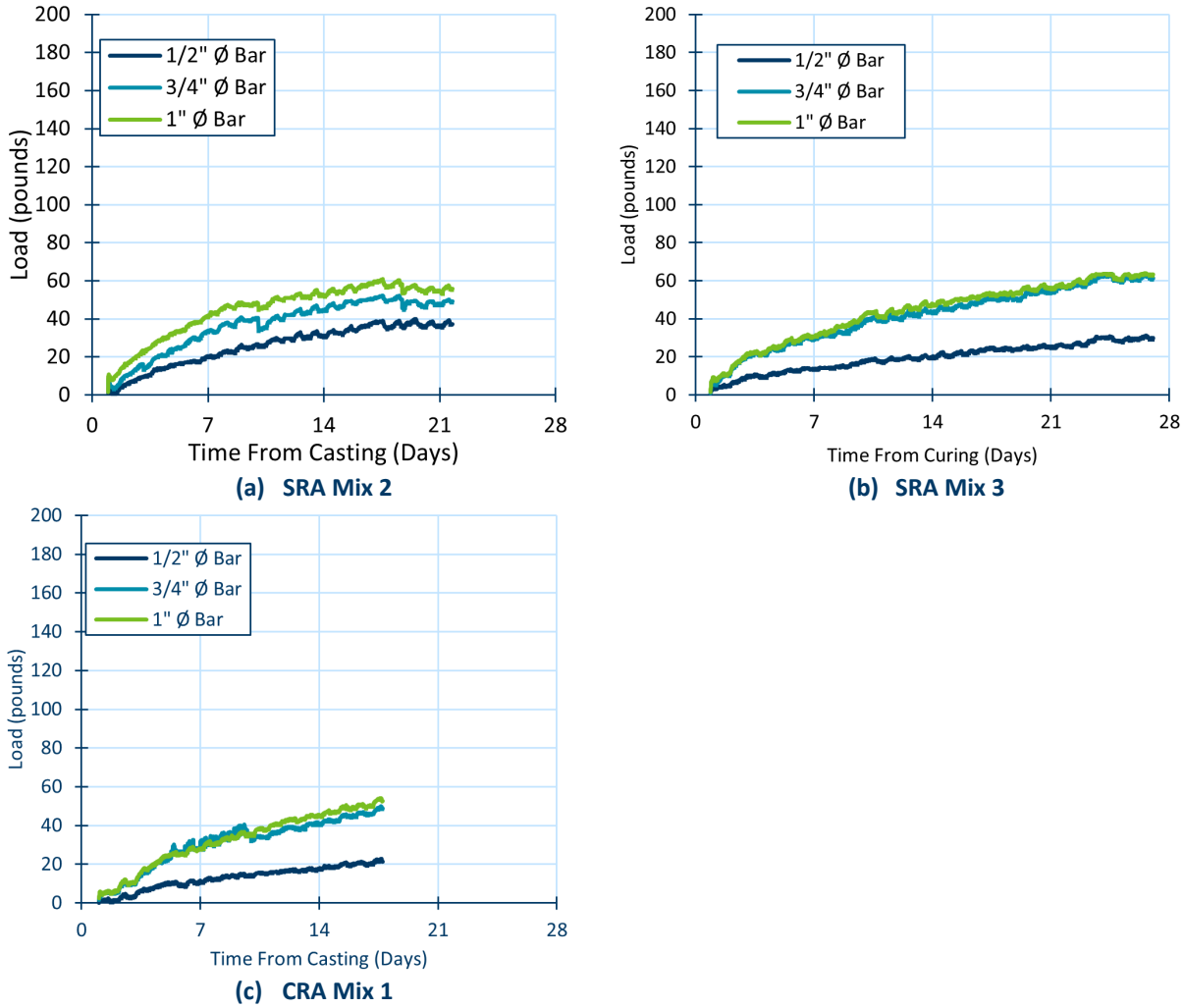


**Figure 4.4.5. Force due to restrained shrinkage for SRA Mixes**

Restrained shrinkage prisms for Fiber Mix 1 were demolded after 24 hours and placed into the restrained shrinkage apparatuses, with data being recorded for 19 days. Results for strain due to restrained shrinkage are shown in Figure 4.4.6. It can be observed that the maximum forces were 154, 109, and 82 pounds for the 1-inch, 0.75-inch, and 0.5-inch bars, respectively.

Restrained shrinkage prisms for Fiber Mix 2 were also demolded after 24 hours and placed into the restrained shrinkage apparatuses, with data being recorded for 29 days. Results for strain due to restrained shrinkage are shown in Figure 4.4.6. It can be observed that the maximum forces were 135, 78, and 56 pounds for the 1-inch, 0.75-inch, and 0.5-inch bars, respectively.

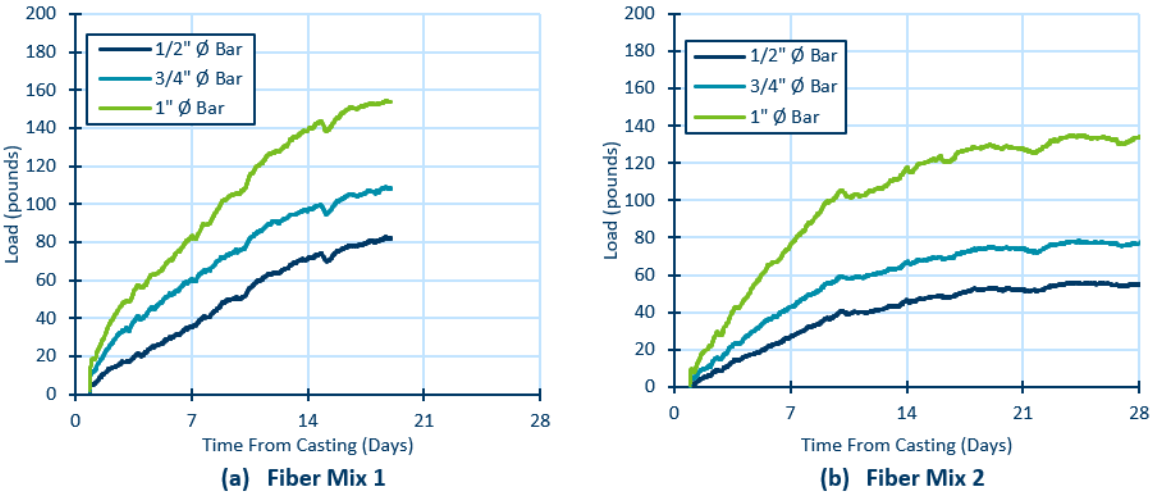


**Figure 4.4.6. Force due to restrained shrinkage for Fiber Mixes**

# Chapter 5: Computational Modeling Results

## 5.1 Initial Computational Testing

The primary output of the model was the concrete deck stress in the longitudinal direction, which may lead to transverse cracking if exceeding the tensile capacity of the concrete. The investigated loading scenarios were uniform temperature changes, thermal gradients, deck concrete shrinkage, and relative temperature difference between deck and girders. Stresses throughout are reported at the top surface of the deck, as tension here would lead to the initiation of deck cracking.

### 5.1.1 Uniform Temperature Change

A uniform temperature change represents an increase or decrease in temperature to all components and materials in the bridge simultaneously. Because the bridge is simply supported, uniform temperature changes only create stresses due to differential expansion in the rebar and concrete, which would not normally be large enough to induce cracking. An initial temperature increase of 50°F was arbitrarily chosen to verify that the model was operating correctly; any observed stresses may be scaled linearly with temperature change. As shown in Figure 5.1.1, longitudinal stresses in the deck did not exceed 10 psi for the selected temperature increase. It can be noted that stress contours outline where girders are located, indicating increased stress above the girders.

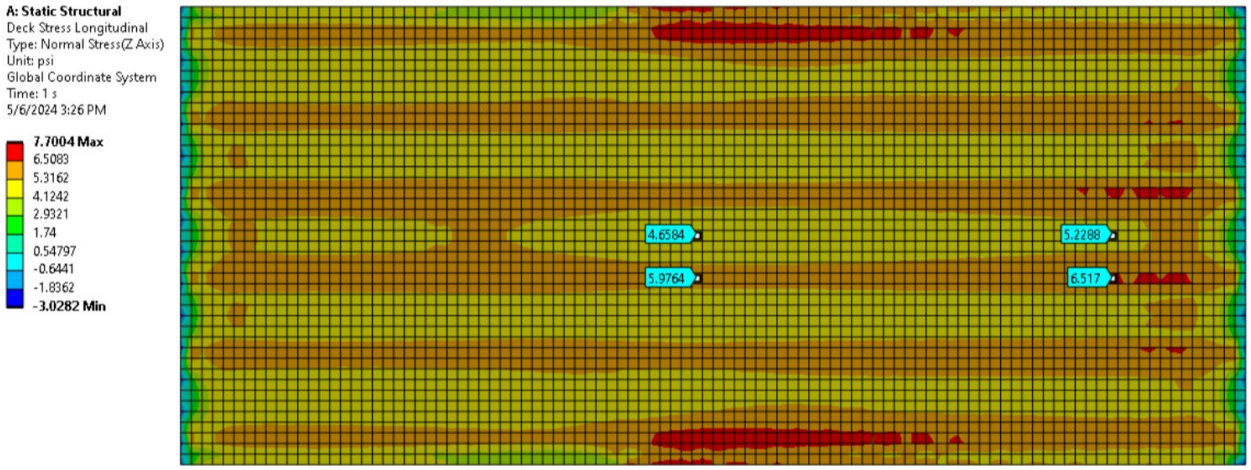


**Figure 5.1.1. Longitudinal deck stresses due to applied uniform temperature change**

According to AASHTO LRFD (2020), a concrete bridge deck in Minnesota may experience a uniform temperature range of –20°F to 110°F, for a total temperature change of 130°F. In this case, deck stresses would be approximately 2.6 times larger than the provided results caused by the 50°F temperature change, resulting in at most 20 psi of tension. However, this would only occur if the bridge deck were cast at the extreme low or extreme high temperature since the changes are based on the initial state of the bridge deck. Regardless, uniform temperature changes would result in negligible stresses in the bridge deck unless there was an exterior restraint to longitudinal expansion and contraction.

### 5.1.2 Thermal Gradients

When the bridge deck experiences a higher temperature than the girders, it is experiencing a positive gradient. When the bridge deck experiences a lower temperature than the girders, it is experiencing a negative gradient. These thermal gradients cause nonuniform expansion and contraction of the structure, resulting in compatibility stresses. The temperature distributions of these gradients are shown in Figure 3.3.4. Positive thermal gradients result in compressive stresses in the bridge deck as shown in Figure 5.1.2, while negative thermal gradients result in tensile stresses in the bridge deck as shown in Figure 5.1.3.

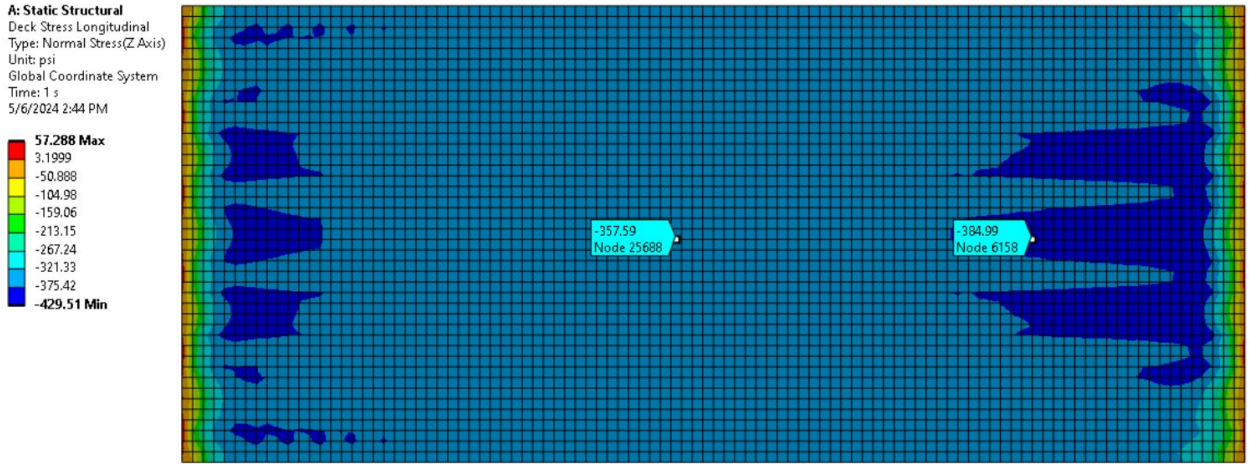


**Figure 5.1.2. Bridge deck longitudinal stresses due to positive thermal gradient**

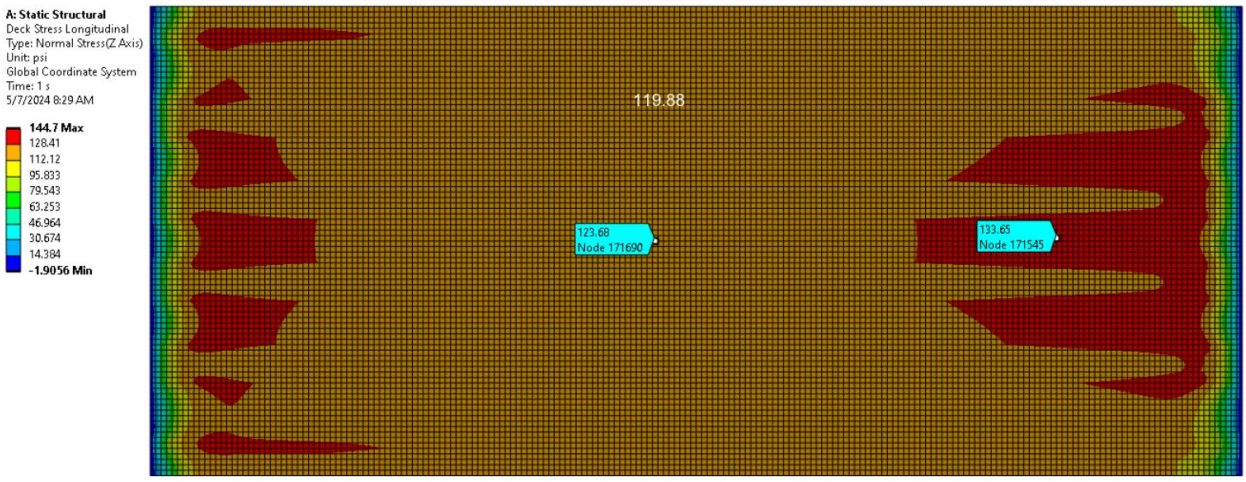


**Figure 5.1.3. Bridge deck longitudinal stresses due to negative thermal gradient**

The stresses remain relatively uniform throughout the entire bridge deck except for at the ends. The positive gradient resulted in a 430-psi maximum compressive stress, while the negative gradient resulted in a 145 psi maximum tensile stress. Although the positive gradient resulted in the larger magnitude stress, it is not a concern for cracking due to the stress being significantly lower than the

required 4000 psi compressive strength of the concrete. The negative gradient is also lower than the expected tensile strength of the concrete of 480 psi per AASHTO LRFD (2020) section 5.4.2.6. However, the negative gradient may act in combination with other mechanisms that induce tensile stresses, such as shrinkage, which may lead to tensile stresses that exceed the tensile strength.

### 5.1.3 Concrete Shrinkage

Shrinkage of the model was investigated in the initial modeling by applying a thermal reduction to the bridge deck concrete only, leaving the embedded rebar and girders with no thermal change. The embedded rebar, being steel, does not experience shrinkage and restrains the shrinking concrete. The girders were assumed to be precast and several months old and were conservatively assumed not to shrink. Given a concrete coefficient of thermal expansion of $5.56 \times 10^{-6}$/°F per degree Fahrenheit, a temperature change of –72°F was applied to the deck concrete to mimic a shrinkage strain of 400 microstrain, which is the allowable shrinkage strain for MnDOT HPC mixes in Minnesota DOT Standard Specifications Table 2401.2-5. As shown in Figure 5.1.4, longitudinal stresses were largest over the girders, similar to the original temperature change model. The maximum tensile stress caused by shrinkage was 250 psi, which is less than the expected tensile capacity of HPC concrete. When combined with the negative thermal gradient, the resulting tension is 385 psi, which is still less than the expected concrete tensile capacity.

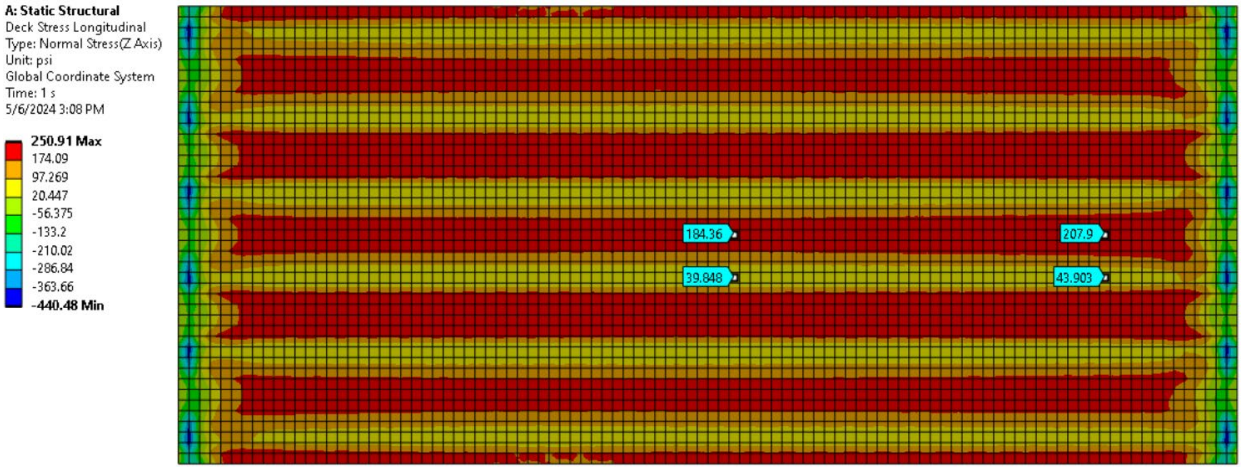


**Figure 5.1.4. Longitudinal stresses in top of deck due to shrinkage**

### 5.1.4 Relative Temperature Difference

If the deck concrete is considerably warmer than the girders onto which it is placed, and this temperature is maintained until the deck concrete sets, then a relative temperature difference can form between the deck and girders. In this case, the deck concrete and reinforcement are all assumed to be the same temperature. When the deck concrete cools, it will contract, inducing tension in the deck. This mechanism is very similar to that of deck shrinkage except that the deck reinforcement does not restrain this deformation. Figure 5.1.5 shows the resulting longitudinal stresses caused by a –72°F temperature change in the concrete, chosen to align with the applied shrinkage in Figure 5.1.4, assuming an

exothermic reaction and resulting cooling of deck during placement. The stresses appear similar to the stresses in Figure 5.1.4, but with a smaller maximum magnitude of 206 psi because the deck reinforcement does not effectively restrain the deck concrete in this case, unlike for shrinkage.

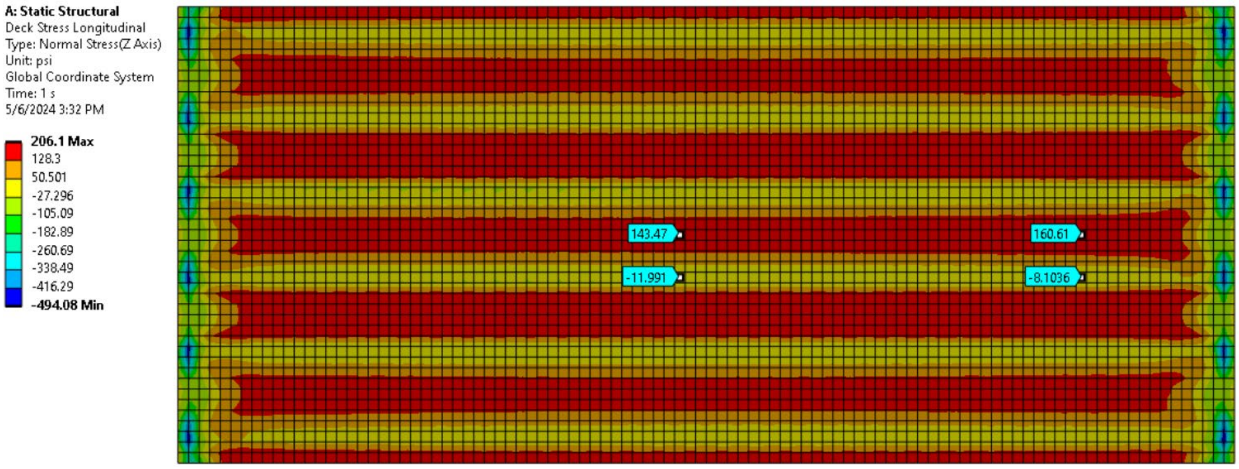


**Figure 5.1.5. Longitudinal stresses in top of deck due to deck cooling**

The temperature drop of –72°F was chosen here merely to show the difference concrete shrinkage and an equivalent temperature change throughout the deck. The results from Figure 5.1.5 may be scaled linearly for different changes in temperature.

## 5.1.5 Verifying Results

Simple hand calculations were performed to verify results found during computational testing. Stress in the deck concrete was estimated assuming a composite section composed of a concrete deck, girders, and deck longitudinal reinforcement. The deck concrete was assumed to shrink 400 microstrain, and this shrinkage was restrained by the girders and deck reinforcement. Only axial shortening was considered for this estimate, and bending of the bridge due to differential shrinkage was ignored. Deck and girder stiffness were estimated using an age-adjusted-effective-modulus to account for 28 days of creep and aging computed per the CPRH Model (Hedegaard et al. 2023) using material properties in Table 3.3.2, though the entire deck was assumed to have a V/S ratio of 4.5 in. and was not varied throughout the deck depth. These age-adjusted-effective-modulus values were 2402 ksi for the deck concrete and 4226 ksi for the girder concrete. Steel remained elastic with a modulus of 29000 ksi.

The estimated stresses from these calculations were 593 psi of tension in the deck, 647 psi of compression in the girders, and 4437 psi in the deck reinforcement. This overestimated the shrinkage stresses in the deck from the ANSYS model in Figure 5.1.4 by nearly a factor of 3. The primary cause of this was that these hand calculations ignored bending. Because the deck is placed on top of the girders, shrinkage of the deck results in a downward displacement of the bridge. Downward deflection normally places the deck into compression and the girders into tension, meaning this deflection would relieve the deck tension and girder compression. Thus, this overestimation of deck tension was expected based on the assumptions of the hand calculations.

## 5.2 Parametric Computational Testing

Similar to the initial computational modeling, the primary output of interest was the tensile stress at the top surface of the deck. The parametric model was investigated for two creep and shrinkage scenarios (constant temperature and cycled thermal gradients) and three elastic scenarios (positive thermal gradient, negative thermal gradient, and relative temperature difference between deck and girders).

### 5.2.1 Summary of Tensile Stresses at Deck Top Surface

Longitudinal stresses on the top surface of the deck are shown in Table 5.2.1 and the following figures below, with positive values representing tension and negative values representing compression. Results for the two creep and shrinkage analyses are taken 28 days after the end of curing. Though thermal changes were included in the creep and shrinkage analysis with cyclic thermal gradients, the presented results are when the temperature state has returned to its initial uniform condition, and therefore this does not directly include stresses from thermal gradients. However, the cycled gradients cause a stress history that affects the creep strain in the concrete, and the creep and shrinkage rates in the CPRH model are temperature dependent (higher temperatures result in faster creep and shrinkage); these effects explain the differences between the two creep and shrinkage analysis results.

**Table 5.2.1. Comparison of maximum tensile stress in each model (psi)**

| Model | 18TLR | 2 Span 18TLR | Flipped 18TLR | 12TLR | 6TLR |
|---|---|---|---|---|---|
| Elastic Analysis – Positive Gradient | -28 | -31 | -30 | -28 | -26 |
| Elastic Analysis – Negative Gradient | 124 | 910 | 125 | 124 | 123 |
| Elastic Analysis – Relative Temperature Difference | 305 | 5356 | 305 | 300 | 295 |
| Creep and Shrinkage at Constant Temperature | 396 | 1541 | 396 | 398 | 402 |
| Creep and Shrinkage with Cycled Thermal Gradients | 538 | 2582 | 538 | 539 | 543 |

Flipping the layering of the reinforcement or changing the spacing between bars had essentially no effect on reducing stresses within the bridge deck. Stresses in the 12TLR and 6TLR models appeared to slightly decrease for the elastic analysis and slightly increase for the two creep and shrinkage loading scenarios. The 2-span model appeared to produce very high tensile and compressive stresses for each of the loading scenarios. These stresses are located at the face at which the boundary condition fixes the slab from movement and reach 5356 psi of tension. These maximum stresses invariably occurred in the negative moment region where the deck was made continuous; once this region has thoroughly cracked, the assumption of two-span continuity would no longer apply. Thus, the remaining discussion of the results focuses on the single-span models.

For the elastic analyses, the thermal gradient stresses were similar to those observed in the initial modeling. These stresses are mainly developed because of compatibility within the deck itself and thus will be similar magnitude whether the gradient is applied immediately after casting or at 28-days, regardless of the stiffness of the girders. However, the stresses due to the relative temperature difference between the deck and girder for this refined analysis were roughly 100 psi larger than observed for the initial modeling. These stresses depend on the relative stiffness of the deck versus the girders. If the deck is only 3 days old when this temperature drop occurs, the stresses increase to roughly 315 psi for 18TLR model, though if the deck is 14 days old before this temperature drop occurs, the stresses are nearly unchanged compared to the 7-day results presented in Table 5.2.1. Adding additional steel to the deck marginally increases the stiffness of the deck, which explains why the decks with reduced spacing also have marginally reduced stresses in these elastic cases.

Though the applied shrinkage strains for the parametric models, shown in Figure 3.3.7, were lower than the 400 microstrain considered for the initial modeling, the resulting stresses are considerably higher. Some of this can be explained by the difference in deck versus girder stiffness, as was the case for the elastic analysis. However, a large portion of this increased stress is due to the nonuniform shrinkage of the deck. As the top surface of the deck shrinks more quickly than the lower portions of the deck, strain compatibility induces increased tension in the top surface. This is same mechanism that causes stresses under thermal gradients, and indeed comparing the creep and shrinkage results at constant temperature versus those with cycled thermal gradients shows that the cycled gradients exacerbate shrinkage stresses.

Creep and shrinkage with cyclic thermal gradients appeared to provide the highest tensile stress in all of the single span models, reaching about 540 psi. These tensile stresses exceed the expected tensile capacity of the deck concrete of 480 psi. Recall that this recorded stress is at the end of the 28-day analysis when the temperature has returned to its initial state, meaning in the extreme case, this stress could be added to those from the elastic analysis of a negative thermal gradient. Adding the tensile stress from the creep and shrinkage analysis with cycled gradients to the tensile stress from the negative gradient analysis returns a tensile stress of nearly 660 psi, which is much higher than the expected tensile stress. Creep and shrinkage alone produced tensile stresses of around 400 psi for the single span models, which, although it does not exceed the expected tensile capacity, is a large amount of tensile stress that may lead to cracking in conjunction with other factors. Finally, relative temperature differences between the deck and girders during casting could add to these stresses. The predicted 300 psi of tension was the result of a 72°F temperature difference, which is admittedly rather extreme. These stresses can be scaled linearly for other temperature difference values.

Further plots showing the results of all the parametric analyses are provided in Appendix A.

### 5.2.2 Stresses through Depth of Deck

While the stress at top surface of the deck would likely lead to crack initiation, stress through the depth of deck may illustrate the extent of cracking. Stress distributions through the depth of the deck for the 6TLR model are shown in Figures 5.2.1 through 5.2.5 to show the distribution of tensile stresses. Other

models were similar (except for the 2-span model, which obviously had different stress distribution near the continuous support, but after cracking would be expected to be similar to the other models). Stress flags in the figures are spaced every 1.5 in. through the depth of the deck.

From the elastic analysis results from Figures 5.2.1 through 5.2.3, positive gradients put the bottom of the deck into tension, though these stresses are small enough to be unlikely to cause cracking. Negative thermal gradients primarily concentrate tensile stresses in the top 1.5 in. of the deck. Relative temperature difference between the deck and girders causes the largest tension at the bottom of the deck, though the entire deck is placed into tension. Recall that this represents a deck that is cooled (that is, contracts) relative to the girders. This could happen when a warm deck poured on cold girders; after the deck cools to the girder temperature, the entire deck will have built-in tension. If combining a positive thermal gradient with a large relative temperature difference, the stresses at the bottom of the deck could be large enough to initiate cracking up from the bottom.

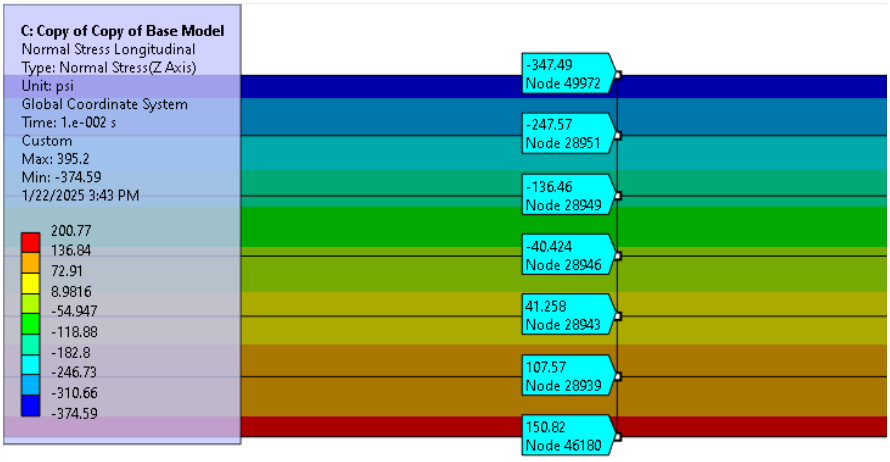


**Figure 5.2.1. Stress distribution through deck of 6TLR model for Elastic Analysis – Positive Gradient**

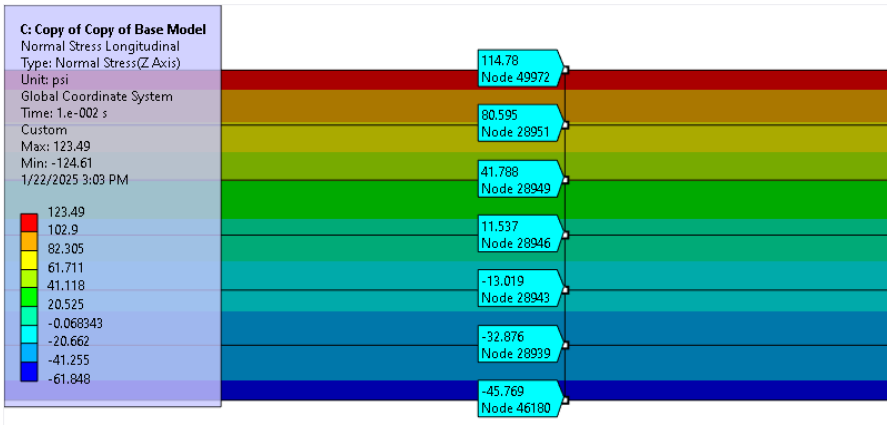


**Figure 5.2.2. Stress distribution through deck of 6TLR model for Elastic Analysis – Negative Gradient**

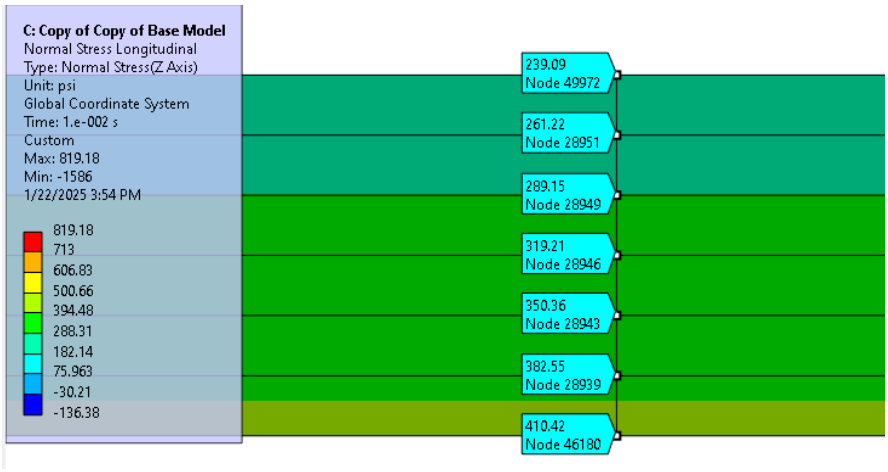


**Figure 5.2.3. Stress distribution through deck of 6TLR model for Elastic Analysis – Relative Temperature Difference**

Results from the shrinkage analyses are given in Figures 5.2.4 and 5.2.5. Shrinkage mainly concentrates the tensile stresses within the top 1.5 in. of the deck. This is exacerbated by the addition of cycled gradients, which return the bottom of the deck to a slightly compressive stress state. While this analysis implies that shrinkage stresses are mostly concentrated at the top surface, that may change for longer durations as the lower portion of the deck continues to shrink after the top surface has completed its shrinkage. Therefore, cracks that initiate at the top surface would likely progress downward with time.

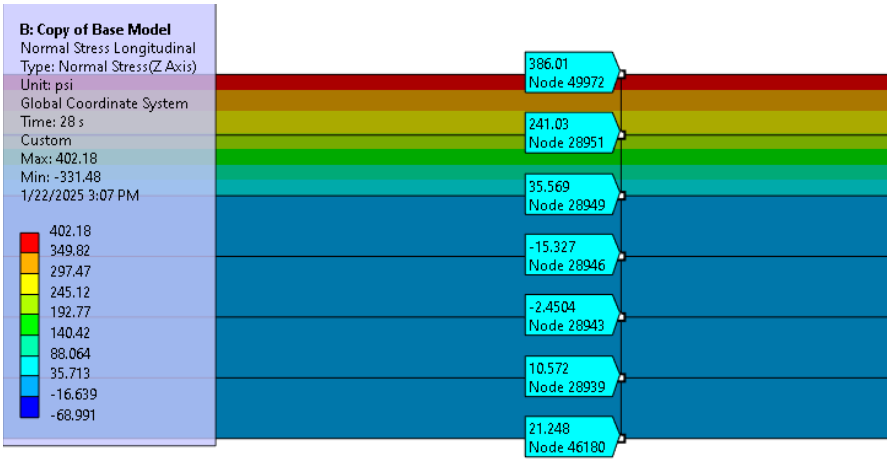


**Figure 5.2.4. Stress distribution through deck of 6TLR model for Creep and Shrinkage with Constant Temperature**

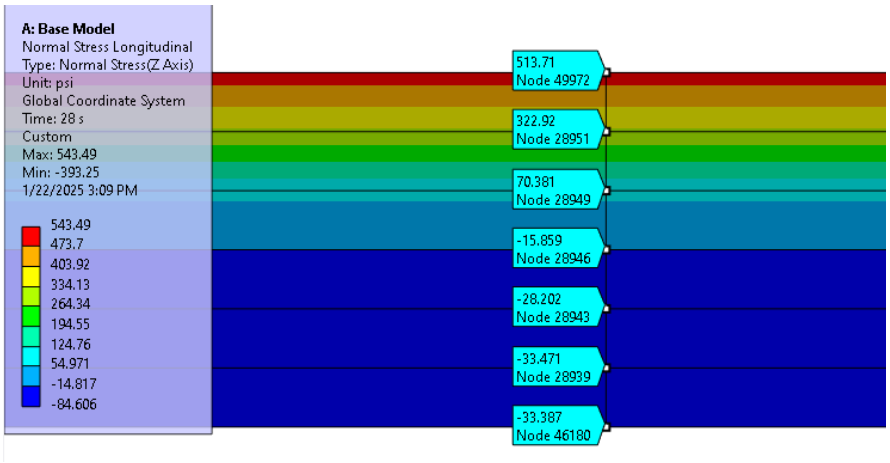


**Figure 5.2.5. Stress distribution through deck of 6TLR model for Creep and Shrinkage with Cycled Gradients**

Thus, the combination of different actions may result in through-depth cracks in the bridge deck. The top surface tensile stresses are maximized by shrinkage and negative thermal gradients, which are both nearly certain to occur within the first month after deck casting, while positive thermal gradients, large deck-to-girder temperature differences, and continued shrinkage may extend the cracking through the deck.

### 5.2.3 Stress With Variable Curing Duration

Adjusted curing durations were also tested for the control model 18TLR bridge, investigating 3-day cure, 7-day cure, and 14-day cure periods. Creep and shrinkage alone and creep and shrinkage with cycled thermal gradients were investigated for the specified cure periods. Material properties matched those in Table 3.3.2, but with dates shifted back by 4 days for the 3-day cure model and dates shifted ahead by 7 days for the 7-day cure model. The CPRH model predicts very slightly lower shrinkage strains given longer curing durations, on the order of 4 microstrain difference between 3 days and 14 days of curing, but nowhere near the reductions observed in lab tested presented in Section 4.4.1. Thus, these model results may be interpreted as the stresses developed under roughly the same magnitudes of shrinkage strain.

Based on results from the model looking at creep and shrinkage stresses alone, increasing the curing duration from 7 to 14 days increased stresses by roughly 6%, while decreasing curing duration from 7 to 3 days decreased stress by roughly 8%, as shown in Figure 5.2.6. Results are similar when looking at creep and shrinkage with cycled thermal gradients, shown in Figure 5.2.7. Longer curing durations resulted in the highest stresses again, though the thermal cycles reduced the stress differences of 3- or 14-day curing with respect to 7-day curing to roughly 2% to 3%. This may seem counterintuitive, but a deck that is cured for longer has increased stiffness and reduced creep, whereas lower stiffness and higher creep allow for greater relaxation of shrinkage-induced stresses. Again, these results effectively assumed the shrinkage strain was unaffected by the curing duration, but lab results indicated a reduction in shrinkage. Taken together, however, these effects cancel each other out, meaning increasing curing duration is unlikely to reduce deck stresses. These results indicate that the only benefit

of increased curing duration is a possible increase in modulus of rupture of the concrete, which was not observed in lab testing as described in Section 4.3.

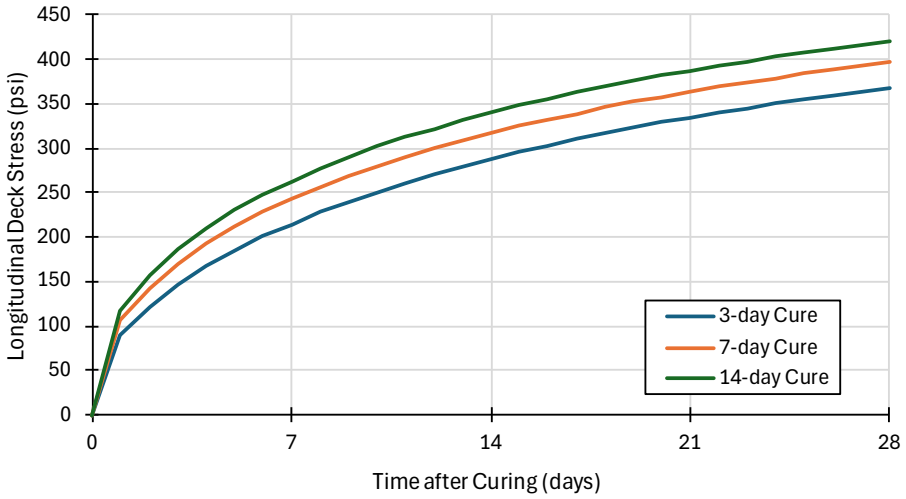


**Figure 5.2.6. Creep and shrinkage alone with adjusted curing durations**

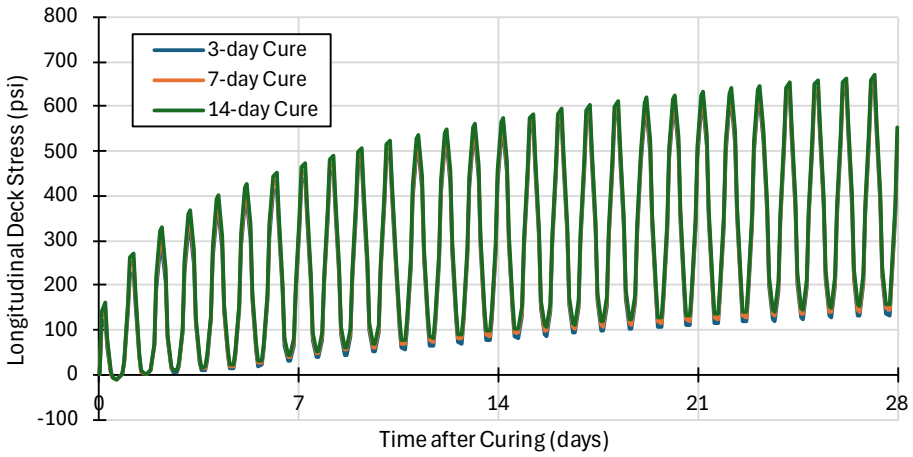


**Figure 5.2.7. Creep and shrinkage with cycled thermal gradients with adjusted curing durations**

# Chapter 6: Conclusions and Recommendations

## 6.1 Research Summary

Early-age cracking in concrete bridge decks causes rapid deterioration of steel reinforcement leading to costly maintenance procedures and a reduction in the life span of a bridge. This research investigated the causes of early age cracking along with potential solutions that can be implemented to reduce early age cracking. Investigations included laboratory testing of different concrete mixes based on current MnDOT mix requirements, along with computational modeling using finite element analysis.

Laboratory testing included eleven total concrete mixes to investigate how introducing shrinkage-reducing admixtures or adjusting fiber content may affect the currently accepted HPC mix design. Results suggested that the inclusion of SRAs into the mix effectively reduced unrestrained shrinkage strain and force due to restrained shrinkage while maintaining quality compressive and flexural strength. However, we observed that the inclusion of SRAs appeared to negatively impact workability of the concrete, increasing the amount of water or superplasticizer necessary to achieve the desired workability. Results also indicated that increasing or decreasing fiber content had little to no impact on reducing unrestrained shrinkage strain or force due to restrained shrinkage. Increasing the fiber content also had a negative impact on the workability of the concrete.

Computational modeling consisted of initial bridge modeling and testing followed by parametric testing. Results indicated significantly higher stress in the multi-span model compared to the other models. However, these locations of significantly high stress were localized to the negative moment region, indicating that cracking would occur at the junction of the spans as expected. However, even for single-span bridges, the models indicated that creep- and shrinkage-induced stresses would likely be high enough to initiate cracking, especially if acting in conjunction with a negative thermal gradient. We observed that decreasing the spacing of longitudinal reinforcement in the top mat of the deck did not provide any benefits in reducing tensile stresses in the deck. Regardless, decreasing rebar spacing may aid in crack control, especially if reinforcement is sized to prevent steel yielding along with maintaining bars with smaller area to circumference ratios to improve bond to the surrounding concrete.

## 6.2 Discussion

Changing the layering or spacing of the deck reinforcement appears to have little to no effect on reducing tensile stresses in the deck. Reduced bar spacing may result in improved performance with respect to cracking simply because more bars cross a potential crack, but not because of reduction in concrete tensile demand or redistribution of stresses to the steel. Furthermore, modeling results indicate that the highest tensile stresses act within the top few inches of the bridge deck, above even the topmost reinforcement layer. Thus, the longitudinal steel cannot have any benefit for reducing crack initiation.

While adjusting reinforcement may not have affected tensile stresses in the model, that does not necessarily indicate the total effect it may have on crack control. Currently, MnDOT standards use #4 bars spaced at 18 inches on center for top longitudinal reinforcement and #4 bars spaced at 8 inches on center for bottom longitudinal reinforcement. This equates to an area of steel of 0.13 in.$^2$/ft for the top mat and 0.29 in.$^2$/ft for the bottom mat, or a total of 0.42 in.$^2$/ft for the bridge deck. Following Equation (2-2) from Frosch et al. (2002) for Indiana DOT, assuming $f_c'$ = 4000 psi, $f_y$ = 60,000 psi, and $A_g$ = 108 in.$^2$ (corresponding to a 12-in. wide strip of a 9-in. thick deck), then $A_s$ = 0.68 in.$^2$/ft. To achieve this ratio, 4 bars would need to be spaced at an average of 7 in. within both the top and bottom mats. For example, 6-in. spacing on bottom plus 8-in. spacing on top would be adequate, or 7-in. spacing on both top and bottom would also be acceptable. Frosch et al. further recommended a maximum 6-inch rebar spacing, which if using #4 bars would clearly satisfy the specified ratio. Following observations by Texas DOT discussed in NCHRP Synthesis 500, Texas DOT determined that the optimal top mat longitudinal reinforcement layout includes #4 bars spaced at 9-inches on center, meeting a reinforcement ratio of 0.27 in.$^2$/ft for the top mat. While this standard is less than Indiana DOT recommendations, it would still suggest increasing the top mat reinforcement ratio by 100%, or overall reinforcement ratio by 33%.

To reduce the initiation of cracking, the three ways to substantially reduce deck stresses are to reduce the shrinkage of the deck concrete, maintain similar temperature between the deck concrete and the girders during casting, or to reduce the stiffness of the girders. The third option is likely untenable, as this has major ramifications for the entirety of the superstructure design. However, tests of HPC mixes with SRA showed promise at reducing the unrestrained shrinkage by 25% and the forces developed by restrained shrinkage by up to 50%. Developing more directed specification language for controlling temperature differences between deck and girder concrete may also effectively reduce early-age cracking.

Based on the modeling results, an approximate equation has been proposed to predict the maximum deck tensile stresses:

$$\sigma = 1\varepsilon_{sh} + 4\Delta T + 125 < f_t \qquad (6\text{-}1)$$

where σ is the deck stress in psi, $\varepsilon_{sh}$ is the 28-day shrinkage strain in microstrain and measured in the laboratory per ASTM C157, $\Delta T$ is the temperature difference in degrees Fahrenheit between the placed concrete deck and the girders, 125 (units of psi) represents the inevitable stresses caused by negative thermal gradients, and $f_t$ is the concrete modulus of rupture (i.e., tensile strength) in psi. This is not intended as a substitute for more detailed analysis but should still provide rough indication on the likelihood of cracking. For typical 4000-psi concrete with an expected tensile strength $f_t$ = 480 psi, a concrete with 355 microstrain of shrinkage and no deck-girder temperature difference would likely have little to no deck cracking. This is, admittedly, a tight limit; complete elimination of deck cracking may not be possible. However, minimization of these tensile demands should still reduce the initiation of cracks, and inclusion of additional reinforcement may minimize the widths of cracks that do inevitably form.

## 6.3 Recommendations

Based on data collected from this research, multiple courses of action can be taken to reduce early age concrete bridge deck cracking. The first option is to reduce shrinkage by using a shrinkage reducing admixture. As depicted in the laboratory testing results, incorporating SRA's in the standard HPC mix effectively reduced unrestrained shrinkage by 20-30% for each specimen. It can also be seen that the incorporation of SRA's effectively reduced the force due to restrained shrinkage by 40-60% for each specimen. Given that the maximum potential tensile stress in the deck due to cyclic creep and shrinkage may reach up to 540 psi, incorporating SRA's may reduce shrinkage sufficiently enough to greatly reduce or eliminate early age shrinkage cracking.

Changes to the specification language for the shrinkage limit for acceptable HPC mixes may result in more reliable control of bridge deck shrinkage stresses. For example, MnDOT Standard Specifications provide only a limit of 400 microstrain (0.04%) according to ASTM C157. However, this ASTM standard provides some leeway in conducting shrinkage tests that may impact shrinkage results and ultimate acceptance of certain mixes. For example, both 3-in. and 4-in. prisms are acceptable according to ASTM C157, but 4-in. prisms will have less shrinkage over 28 days than a 3-in. prism. Furthermore, using a curing duration of 28-days prior to drying will reduce measured shrinkage strains, but this does not align with the standard 7-day cure of MnDOT bridge decks.

Another solution is to decrease rebar spacing. In theory, rebar spacing could have two competing effects on deck cracking. First, reduced steel spacing may control crack widths, as highlighted by NCHRP Synthesis Report 500. However, more steel could also theoretically increase tension stresses due to shrinkage because of the increased amount of restraint. However, results from the finite element models revealed that rebar spacing has nearly no effect on peak tensile stresses. Therefore, most of the restraint that generates tension in the deck is caused by the composite connection to the girders. Consequently, increasing the amount of rebar is likely to provide benefits for crack control. Based on the equation provided by Frosch et al. (2002), the minimum area of steel required to eliminate yielding is 0.68 $in.^2$/ft. Rather than using larger bars spaced farther apart, maintaining the smaller sized #4 rebar spaced at 6 inches on center would provide better crack control. Maintaining a smaller bar size provides a smaller area to circumference ratio, resulting in improved bond to the surrounding concrete compared to larger bars. This aids in crack control performance but will not prevent crack initiation. The maximum potential tensile stress in the deck may reach 660 psi when a negative thermal gradient acts in conjunction with creep and shrinkage, regardless of how much steel is used, and this demand is invariably greater than the tensile strength of the deck concrete.

The recommendations given above will add some material costs to the initial construction of the bridge deck, but these costs are likely to be more than offset by a reduction in deterioration of the bridge deck and the associated maintenance costs. For example, for an example bridge deck 43-ft wide by 100-ft long, the current reinforcement layout using 18-inch spacing for the top longitudinal reinforcement costs approximately $26,475 for the entire deck, assuming $1.65 per pound of steel (equivalently, $1.1022 per foot of #4 reinforcement). Adopting a 9-inch spacing for the top reinforcement but leaving the rest of the reinforcement the same results in a $3,306 increase in costs (12.5% increase in

reinforcement costs for the deck alone). Similarly, adopting a 6-inch spacing for the top reinforcement increases rebar costs by $6,613 (25% increase in rebar costs for deck alone). Similar costs are associated with including SRA into the bridge deck. The example bridge deck contains roughly 120 cubic yards of concrete; estimating a cost of $50/gallon of SRA at a dosage of 1 gallon per cubic yard results in an increase of $6,000 for the deck. If such upfront costs can extend the time to maintenance by even only one or two years, this will likely lead to overall improved lifecycle costs.

Increasing fiber content may also have benefits for crack control, though generally at a cost to concrete workability. Testing did not conclusively show that higher fiber dosage increases mechanical performance; literature (e.g., Kazemian and Shafei 2022) indicate that increasing the amount of synthetic fibers may have a negligible (and sometimes negative, per Ghadban et al. 2018) impact on compressive strength but may marginally increase the modulus of rupture. However, samples with increased fiber content developed less force during restrained shrinkage tests. Other references (e.g., Hsie et al. 2008) show reductions in unrestrained shrinkage strain for increasing fiber dosage. Furthermore, fibers may provide additional control of crack width by providing more bridging sites across cracks, similar to increasing the amount of reinforcing steel but more dispersed throughout the structure.

A final possibility would be to increase typical curing periods from 7 days to 14 or even 28 days. Increasing the curing duration beyond 3 to 7 days, investigated using Control Mix 4, does not have a significant benefit on concrete strength (Poole 2006). Furthermore, curing duration did not appear to have a significant effect on concrete modulus of rupture, as investigated using Control Mix 6. However, based on results from the unrestrained shrinkage data, specimens that were cured for 28 days provided an average 14% decrease in shrinkage strain compared to specimens cured for 7 days. The delay in the onset of drying shrinkage may also reduce deck cracking, as the deck concrete is more mature before being subjected to these reduced shrinkage strains. According to the finite element model results, this reduction in shrinkage strains may be sufficient to reduce peak deck stresses caused by shrinkage alone below cracking levels but may not provide a large enough stress reduction to combat the maximum possible tensile stresses due to a combination of creep, shrinkage, and cycled thermal gradients. Furthermore, shrinkage that develops later acts on stiffer deck concrete, and restraint stresses depend on the relative stiffness between the deck and the girders. Thus, even though an increased curing duration would reduce shrinkage strains, this would be counteracted by an increased magnitude of stress per unit strain. In summary, increasing curing duration may have negligible benefits in preventing cracking, and is unlikely to be as effective as including SRA or increasing the amount of longitudinal deck steel. Estimating a cost of $1,000 per day of additional curing plus additional costs due to delays to schedule further reduce the desirability of this option.

# References


AASHTO (2020). *AASHTO LRFD bridge design specifications, 9th Ed.*, Washington, DC.

Abdigaliyev, A., Kim, Y. R., & Hu, J. (2020). Application of Internal Curing to Improve Concrete Bridge Deck Performance. *Nebraska Department of Transportation; Research Report SPRRR-P1(19) M083.*

Andrawes, B., Perez Claros, E. A., & Zhang, Z. (2022). Bond characteristics and experimental behavior of textured epoxy-coated rebars used in concrete bridge decks. *FHWA-ICT-22-001*.

Ardeshirilajimi, A., Wu, D., Chaunsali, P., Mondal, P., Chen, Y. T., Rahman, M. M., ... & Hindi, R. (2016). Bridge decks: mitigation of cracking and increased durability. *Illinois Center for Transportation Series No. 16-018; Research Report No. FHWA-ICT-16-016*.

Bažant, Z.P., and Xi, Y. (1995). Continuous retardation spectrum for solidification theory of concrete creep. *Journal of Engineering Mechanics*, 121(2), 281–288.

California Department of Transportation (2022). *Standard Specifications.*

Carrasquillo, R.L., Nilson, A.H., and Slate, F.O. (1981). Properties of High Strength Concrete Subject to Short-Term Loads. *ACI Journal*, 78(3), 171-178.

French. C.E., Eppers, L.J., Le, Q.T.C., and Hajjar, J.F. (1999). *Transverse Cracking in Bridge Decks*. Report Mn/RC – 1999-05. Minnesota Department of Transportation, St. Paul, MN.

Frosch, R.J., Blackman, D.T., and Radabaugh, R.D. (2003). *Investigation of Bridge Deck Cracking in Various Bridge Superstructure Systems* (Report No. FHWA/IN/JTRP-2002/25). Indiana Department of Transportation.

Ge, X., Munsterman, K., Deng, X., Reichenbach, M., Park, S., Helwig, T., ... and Bayrak, O. (2021). *Designing for Deck Stress Over Precast Panels in Negative Moment Regions* (No. FHWA/TX-21/0-6909-1/5-6909-01-1). University of Texas at Austin. Center for Transportation Research.

Ghadban, A.A., Wehbe, N.I., and Underberg, M. (2018). Effect of fiber type and dosage on flexural performance of fiber-reinforced concrete for highway bridges. *ACI Materials Journal*, 115(3), 413-424.

Hamid, W. K., Steinberg, E. P., Khoury, I., Walsh, K. K., Ahmed, S., & Semendary, A. (2022). Determination of Concrete Shrinkage Initiation in Internally Cured and Conventional Concrete Decks. *Journal of Testing and Evaluation*, *50*(3), 1673-1682.

Hedegaard, B.D., Clement, T.J., and Hubler, M.H. (2023). Coupled pore relative humidity model for concrete creep and shrinkage. *ACI Materials Journal*, 120(3), 103-116.

Hedegaard, B.D., French, C.E.W., and Shield, C.K. (2013). Investigation of thermal gradient effects in the I-35W St. Anthony Falls Bridge. *Journal of Bridge Engineering*, 18(9), 890-900.

Hsie, M., Tu, C., and Song, P.S. (2008). Mechanical properties of polypropylene hybrid fiber-reinforced concrete. *Materials Science and Engineering A*, 494, 153-157.

Kazemian, M., and Shafei, B. (2022). Mechanical properties of hybrid fiber reinforced concretes made with low dosages of synthetic fibers. *Structural Concrete*, 24, 1226-1243.

Khayat, K. H., & Abdelrazik, A. (2019). *Field Implementation of super-workable fiber-reinforced concrete for infrastructure construction* (No. CMR 19-001). Missouri University of Science and Technology. Dept. of Civil, Architectural, and Environmental Engineering.

Kim, K. H. E., & Andrawes, B. (2018). Behavior of epoxy-coated textured reinforcing bars. *FHWA-ICT-18-004*.

Lee, B. J., & Kim, Y. Y. (2018). Durability of latex modified concrete mixed with a shrinkage reducing agent for bridge deck pavement. *International Journal of Concrete Structures and Materials*, *12*(1), 1-9.

Minnesota Department of Transportation (2023). *Mn/DOT LRFD bridge design manual*. https://www.dot.state.mn.us/bridge/lrfd.html

Minnesota Department of Transportation (2023). *Mn/DOT service life design guide for bridges*. https://edocs-public.dot.state.mn.us/edocs_public/DMResultSet/download?docId=15850393

Minnesota, Department of Transportation (2020). *Mn/DOT standard specifications for construction*. https://www.dot.state.mn.us/pre-letting/spec/

National Cooperative Highway Research Program (2017). *NCHRP Synthesis 500: Control of Concrete Cracking in Bridges.* Washington, DC.

Ozyildirim, H. C., & Nair, H. (2018). Durable Concrete Overlays in Two Virginia Bridges. *Transportation Research Record*, *2672*(27), 78-87.

Pacheco, J., Vaddey, P., Amini, K., & Vosahlik, J. (2021). *Internal Curing of Bridge Decks and Concrete Pavement to Reduce Cracking* (No. WHRP 0092-19-02). Wisconsin. Dept. of Transportation. Research and Library Unit.

Patnaik, A. (2017). *Reduction of Bridge Deck Cracking through Alternative Material Usage* (No. FHWA/OH-2017/44). Ohio. Dept. of Transportation. Office of Statewide Planning and Research.

Poole, T.S. (2006). *Guide for Curing of Portland Cement Concrete Pavements, Volume II* (Publication No. FHWA-HRT-05-038). Federal Highway Administration, Turner-Fairbank Highway Research Center.

Priestley, M.J.N. (1978). Design of concrete bridges for temperature gradients, *ACI Journal*, Vol. 75, No. 5, pp. 209-217.

Rahman, M., Chen, Y., Ibrahim, A., Lindquist, W., Tobias, D., Krstulovich, J., ... & Hindi, R. (2020). Study of drying shrinkage mitigating concrete using scaled bridge bays. *International Journal of Civil Engineering*, *18*, 65-73.

Rettner, D. L., Fiegen, M. S., Snyder, M. B., & MacDonald, K. A. (2014). Analysis of Bridge Deck Cracking Data: A Review of Mechanisms, Analysis of MnDOT Bridge Construction Data, and Recommendations for Treatment and Prevention.

Ross, B., Poursaee, A., Sreedhara, S., & Mueller, M. (2021). *Textured Epoxy Coated and Galvanized Reinforcement To Reduce Cracking in Concrete Bridge Decks and Components* (No. WisDOT ID no. 0092-19-01). Wisconsin. Dept. of Transportation. Research and Library Unit.

Saje, D., Bandelj, B., Šušteršič, J., Lopatič, J., & Saje, F. (2011). Shrinkage of polypropylene fiber-reinforced high-performance concrete. *Journal of materials in civil engineering*, *23*(7), 941-952.

Shafei, B., Taylor, P., Phares, B., & Kazemian, M. (2021). Fiber-Reinforced Concrete for Bridge Decks. *The Bridge*, *515*, 294-8103.

Simonton, E., & Shearer, C. R. (2021). *Low Shrinkage Mix Designs to Reduce Early Cracking of Concrete Bridge Decks* (No. SD2018-04-F). South Dakota Department of Transportation. Office of Research.

Tunstall, L. E., Ley, M. T., & Scherer, G. W. (2021). Air entraining admixtures: Mechanisms, evaluations, and interactions. *Cement and Concrete Research*, *150*, 106557.

Utah Department of Transportation (2022). *Structures Design and Detailing Manual.* https://www.udot.utah.gov/connect/business/structures-geotechnical-guidance-manuals/structures-design-detailing-manual/

Virginia Department of Transportation (2020). *Road and Bridge Specifications.* https://www.vdot.virginia.gov/doing-business/technical-guidance-and-support/technical-guidance-documents/road-and-bridge-specifications/

Washington State Department of Transportation (2024). *Standard Specifications for Road, Bridge, and Municipal Construction.* https://wsdot.wa.gov/engineering-standards/all-manuals-and-standards/manuals/standard-specifications-road-bridge-and-municipal-construction

Wisconsin Department of Transportation (2023). *Bridge Manual.* https://wisconsindot.gov/Pages/doing-bus/eng-consultants/cnslt-rsrces/strct/bridge-manual.aspx

# Appendix A
# Parametric Modeling Results

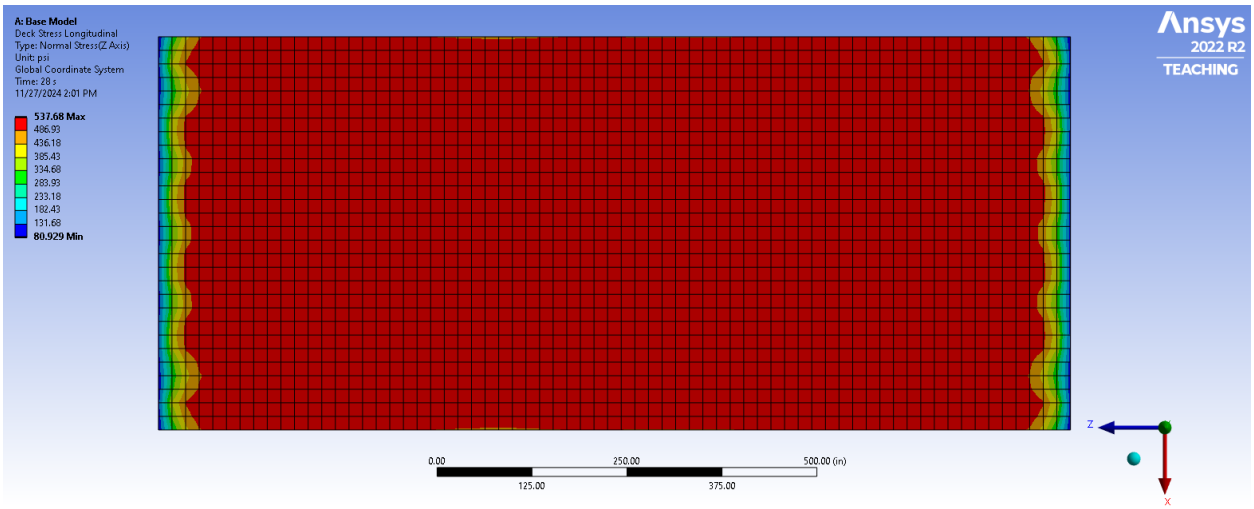


**Figure A.1. Stress in 18TLR model due to creep and shrinkage with cycled thermal gradients**

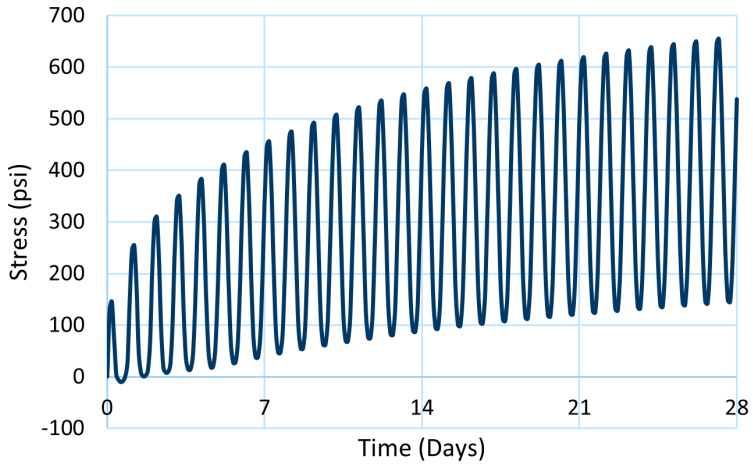


**Figure A.2. Stress in 18TLR model due to creep and shrinkage with cycled thermal gradients**

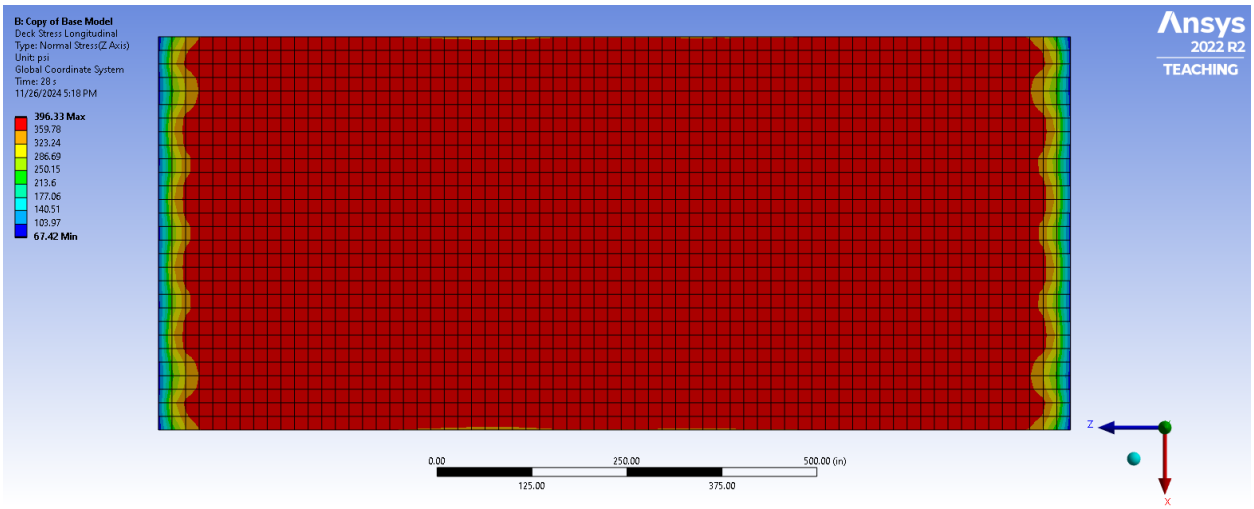


**Figure A.3. Stress in 18TLR model due to creep and shrinkage alone**

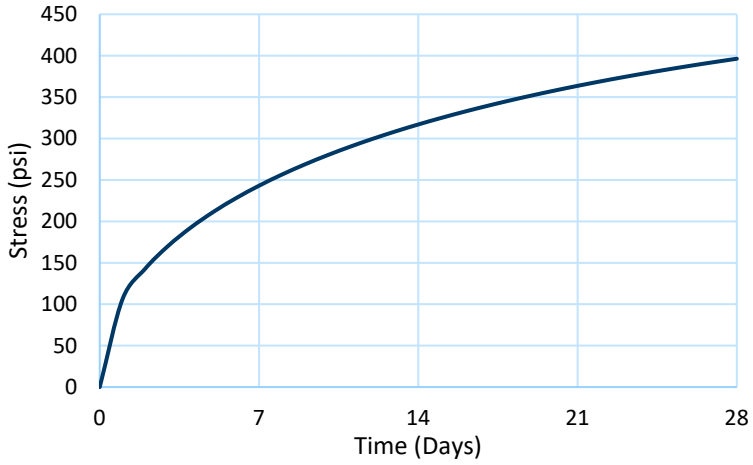


**Figure A.4. Stress in 18TLR model due to creep and shrinkage alone**

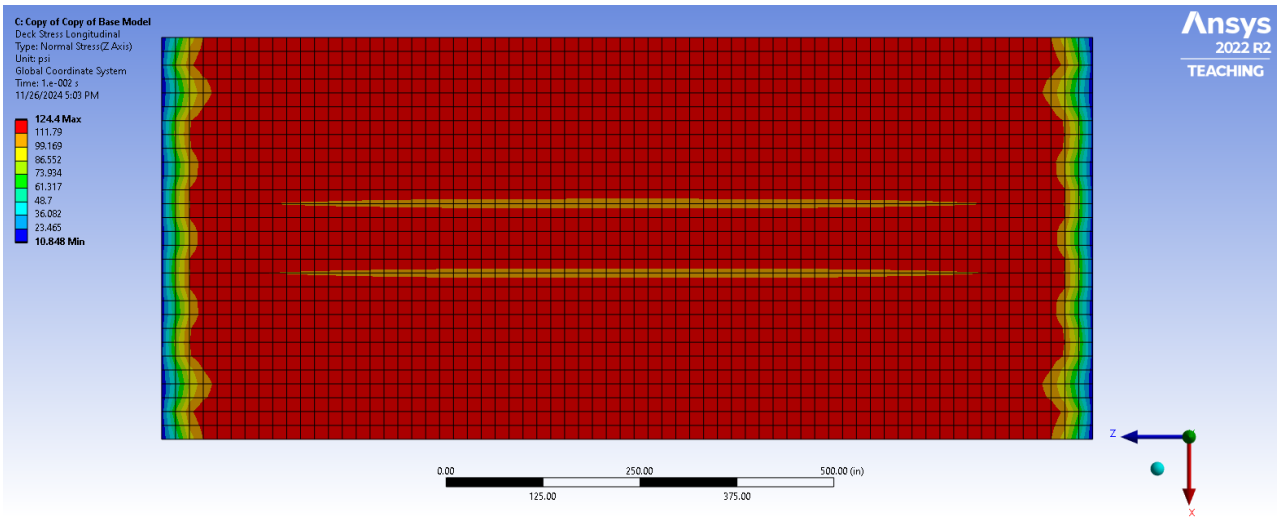


**Figure A.5. Stress in 18TLR model – elastic analysis with negative gradient**

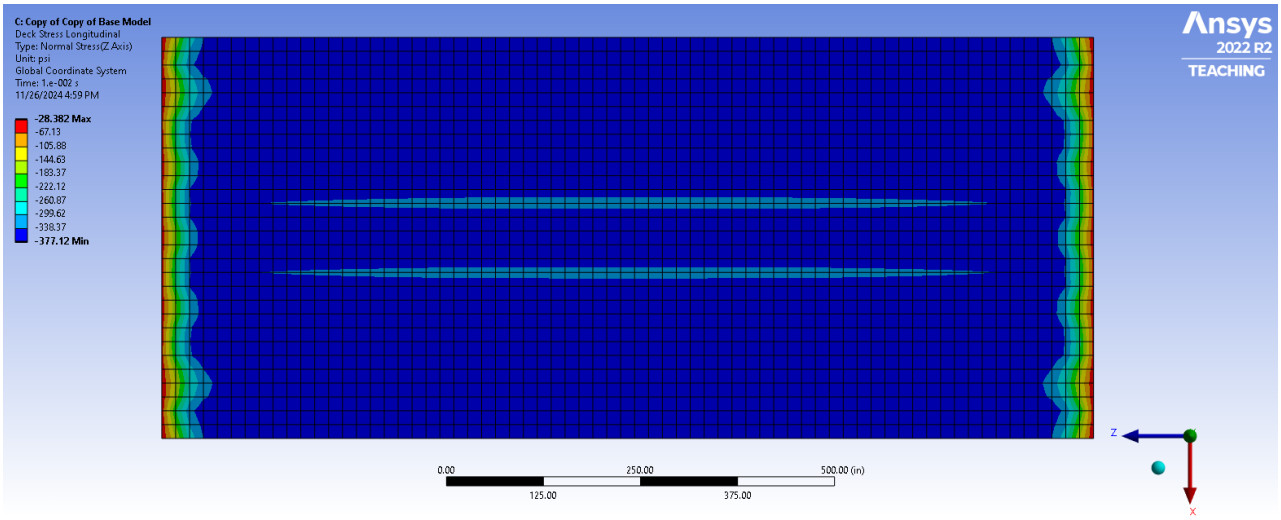


**Figure A.6. Stress in 18TLR model – elastic analysis with positive gradient**

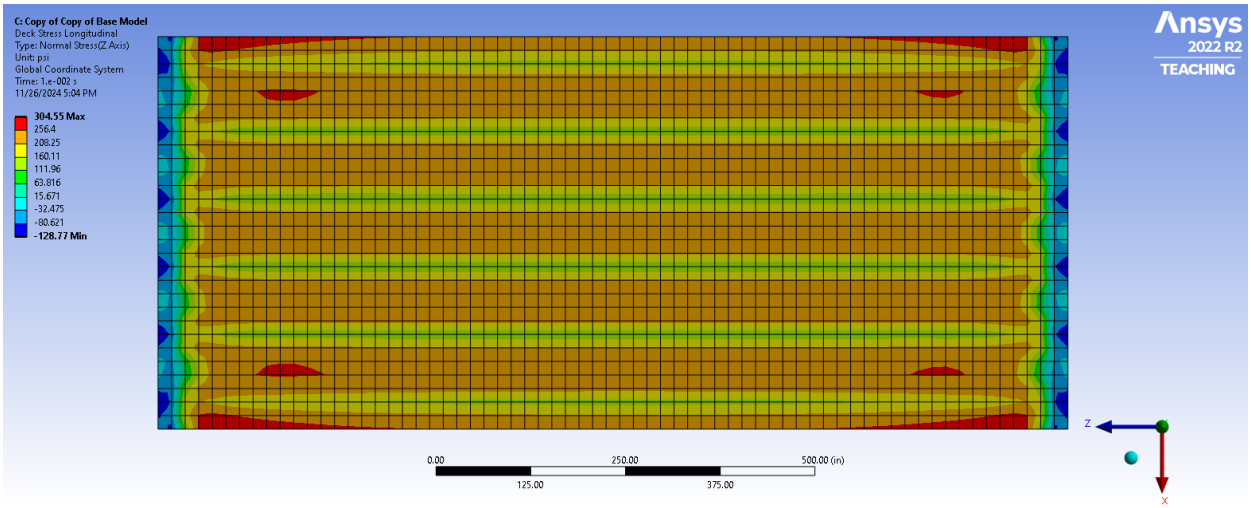


**Figure A.7. Stress in 18TLR model – elastic analysis with relative temperature difference between deck and girders**

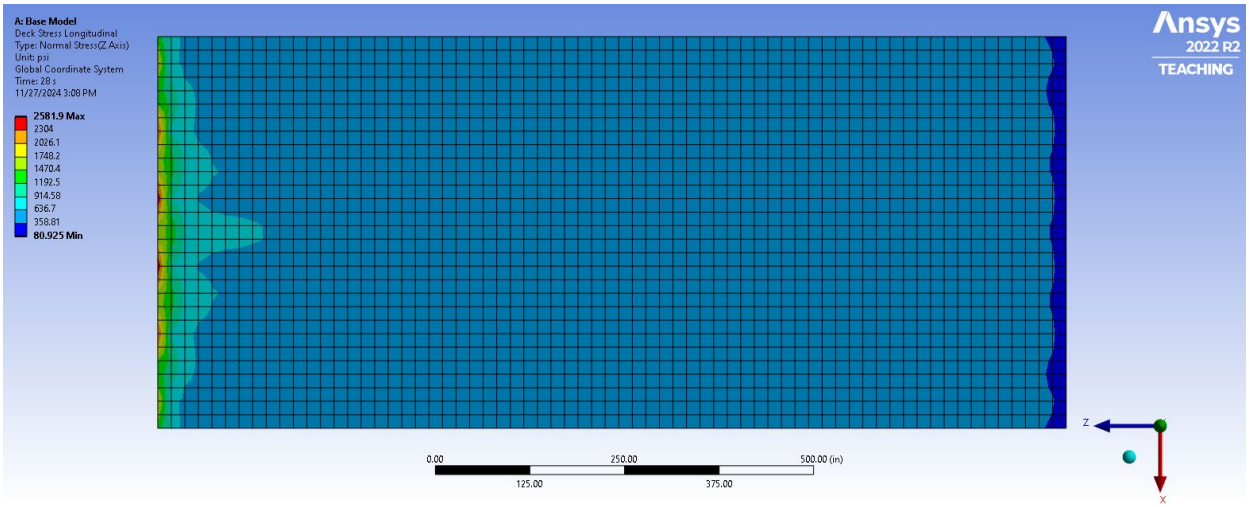


**Figure A.8. Stress in 2 span 18TLR model due to creep and shrinkage with cycled thermal gradients**

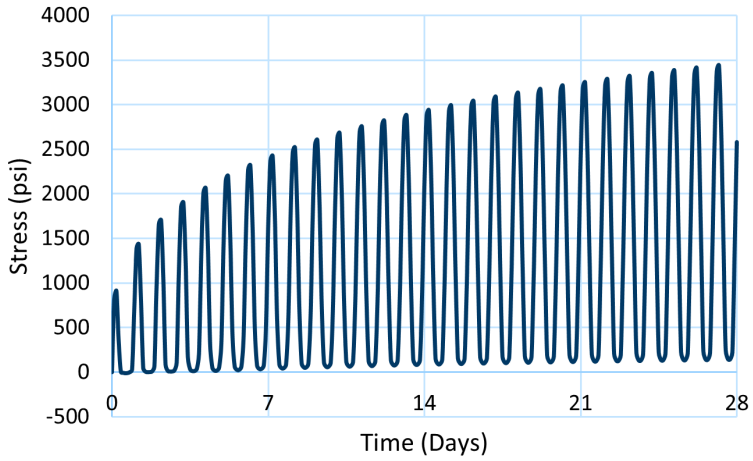


**Figure A.9. Stress in 2 span 18TLR model due to creep and shrinkage with cycled thermal gradients**

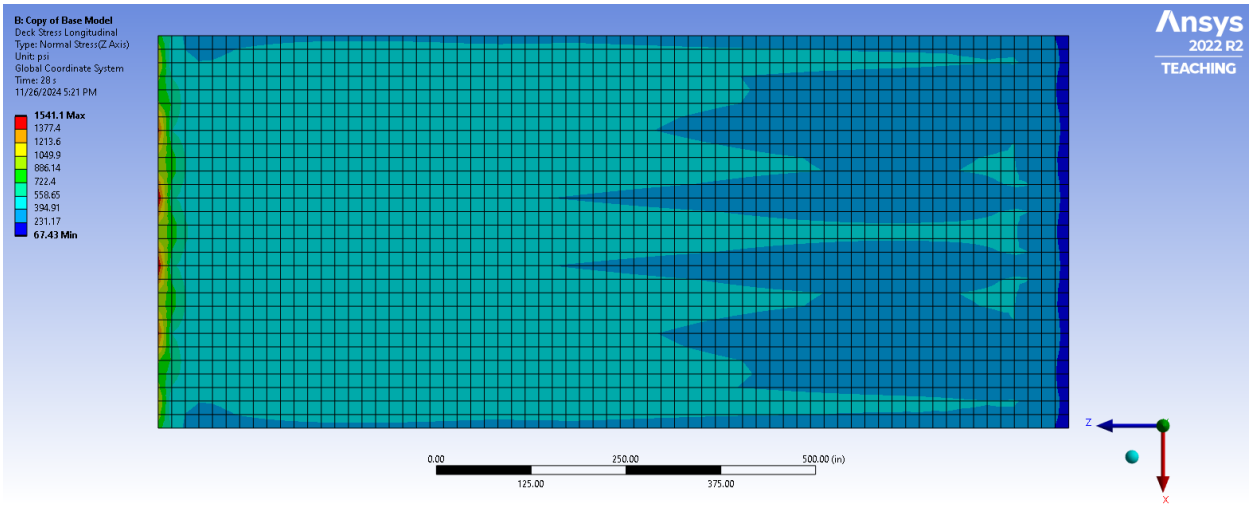


**Figure A.10. Stress in 2 span 18TLR model due to creep and shrinkage alone**

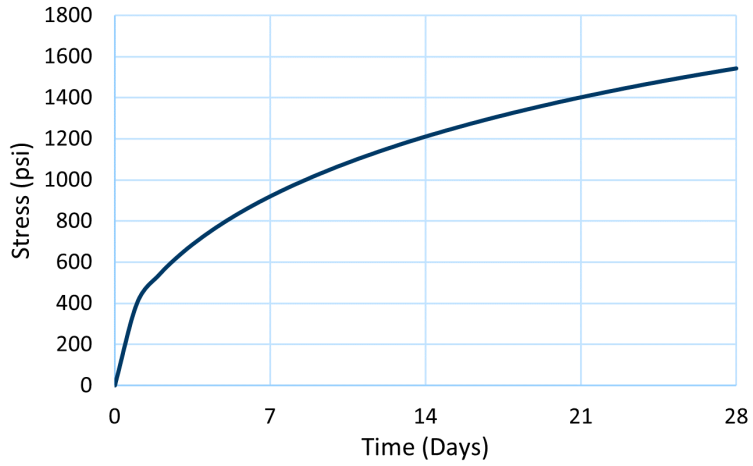


**Figure A.11. Stress in 2 span 18TLR model due to creep and shrinkage alone**

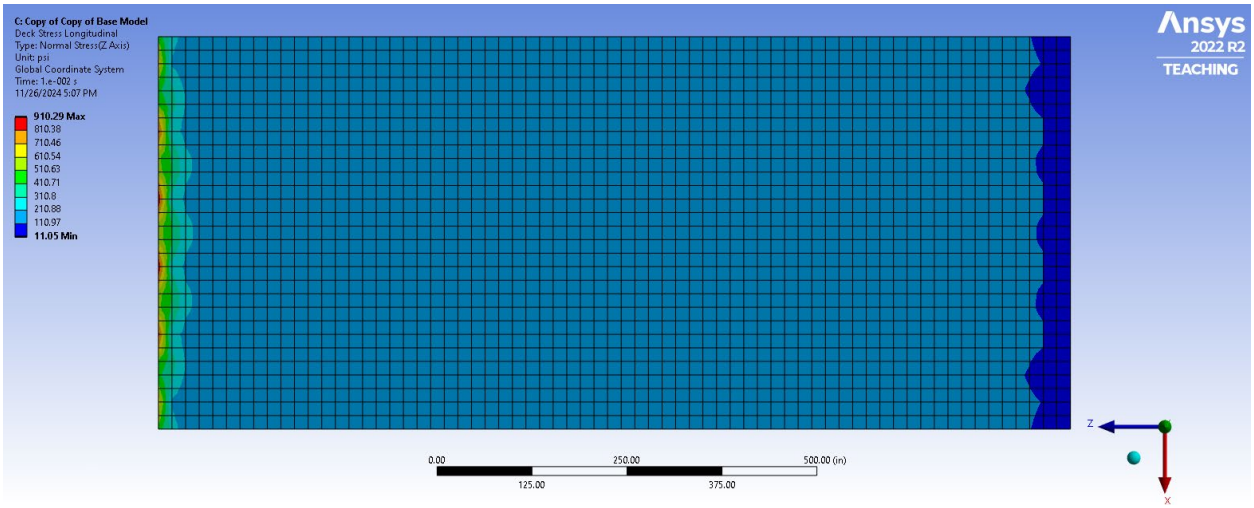


**Figure A.12. Stress in 2 span 18TLR model – elastic analysis with negative gradient**

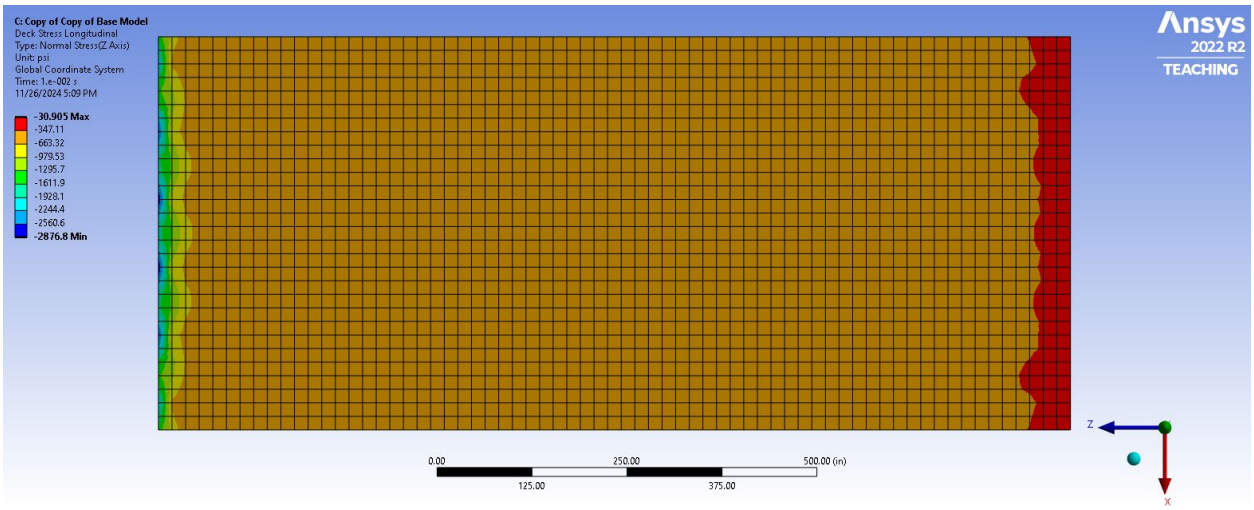


**Figure A.13. Stress in 2 span 18TLR mode – elastic analysis with positive gradient**

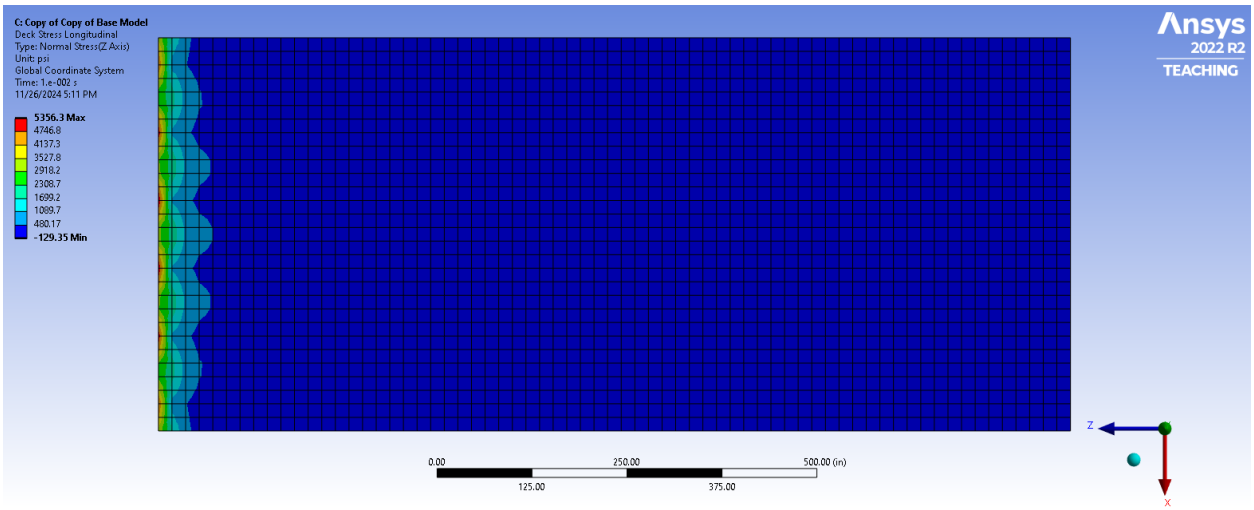


**Figure A.14. Stress in 2 span 18TLR model – elastic analysis with relative temperature difference between deck and girders**

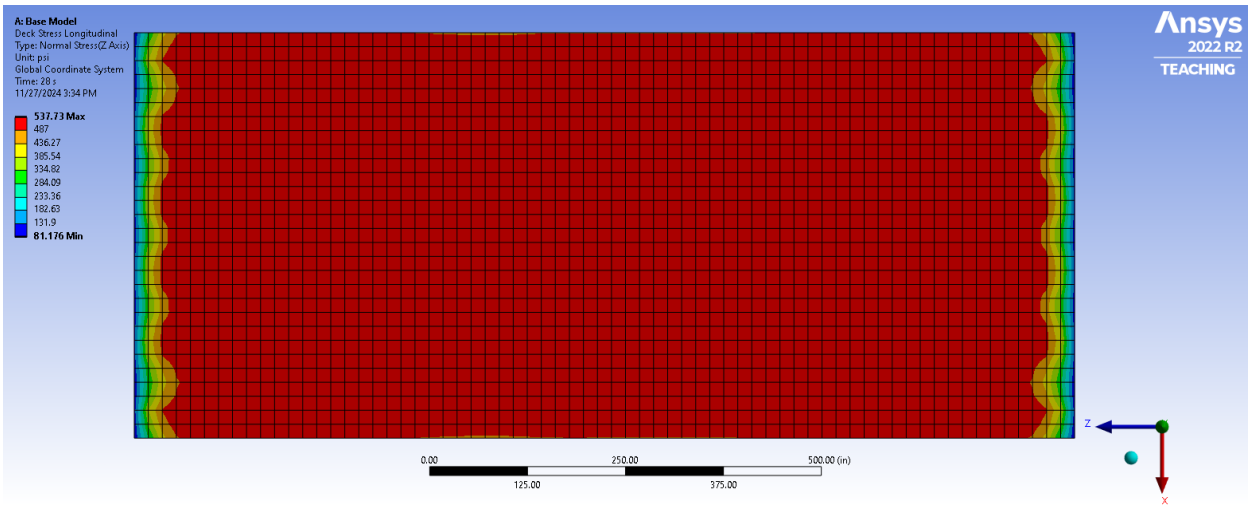


**Figure A.15. Stress in flipped 18TLR model due to creep and shrinkage with cycled thermal gradients**

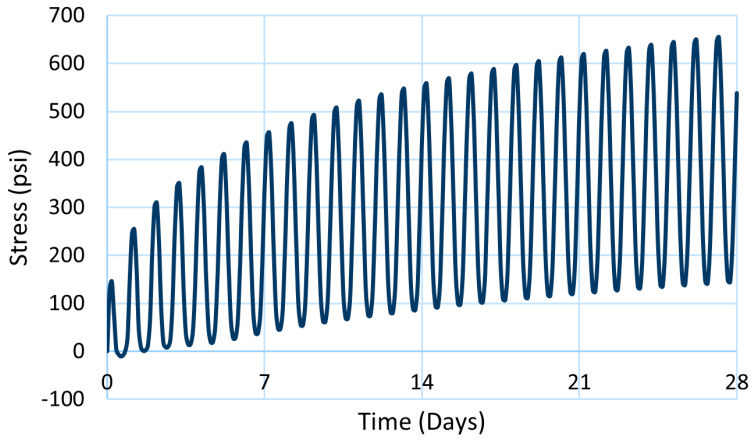


**Figure A.16. Stress in flipped 18TLR model due to creep and shrinkage with cycled thermal gradients**

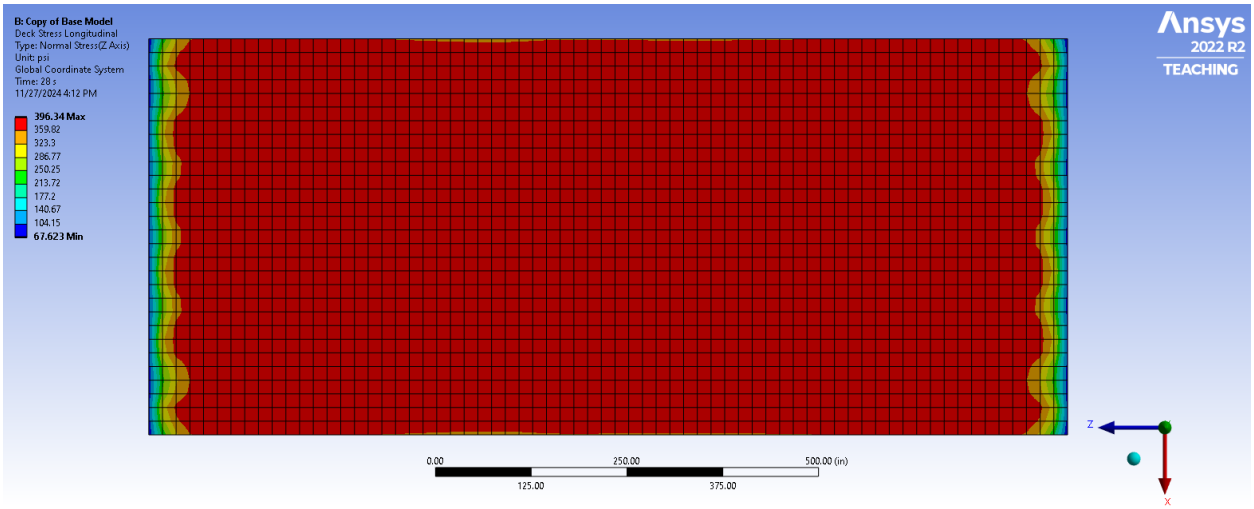


**Figure A.17. Stress in flipped 18TLR model due to creep and shrinkage alone**

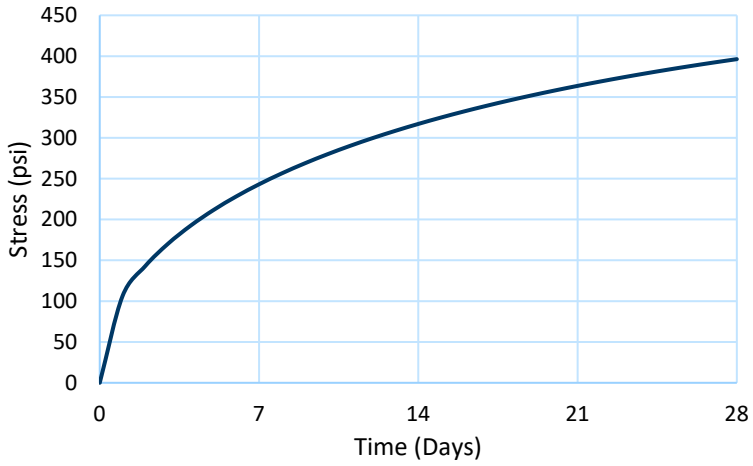


**Figure A.18. Stress in flipped 18TLR model due to creep and shrinkage alone**

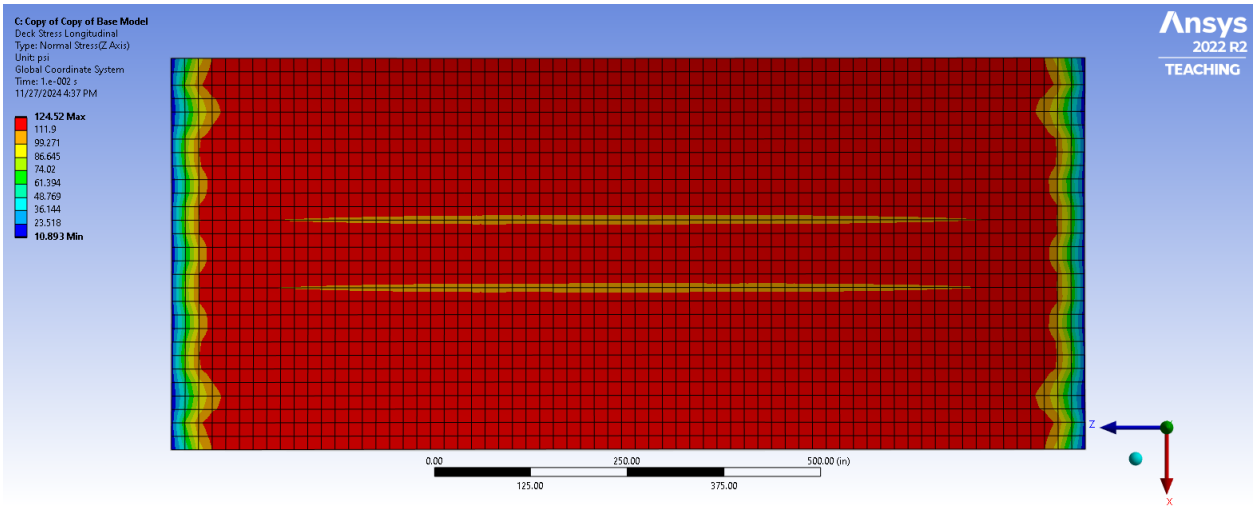


**Figure A.19. Stress in flipped 18TLR model – elastic analysis with negative gradient**

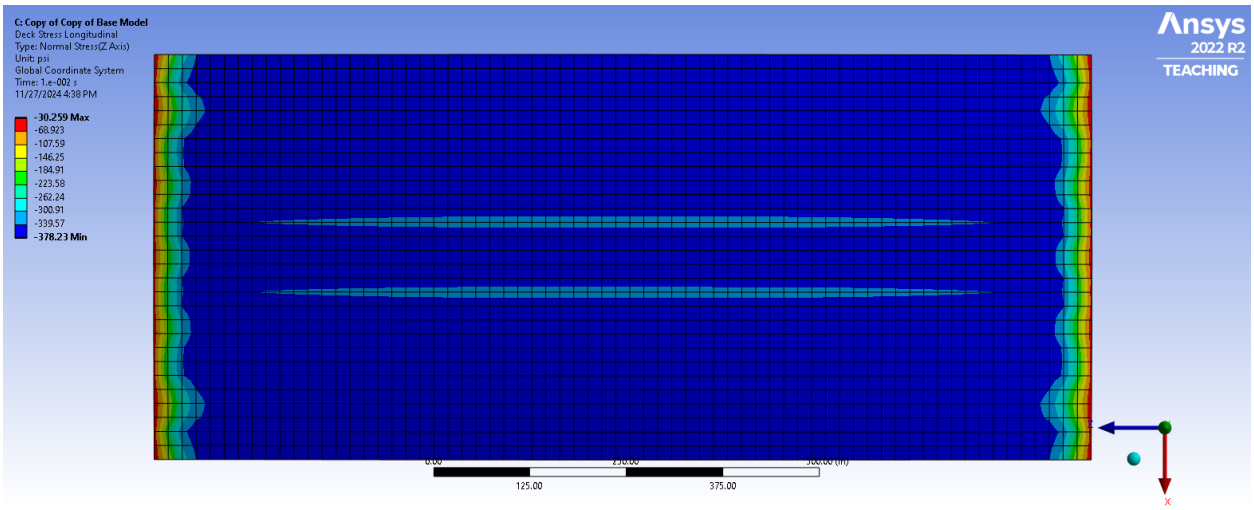


**Figure A.20. Stress in flipped 18TLR model – elastic analysis with positive gradient**

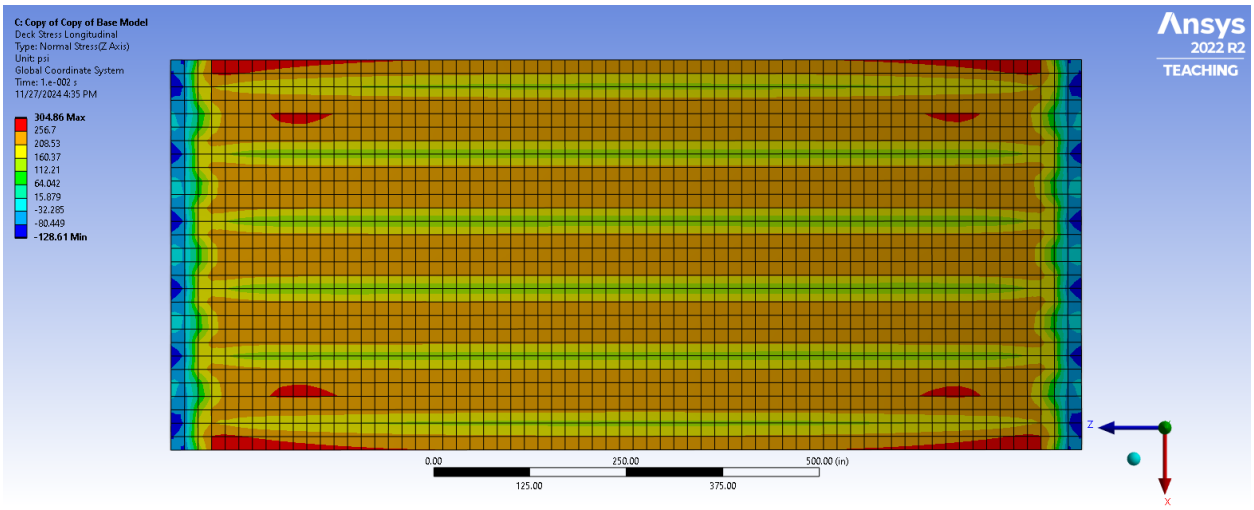


**Figure A.21. Stress in flipped 18TLR model – elastic analysis with relative temperature difference between deck and girders**

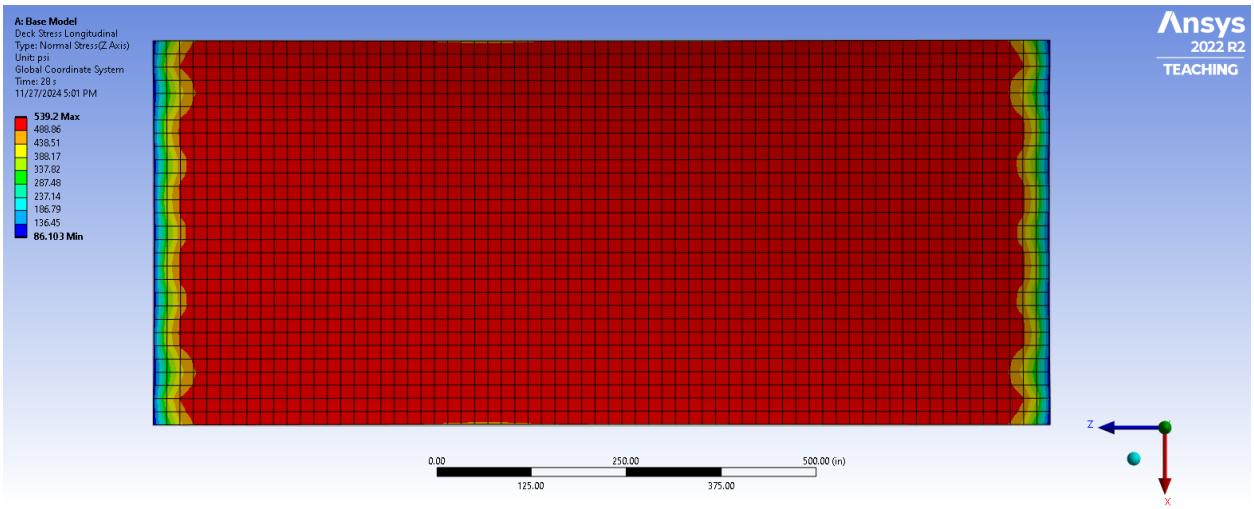


**Figure A.22. Stress in 12TLR model due to creep and shrinkage with cycled thermal gradients**

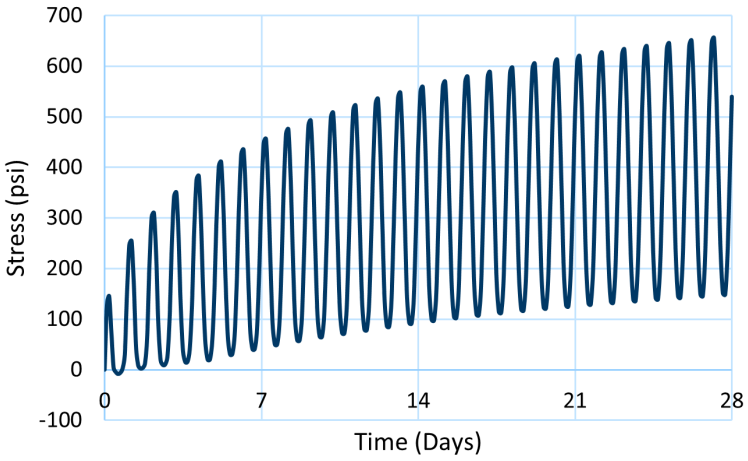


**Figure A.23. Stress in 12TLR model due to creep and shrinkage with cycled thermal gradients**

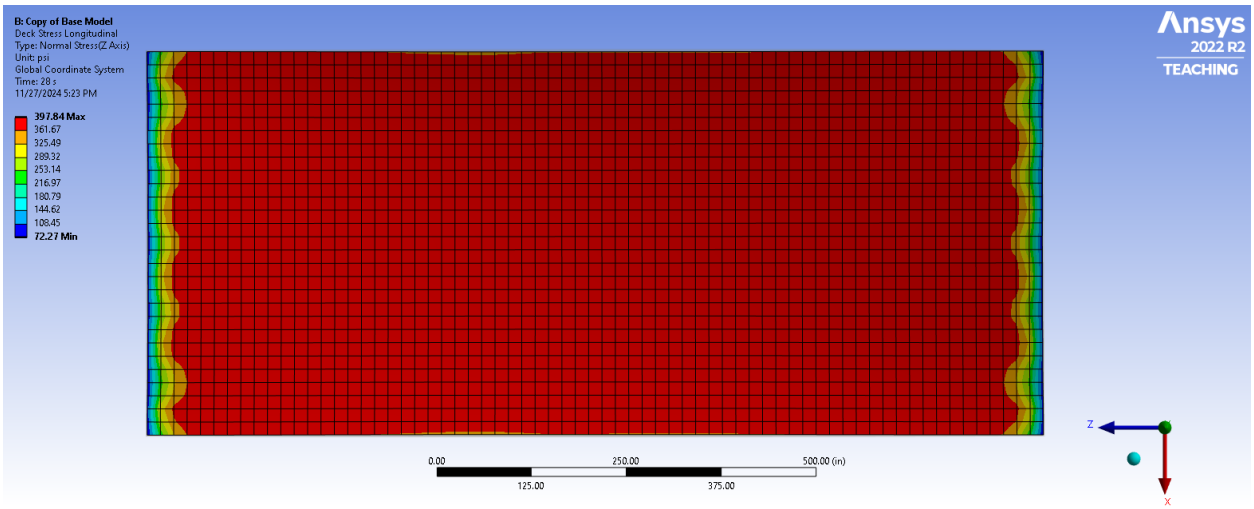


**Figure A.24. Stress in 12TLR model due to creep and shrinkage alone**

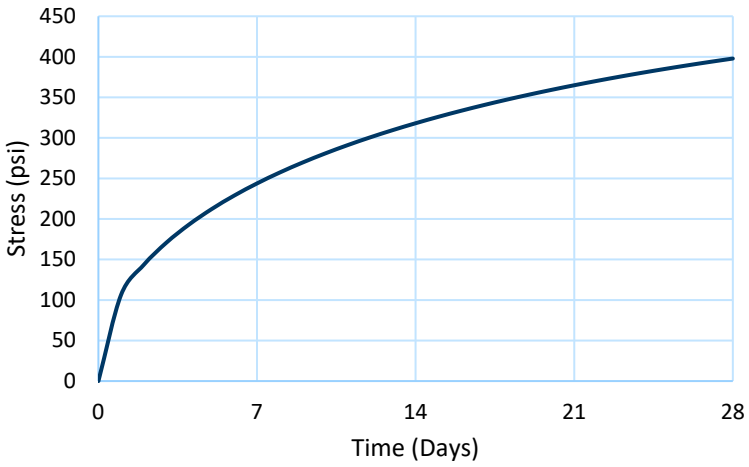


**Figure A.25. Stress in 12TLR model due to creep and shrinkage alone**

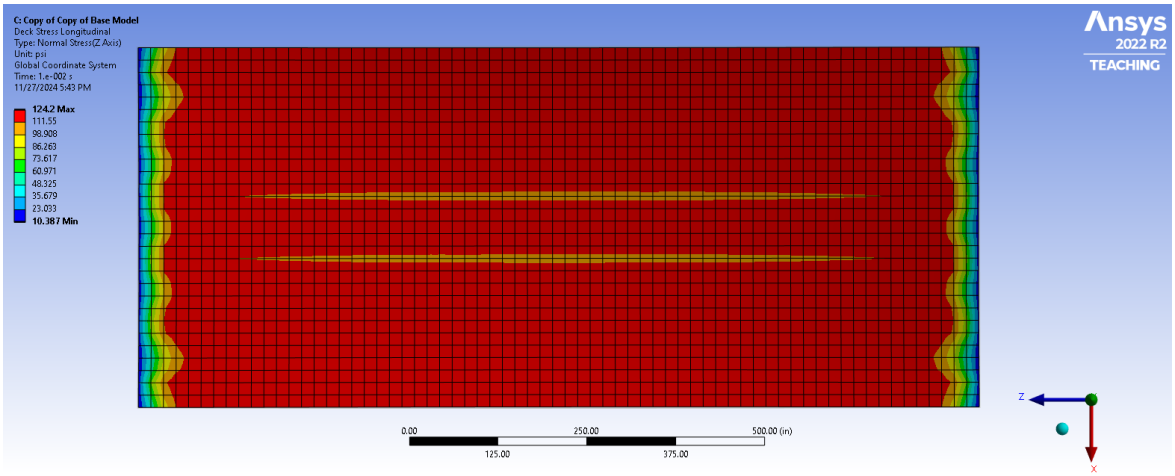


**Figure A.26. Stress in 12TLR model – elastic analysis with negative gradient**

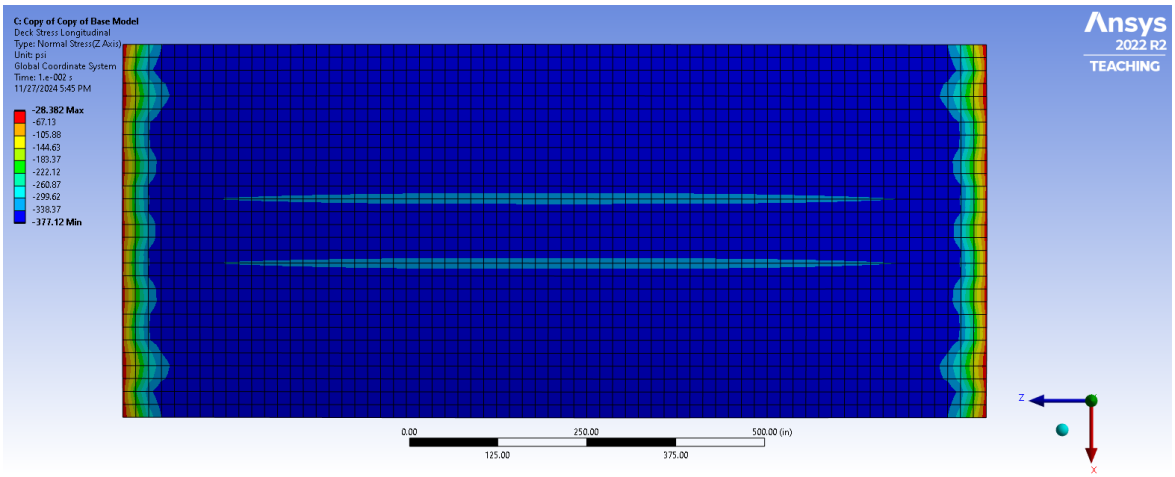


**Figure A.27. Stress in 12TLR model – elastic analysis with negative gradient**

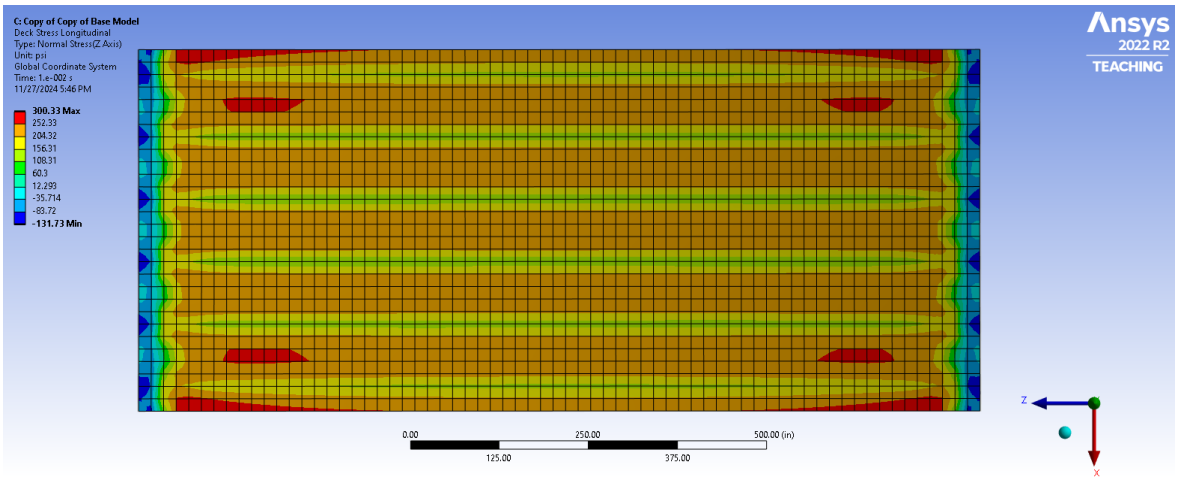


**Figure A.28. Stress in 12TLR model – elastic analysis with relative temperature difference between deck and girders**

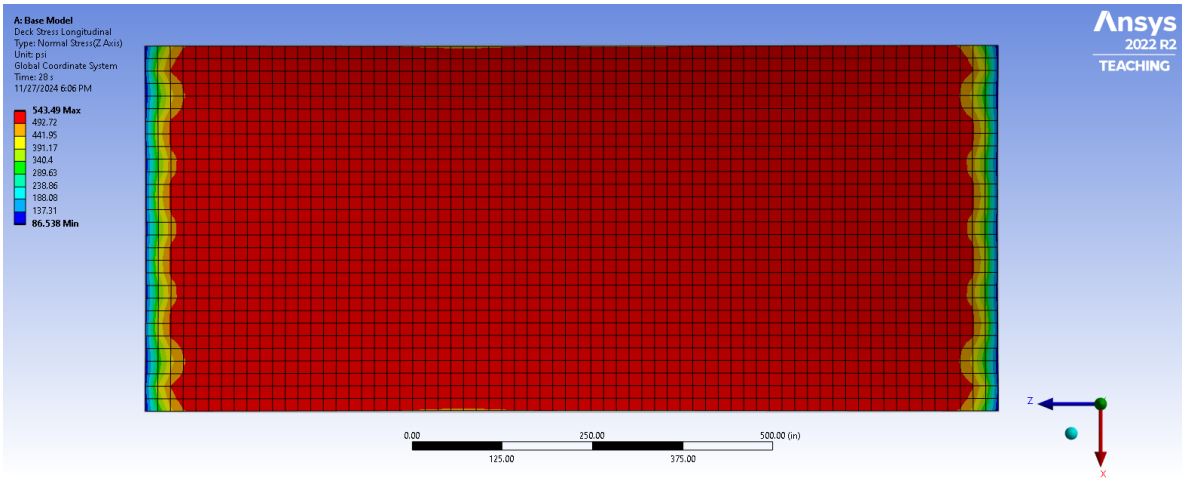


**Figure A.29. Stress in 6TLR model due to creep and shrinkage with cycled thermal gradients**

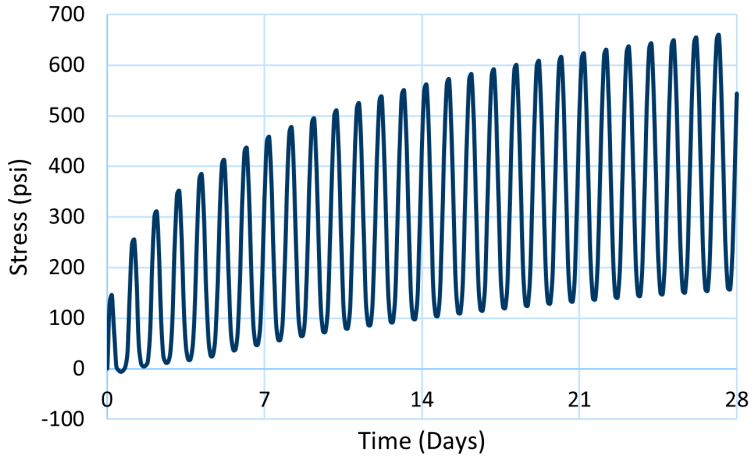


**Figure A.30. Stress in 6TLR model due to creep and shrinkage with cycled thermal gradients**

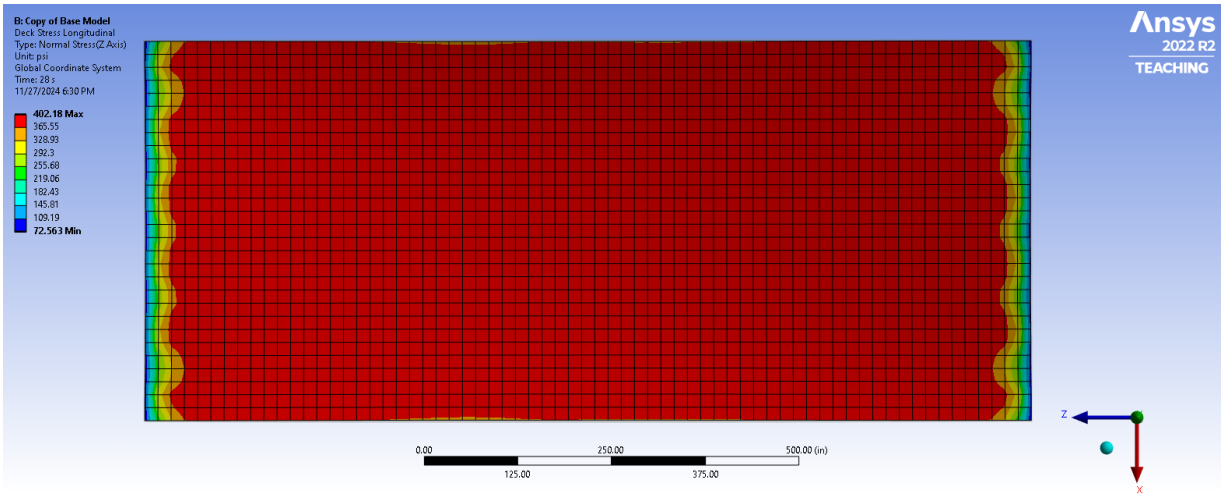


**Figure A.31. Stress in 6TLR model due to creep and shrinkage alone**

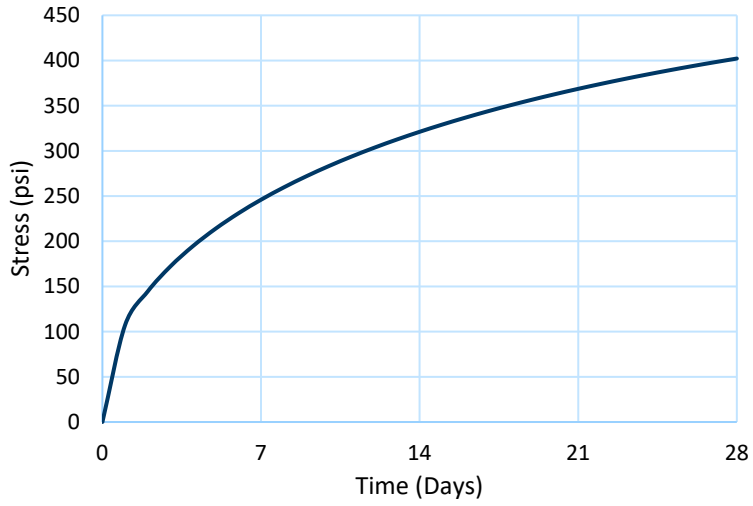


**Figure A.32. Stress in 6TLR model due to creep and shrinkage alone**

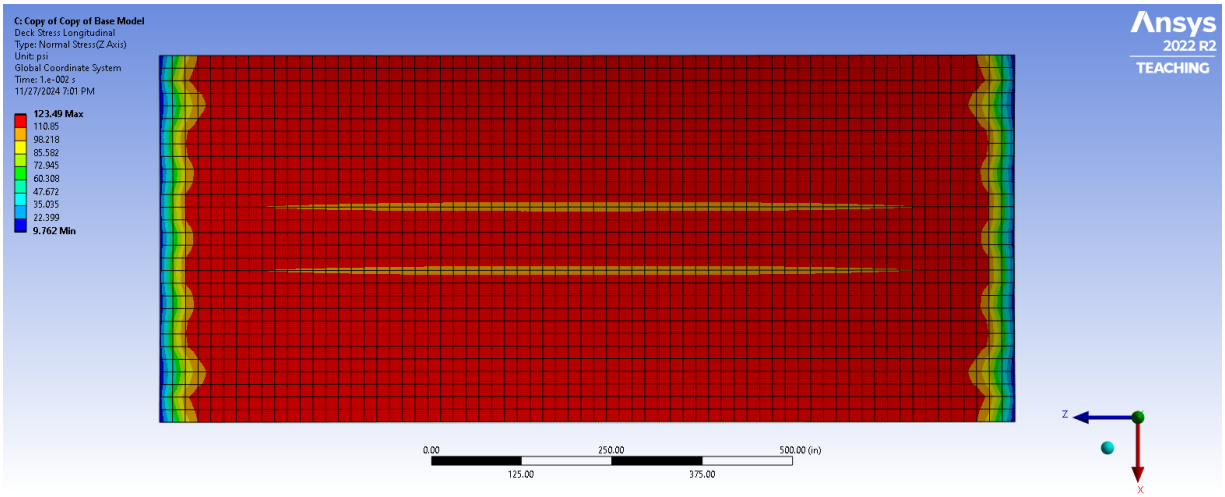


**Figure A.33. Stress in 6TLR model – elastic analysis with negative gradient**

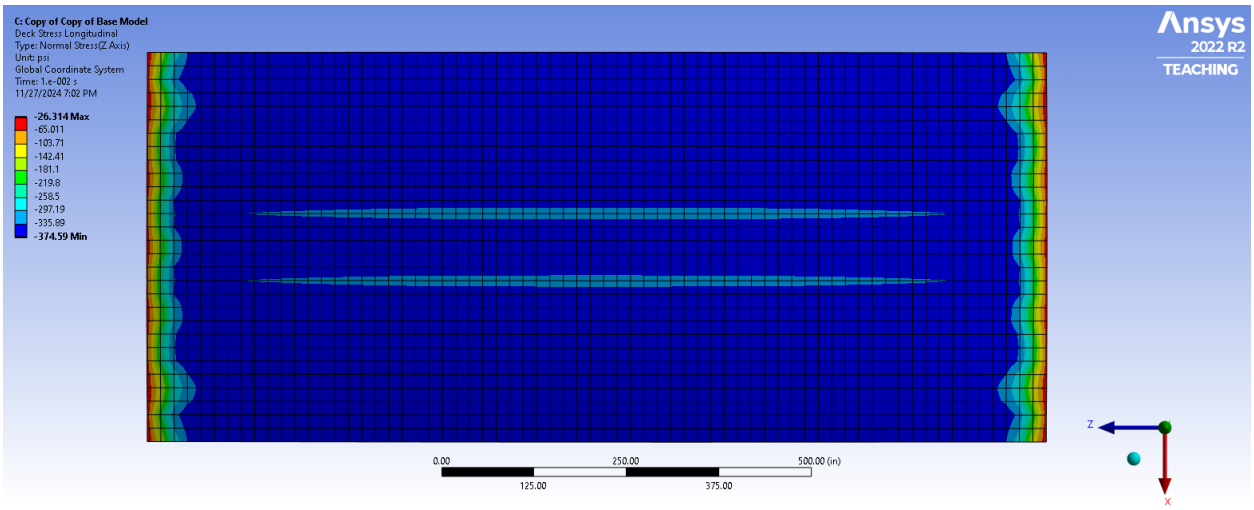


**Figure A.34. Stress in 6TLR model – elastic analysis with positive gradient**

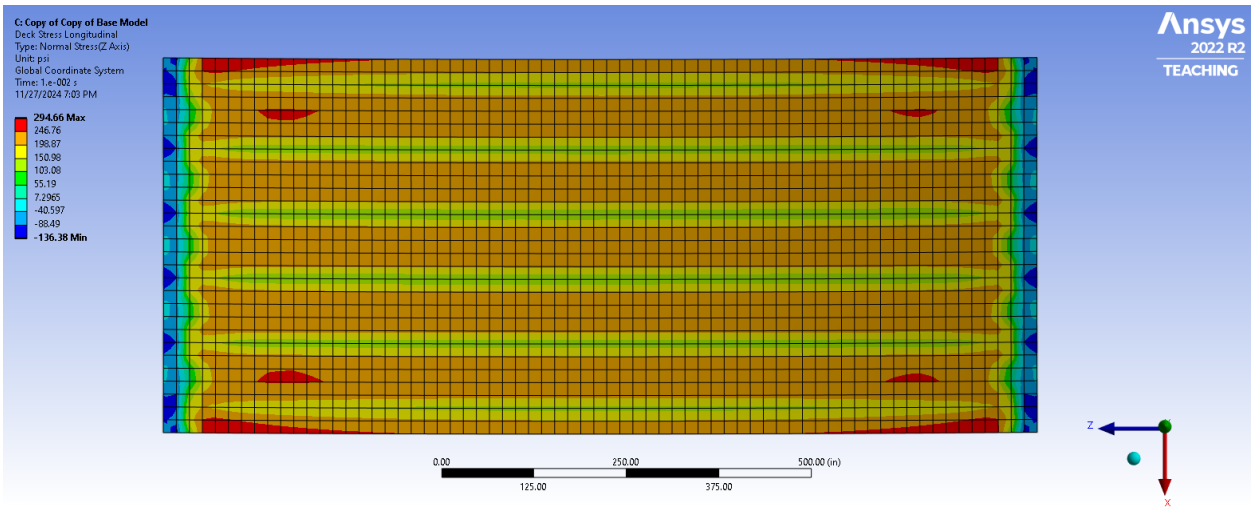


**Figure A.35. Stress in 6TLR model – elastic analysis with relative temperature difference between deck and girders**